



Akademie věd České republiky

Teze disertace  
k získání vědeckého titulu "doktor věd"  
ve skupině věd **Technické vědy**

**Analytical Models of Thermal Stresses in Multi-Component Materials**

název disertace

Komise pro obhajoby doktorských disertací v oboru

**Mechanika těles, konstrukcí, mechanismů a prostředí**

Jméno uchazeče: Ladislav Ceniga

Pracoviště uchazeče: Ústav materiálového výskumu  
Slovenská akadémia vied  
Košice, Slovenská republika

Místo a datum: Praha, 2012

# Contents

<b>Resumé</b>	<b>2</b>
<b>1 Types of multi-component materials. Model systems and cell model</b>	<b>4</b>
1.1 Types of multi-component materials . . . . .	4
1.2 Model systems and cell model . . . . .	4
1.3 Characteristics of the model systems . . . . .	5
1.4 Multi-component materials versus model systems . . . . .	5
<b>2 Selected topics on solid continuum mechanics</b>	<b>6</b>
2.1 Coordinate system and intervals of coordinates . . . . .	6
2.2 Displacement of the infinitesimal spherical cap. Thermal-stress induced radial displacement . . . . .	7
2.3 Fundamental equations of solid continuum mechanics . . . . .	8
2.4 Elastic energy . . . . .	9
2.5 Reason of thermal stresses . . . . .	10
<b>3 Thermal stresses in the model systems with anisotropic components</b>	<b>12</b>
3.1 Radial, tangential and shear stresses . . . . .	12
3.2 Analysis of a number of solutions for the model systems . . . . .	13
3.3 Boundary conditions . . . . .	14
<b>4 Thermal stresses in the model systems with isotropic components</b>	<b>18</b>
4.1 Radial, tangential and shear stresses . . . . .	18
4.2 Analysis of a number of solutions for the model systems . . . . .	19
4.3 Number of solutions for the model systems . . . . .	19
4.4 Thermal stresses in the model systems with isotropic and anisotropic components . . . . .	19
<b>5 Related phenomena</b>	<b>20</b>
5.1 Analytical model of crack formation . . . . .	20
5.2 Analytical model of energy barrier . . . . .	25
5.3 Analytical model of strengthening . . . . .	27
5.4 Methods of lifetime prediction . . . . .	28
<b>6 Conclusions and applications</b>	<b>33</b>
<b>Bibliography</b>	<b>36</b>
<b>List of the author's publications</b>	<b>40</b>

## Resumé

This doctoral dissertation presents scientific results which have been published in papers of international journals [D1]–[D12], in chapters of international books [D13]–[D15], and in the author’s monographs published at an international publisher [D16]–[D18]. Strictly speaking, the scientific results which are published in [D1]–[D15] along with next development of these results are presented in [D16]–[D18]. This doctoral dissertation thus presents the most important results of these three monographs [D16]–[D18]. These *sole-authored* international works [D1]–[D18] deal with the analytical modelling of thermal stresses and thermal-stress induced phenomena in multi-component materials, i.e. in two- and three-component materials which are defined in Sec. 1.2. The thermal stresses and thermal-stress induced phenomena are thus analytically determined in each component of these multi-component materials. With regard to the analytical modelling, these real multi-component materials are replaced by two- and three-component model systems, i.e. multi-particle-matrix and multi-particle-envelope-matrix systems, respectively (see Fig. 1).

The analytical determination of a thermal stress-strain state is based on a cell model which considers a cubic cell (see Fig. 1). The cell model is usually used in case of the analytical and computational modelling of phenomena in periodic model systems [19]–[27]. As presented in [28], the replacing of the real multi-component materials with finite dimensions by model systems with infinite dimensions is considered for mathematical simplicity of analytical solutions which are assumed to exhibit sufficient accuracy due to relatively small material components in comparison with macroscopic material samples, macroscopic structural elements, etc.

The thermal stresses which originate below relaxation temperature (see Sec. 2.5) during a cooling process are a consequence of the difference in dimensions of the components. This difference is a consequence of different thermal expansion coefficients and/or a consequence of the phase-transformation induced strain. This coefficient and strain are included in the coefficient  $\beta_q$  for the spherical particle ( $q = p$ ), the spherical envelope ( $q = e$ ) and the cell matrix ( $q = m$ ) (see Eqs. (9)–(11)). Due to a range of this brochure, this strain is determined in the doctoral dissertation.

The analytical modelling results from fundamental equations of solid continuum mechanics which are represented by the Hooke’s law for an anisotropic and isotropic continuum (see Sec. 2.3), and by the Cauchy’s, compatibility and equilibrium equations which are determined by the spherical coordinates  $(r, \varphi, \nu)$  (see Fig. 2). The analytical models of the thermal stresses are determined for these model systems which consists of either anisotropic, or isotropic, or anisotropic and isotropic components (see Chaps. 3, 4, Sec. 4.3). The thermal stress-strain state in each component of the model systems is determined by several mutually different solutions which fulfil the boundary conditions which are determined in Sec. 3.3. In case of the cell matrix, mandatory and additional boundary conditions are determined. Due to these different solutions, a principle of minimum total potential energy of an elastic solid body [29] is then required to be considered (see Sec. 2.4).

Analytical models of thermal-stress induced phenomena are also determined. These phenomena include the crack formation (see Sec. 5.1), the energy barrier (see Sec. 5.2), the micro- and macro-strengthening (see Sec. 5.3), and the analytical-computational and analytical-computational-experimental methods of the lifetime prediction (see Sec. 5.4).

In addition to experimental methods [30]–[32], crack formation is also investigated analytically and/or computationally [33]–[38]. This investigation is usually applied to an existing crack in a model system. A shape of such existing crack is required to be mathematically defined, e.g. a penny-shaped crack. Strictly speaking, this mathematically defined crack exists in a model system before the loading of the model system. Such analytical and/or computational determination is based on e.g. the finite and boundary element methods, the Green’s functions,  $J$ -integrals, semi-smooth Newton methods, singular integral equations which result from the Lekhnitskii’s complex variable formulation, weight functions, mean-field theory, Mori-Tanaka’s homogenization, Stroh formalism [35]–[38].

As presented in Sec. 5.1, the crack formation in the multi-particle-matrix system includes crack initiation which is followed by crack propagation. With regard to the crack initiation investigated in

this doctoral dissertation, *no* mathematically defined crack is present in this model system *before* the thermal-stress loading. As mentioned above, this is in contrast to the crack formation investigation in [33]–[38] which is based on a concept of a crack existing in a model system before loading of the model system. The crack formation analysis in Sec. 5.1 is based on the comparison of energy which is accumulated in the cubic cell with energy for the creation of a new surface (i.e. a surface of the crack). This comparison is also used e.g. in [39]–[41]. The crack formation analysis considers a curve integral of energy density along a curve in the cubic cell (see Eqs. (50), (51)).

The condition (see Eq. (47)) which defines a limit state with respect to the crack initiation in the cracking plane  $x_i x_j$  ( $i, j = 1, 2, 3; i \neq j$ ; see Fig. 4c) in the spherical particle or cell matrix is determined. The limit state is thus defined by the critical particle radius  $R_{1cq}^{(ij)}$  related to the crack initiation in the spherical particle ( $q = p$ ) or in the cell matrix ( $q = m$ ). With regard to the crack propagation at  $R_1 > R_{1cq}^{(ij)}$ , the condition for the determination of a position of the crack tip in  $x_i x_j$  (see Fig. 4a) in components of the multi-particle-matrix system is determined (see Eq. (48)). Formulae which define the crack shape in the plane  $x_{ij} x_k$  ( $i, j, k = 1, 2, 3; i \neq j \neq k$ ; see Fig. 4c) which is perpendicular to the cracking plane  $x_i x_j$  in components of the multi-particle-matrix system are also determined (see Eqs. (44)–(46)). These crack propagation results are valid for ceramic components which are characterized by a high-speed crack propagation. In contrast to the crack propagation results, the determination of the limit state is applicable disregarding a 'character' of components of the multi-particle-matrix system (ceramic=brittle, elastic, elastoplastic components). Additionally, the crack formation analysis (see Method 2, p. 24) explains paradoxical behaviour of the cracking which is experimentally observed in a real two-component material [39]–[41].

The energy barrier represents a surface integral of the thermal-stress induced elastic energy density  $w$  over a surface in the cubic cell (see Eq. (54)). In addition to experimental methods [42]–[44], strengthening of the multi-component materials is also investigated analytically and/or computationally. Such analytical and/or computational determination is based on e.g. the finite element methods, Orowan and modified Oldroyd models, a simulation of dislocation dynamics [45]–[50]. As presented in Sec. 5.3, the micro- and macro-strengthening (see Eq. (58)), which is defined - within this doctoral dissertation - as thermal-stress resistance against mechanical loading, is also based on a surface integral of the thermal-stress induced elastic energy density  $w_i$  ( $i = 1, 2, 3$ ) over a surface in the cubic cell (see Eq. (56)). In this case,  $w_i$  represents such elastic energy density which is induced by the thermal stress  $\sigma_i$  which act along the axis  $x_i$  (see Fig. 2). The macro-strengthening represents a mean value of the micro-strengthening in the cubic cell. The energy barrier along with micro- and macro-strengthening are determined for both model systems. This brochure presents the determination of this barrier and strengthening for the multi-particle-matrix system only.

The analytical modelling of the lifetime prediction methods is based on a transformation of the 'resistive' effect of the thermal stresses to the 'contributory' effect with respect to mechanical loading. This transformation results in the analytical determination of critical microstructural parameters (a radius of grains; thickness of an envelope which is segregated on a surface of the grains). The lifetime prediction methods also consider computational results which are obtained by a computational simulation of the microstructural parameters during a time-temperature-dependent development of microstructure (analytical-computational method), and also consider experimental results (analytical-computational-experimental method).

Finally, the analytical models of the crack formation, of the energy barrier and of the micro- and macro-strengthening along with the methods of lifetime prediction exhibit a general validity. These analytical models and these lifetime prediction methods are valid for the thermal-stress induced elastic energy density as well as for energy density which is induced by any stresses acting in the model systems (see Fig. 1). In case of the lifetime prediction methods, conditions which are required with respect to this general validity are presented (see page 29). Due to a range of this brochure, The detailed analysis concerning this general validity along with illustrative examples of applications of the analytical models of these phenomena to real engineering materials (superconductive and structural ceramics, a creep-resistant steel) are presented in the doctoral dissertation.

# 1 Types of multi-component materials. Model systems and cell model

**1.1 Types of multi-component materials.** The analytical models of the thermal stresses and the related phenomena (see Chaps. 3–5) are applicable to real multi-component materials which consist of two or three components. The following two types of the two-component materials with finite dimensions consist of

1. precipitates and grains, where the precipitates are distributed in the grains,
2. two types of grains. Crystal lattices of grains of these two types are mutually different.

The following two types of the three-component materials with finite dimensions consist of

3. precipitates, grains and a continuous component on a surface of each of the precipitates, where the precipitates are distributed in the grains,
4. grains with a continuous component on their surface and grains without the continuous component on their surface. Crystal lattices of grains of these two types (i.e. with and without the continuous component) are mutually identical or mutually different.

**1.2 Model systems and cell model.** With regard to analytical modelling of the thermal stresses, the two- and three-component materials with finite dimensions, defined in Sec. 1.1, are replaced by multi-particle-matrix and multi-particle-envelope-matrix systems with infinite dimensions (see Fig. 1), respectively. These **model systems** consist of periodically distributed spherical particles without (see Fig. 1a) and with (see Fig. 1b) a spherical envelope on a surface of each of the spherical particle surfaces. These model systems are characterized by the inter-particle distance  $d$ , the particle radius  $R_1$ , the envelope radii  $R_1, R_2$ , where  $R_1 < R_2$ .

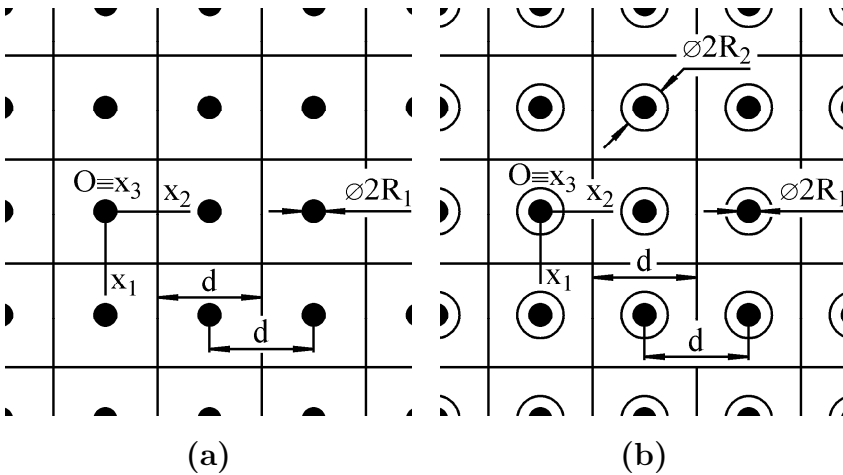


Figure 1: (a) The multi-particle-matrix system and (b) multi-particle-envelope-matrix system as model systems which are applicable to the two- and three-component materials defined in Sec. 1.1, respectively. The imaginary cubic cells with the Cartesian system ( $Ox_1x_2x_3$ ) in the cell centre and with a central spherical particle (with the radius  $R_1$ ) without or with the spherical envelope (with the radii  $R_1, R_2$ ) on the particle surface. The cubic cell dimension  $d$  along the axes  $x_1, x_2, x_3$  is identical to inter-particle distance.

To derive the thermal stresses acting in these model systems, the infinite matrix is **imaginarily** divided into identical cubic cells with the dimension  $d$  along each of the axes  $x_1, x_2, x_3$  of the Cartesian system ( $Ox_1x_2x_3$ ). Each cubic cells contains a central spherical particle without or with the spherical envelope. The beginning  $O$  of the Cartesian system is identical with the particle centre as well as with the centre of the cubic cell. The thermal stresses are thus investigated within the cubic cell, i.e. in the spherical particle, spherical envelope and cell matrix. The cubic cell represents a part of the infinite matrix, and this part is related to one spherical particle. Due to infinity of the matrix, formulae for the thermal stresses which are determined for a certain cubic cell are also valid for any cubic cell of the infinite matrix.

The model systems shown in Fig. 1 are depicted in the plane  $x_1x_2$ . Due to the matrix infinity regarding each of the axes  $x_1, x_2, x_3$ , the same figure is also considered for the planes  $x_1x_3$  and  $x_2x_3$ . As analysed in Sec. 3.3, the surface of the cubic cell represents a set of points for which one of the mandatory boundary conditions (see Eq. (34)) as well as the additional boundary conditions (see Eqs. (36), (37)) for the cell matrix are determined.

Let the model systems have a finite matrix. The analytical modelling of the thermal stresses in such model systems is required to consider a shape and dimensions of the finite matrix as well as a position of each cell in the finite matrix. Boundary conditions related to the surface of the cubic cell are then required to be separately determined for each cell. On the one hand, let the boundary conditions for the surface of the cubic cell in the model systems with a finite matrix be defined. However, an application of such analytical model to real two- and three-component materials results in numerical dependences of the thermal stresses and of the related phenomena (see Chaps. 3–5) on characteristics of the model systems (see Sec. 1.3). On the other hand, such application would be probably time-consuming. Additionally, as presented in [28], the case when an infinite matrix is considered within analytical modelling of phenomena in real multi-component materials with finite dimensions is of particular interest for the mathematical simplicity of analytical solutions. As presented in [28], such analytical solutions are assumed to exhibit sufficient accuracy due to the size of material components (e.g. precipitates, envelopes) which is relatively small in comparison with the size of macroscopic material samples, macroscopic structural elements, etc.

**1.3 Characteristics of the model systems**, i.e.  $R_1, R_2, d$ , the thickness  $t = R_2 - R_1 > 0$  of the spherical envelope and the particle volume fraction  $v \in (0, v_{max})$ , represent microstructural characteristics of the real two- and three-component materials. In case of the multi-particle-matrix and multi-particle-envelope-matrix systems, we get  $v_{max} = \pi/6$  and  $v_{max} = (\pi/6) \times [1 - t/(R_1 + t)]^3$ , respectively. These characteristics are related to the temperature  $T \in \langle T_f, T_r \rangle$ , where  $T_f$  is final temperature of a cooling process, and the relaxation temperature  $T_r$  is analysed in Sec. 2.5. In case of the numerical determination of the thermal stresses in a real two- or three-component material, the temperature dependences  $R_1 = R_1(T), t = t(T), d = d(T)$  are required to be determined for the temperature interval  $T \in \langle T_f, T_r \rangle$  by a suitable experimental-computational method.

**1.4 Multi-component materials versus model systems.** Relationship between components of the multi-component materials defined in Items 1–4, Sec. 1.1 and components of the model systems defined (see Fig. 1) are as follows.

Two-component materials. The precipitates and grains of the two-component material defined in Item 1, Sec. 1.1 correspond to the spherical particles and infinite matrix of the multi-particle-matrix system, respectively.

Let the grains  $A$  and  $B$  of the two-component material defined in Item 2, Sec. 1.1 be characterized by the volume fractions  $v_A$  and  $v_B = 1 - v_A$ , respectively. If  $v_A > v_{max} = \pi/6$  (see Sec. 1.3), then the grains  $A$  are considered to represent the infinite matrix of the multi-particle-matrix system. If  $v_B > v_{max} = \pi/6$ , then the grains  $B$  are considered to represent the infinite matrix of the multi-particle-matrix system.

Let  $v_A < v_{max}$  and  $v_B < v_{max}$  be valid. Let  $W_{cAB} = W_{pA} + W_{mB}$  (see Sec. 2.4) represent thermal-stress induced elastic energy of the cubic cell of such multi-particle-matrix system when the grains  $A$  and  $B$  are considered to represent the spherical particle and cell matrix within the analytical modelling of the thermal stresses, respectively.

Let  $W_{cBA} = W_{pB} + W_{mA}$  (see Sec. 2.4) represent thermal-stress induced elastic energy of the cubic cell of such multi-particle-matrix system when the grains  $B$  and  $A$  are considered to represent the spherical particle and cell matrix, respectively.

If  $W_{cAB} < W_{cBA}$ , then the grains  $A$  and  $B$  of this real two-component material are considered to represent the spherical particle and cell matrix, respectively. If  $W_{cAB} > W_{cBA}$ , then the grains  $B$  and  $A$  of this real two-component material are considered to represent the spherical particle and cell matrix, respectively.

Three-component materials. The precipitates, continuous component and grains of the three-component material defined in Item 3, Sec. 1.1 correspond to the spherical particles, spherical envelope and infinite matrix of the multi-particle-envelope-matrix system, respectively.

With regard to Item 4, Sec. 1.1, the continuous component, the grains with the continuous component and the grains without the continuous component of the correspond to the spherical envelope, spherical particle and infinite matrix of the multi-particle-envelope-matrix system, respectively.

## 2 Selected topics on solid continuum mechanics

**2.1 Coordinate system and intervals of coordinates.** Thermal stresses are investigated at the arbitrary point  $P$  of a solid continuum along the axes  $x'_1, x'_2, x'_3$  of the Cartesian system ( $Px'_1x'_2x'_3$ ) (see Fig. 2). A position of the arbitrary point  $P$  regarding the Cartesian system ( $Ox_1x_2x_3$ ) is determined by the spherical coordinates  $(r, \varphi, \nu)$ , where  $O$  is a centre of the spherical particle (see Fig. 1). The spherical coordinates  $(r, \varphi, \nu)$  and the infinitesimal spherical cap<sup>1</sup> in Fig. 2 are considered due to the spherical shape of the particles and envelopes of the model systems (see Fig. 1).

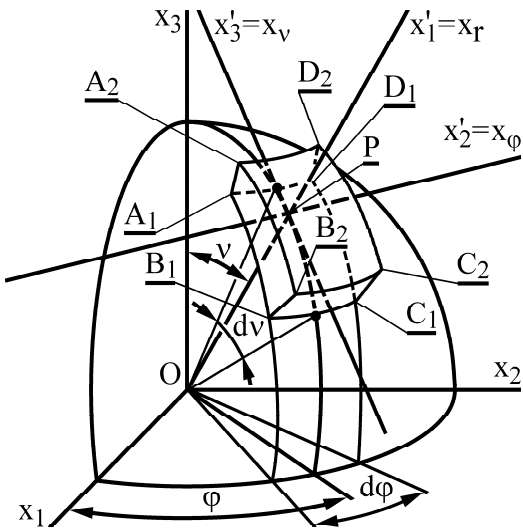


Figure 2: The arbitrary point  $P$  with a position determined by the spherical coordinates  $(r, \varphi, \nu)$  regarding the Cartesian system ( $Ox_1x_2x_3$ ), where  $O$  is a centre of the spherical particle (see Fig. 1), and  $r = |OP|$ . The axes  $x'_1 = x_r$  and  $x'_2 = x_\varphi$ ,  $x'_3 = x_\nu$  thus represent radial and tangential directions, respectively, where  $x_\varphi \parallel x_1x_2$ . The infinitesimal spherical cap at the point  $P$  with the surfaces  $S_r = A_1B_1C_1D_1$  and  $S_{r+dr} = A_2B_2C_2D_2$  at the radii  $r = |OP|$  and  $r + dr$ , respectively. The axis  $x'_1$  represents a normal of  $S_r$  and  $S_{r+dr}$ . Dimensions of the infinitesimal spherical cap are as follows:  $|A_1A_2| = |B_1B_2| = |C_1C_2| = |D_1D_2| = dr$ ,  $|A_1D_1| = |B_1C_1| = r \times d\varphi$ ,  $|A_1B_1| = |C_1D_1| = r \times d\nu$ ,  $|A_2D_2| = |B_2C_2| = (r + dr) \times d\varphi$ ,  $|A_2B_2| = |C_2D_2| = (r + dr) \times d\nu$ .

The thermal stresses are sufficient to be investigated within one eighth of the cubic cell, i.e. for  $\varphi \in \langle 0, \pi/2 \rangle$  and  $\nu \in \langle 0, \pi/2 \rangle$ . This is a consequence of symmetry of the model systems. This symmetry results from the matrix infinity and from the periodical distribution of the spherical particles and spherical envelopes. The intervals  $\varphi \in \langle 0, \pi/2 \rangle$  and  $\nu \in \langle 0, \pi/2 \rangle$  are also considered due to a homogeneous temperature change during the cooling process. The homogeneous temperature change which is considered in this doctoral dissertation is then characterized by the condition  $\partial T/\partial r = \partial T/\partial \varphi = \partial T/\partial \nu = 0$ , where  $T$  is temperature. The interval  $r \in \langle 0, R_1 \rangle$  is related to the spherical particle of the model systems (see Fig. 1). The interval  $r \in \langle R_1, R_2 \rangle$  is related to the spherical envelope of the multi-particle-envelope-matrix system. The intervals  $r \in \langle R_1, r_c \rangle$  and  $r \in \langle R_2, r_c \rangle$  are related to the cell matrix of the multi-particle-matrix and multi-particle-envelope-matrix systems, respectively. The integral boundary  $r_c$  represents a distance along a radial direction (i.e. along the axis  $x'_1 = x_r$ ) from the point  $O$  to a point on a surface of the cubic cell, where  $r_c$  is derived as

$$r_c = \frac{R_1 \times \sqrt{1 + c_\varphi^2}}{2(\sin \nu' + c_\varphi \cos \nu')} \left( \frac{4\pi}{3\nu'} \right)^{1/3} \quad \text{for } \nu' \in \langle 0, \nu^* \rangle; \quad \nu' = \nu^* - \nu,$$

$$r_c = \frac{R_1}{2c_\varphi \sin \nu} \left( \frac{4\pi}{3\nu} \right)^{1/3} \quad \text{for } \nu \in \left\langle \nu^*, \frac{\pi}{2} \right\rangle,$$

$$\nu^* = \arctan \left( \frac{1}{c_\varphi} \right); \quad c_\varphi = \cos \varphi \quad \text{for } \varphi \in \left\langle 0, \frac{\pi}{4} \right\rangle; \quad c_\varphi = \sin \varphi \quad \text{for } \varphi \in \left\langle \frac{\pi}{4}, \frac{\pi}{2} \right\rangle. \quad (1)$$

<sup>1</sup>With regard to  $x'_1 = x_r$ ,  $x'_2 = x_\varphi$ ,  $x'_3 = x_\nu$  (see Fig. 2), the conventional subscripts  $r, \varphi, \nu$  in a connection with the spherical coordinates  $(r, \varphi, \nu)$  are replaced by the subscripts 1, 2, 3, respectively, due to the mathematical techniques in Sec. 3.1 (see e.g. Eqs. (16), (39)).

**2.2 Displacement of the infinitesimal spherical cap. Thermal-stress induced radial displacement.** Let the multi-particle-matrix system be considered (see Fig. 1a). The thermal stresses in this model system originate as a consequence of the condition  $\beta_p \neq \beta_m$ . A detailed analysis of the coefficient  $\beta_q$  (see Eqs. (9)–(12)) is presented in Sec. 2.5, where the subscript  $q = p$  and  $q = m$  is related to the spherical particle and cell matrix, respectively. The thermal stresses originate at the temperature  $T \in \langle T_f, T_r \rangle$ , where  $T_f$  is final temperature of a cooling process, and the relaxation temperature  $T_r$  is analysed in Sec. 2.5. As presented in Sec. 2.1, this cooling process is characterized by a homogeneous temperature change. The homogeneous temperature change which is considered in this doctoral dissertation is then characterized by the condition  $\partial T / \partial r = \partial T / \partial \varphi = \partial T / \partial \nu = 0$ .

If  $T \in \langle T_f, T_r \rangle$  and  $\beta_m - \beta_p > 0$ , then the cell matrix is pushed by the spherical particle, and the spherical particle is pushed by the cell matrix. If  $T \in \langle T_f, T_r \rangle$  and  $\beta_m - \beta_p < 0$ , then the cell matrix is pulled by the spherical particle, and the spherical particle is pulled by the cell matrix.

An analysis of the pulling or pushing, i.e. an analysis of displacement of the infinitesimal spherical cap, is as follows. As presented in Sec. 2.1, the multi-particle-matrix system is symmetric. Due to this symmetry, the pulling or pushing of an arbitrary point at the particle-matrix boundary is realized along a normal to this surface (i.e. to the particle-matrix boundary) at this arbitrary point.

Let  $P$  (see Fig. 2) be such arbitrary point at the particle-matrix boundary, thus for  $r = R_1$ . The point  $P$  as well as the infinitesimal spherical cap at the point  $P$  thus exhibit a displacement along a normal to the surfaces  $S_r$  and  $S_{r+dr}$  of the spherical the infinitesimal spherical cap (see Fig. 2). The normal to the surfaces  $S_r, S_{r+dr}$  is represented by the axis  $x'_1$  which defines the radial direction regarding the Cartesian system ( $Ox_1x_2x_3$ ) (see Fig. 2). The infinitesimal spherical cap in the point  $P$  at the particle-matrix boundary exhibits a displacement along the axis  $x'_1$ , i.e. a radial displacement.

The condition  $\beta_p \neq \beta_m$  is a reason of the radial stress  $p_1$  acting at the particle-matrix boundary along the axis  $x'_1$ . A condition for the determination of  $p_1 = p_1(\varphi, \nu)$  is derived in Sec. 2.6 (see Eq. (13)). The radial stress  $p_1$  is a reason of the fact that this analysis concerning the radial displacement of the infinitesimal spherical cap in the point  $P$  at the particle-matrix boundary (i.e. for  $r = R_1$ ) is also valid for each point of the axis  $x'_1$  (i.e. for  $r \in \langle 0, r_c \rangle$ ).

The same is also valid for the multi-particle-envelope-matrix system. In this case,  $p_1$  and  $p_2$  acting at the particle-envelope and matrix-envelope boundaries are a consequence of the conditions  $\beta_p \neq \beta_e$  and  $\beta_e \neq \beta_m$ , where  $\beta_e$  is a thermal expansion coefficient of the spherical envelope (see Eqs. (9)–(12)). The radial stresses  $p_1 = p_1(\varphi, \nu)$  and  $p_2 = p_2(\varphi, \nu)$  are determined by Eqs. (14) and (15), respectively,

The infinitesimal spherical cap (see Fig. 2) in the arbitrary point  $P$  (see Fig. 2) with a position described by the spherical coordinates  $(r, \varphi, \nu)$  exhibits the **radial displacement**  $u'_1 = u_r$  only, along the axis  $x'_1$  (see Fig. 2).

Additionally, the following analysis concerning the radial displacement  $u'_1 = u_r$  is required to be considered. This analysis is based on a concept of imaginary separation which is also considered within mathematical procedures which are used for the determination of the Eshelby's model [51].

Let the multi-particle-matrix system be considered. Let the spherical particles and infinite matrix be imaginarily separated, and then spherical hollows are periodically distributed in the infinite matrix.

Let  $T \in \langle T_f, T_r \rangle$  represent temperature of the separated spherical particles and of the infinite matrix with the spherical hollows. If the temperature  $T$  increases or decreases within the interval  $\langle T_f, T_r \rangle$ , then the components which are imaginarily separated expand or contract, respectively. The expansion and contraction result in displacements of points in the components. Due to the imaginary separation, these displacements result from the temperature change, and not from the difference  $\beta_m - \beta_p \neq 0$  (see Eqs. (9)–(12)).

Let the spherical particles be embedded in the infinite matrix. Let  $\Delta T = T - T_r \neq 0$  represent the temperature change. Let the condition  $\beta_p = \beta_m$  be considered. Due to  $\beta_p = \beta_m$ , the thermal stresses do not originate in the multi-particle-matrix system, and the infinitesimal spherical cap is thus shifted due to the temperature change.

Let  $R_{1p} = R_{1p}(T)$  and  $R_{1m} = R_{1m}(T)$  represent temperature-dependent functions of radii of

these separated spherical particle and the spherical hollows, respectively. Due to  $T < T_r$ , we get  $R_{1q}(T) < R_{1q}(T_r)$  ( $q=p,m$ ), where  $R_{1q}(T_r) = R_{1T_r}$ . The same, i.e.  $d(T) < d(T_r)$ , is also valid for the temperature-dependent function  $d = d(T)$  of the inter-particle distance  $d$ .

Due to  $\beta_q = \beta_q(\varphi, \nu)$  (see Eqs. (9)–(12)), we get  $R_{1q} = R_{1q}(\varphi, \nu, T)$ . Consequently,  $R_{1p} = R_{1p}(\varphi, \nu, T)$  is a distance from the particle centre to a point on a surface of the separated particle along the axis  $x'_1$  which represents the radial direction defined by the angles  $\varphi, \nu$ . Similarly,  $R_{1m} = R_{1m}(\varphi, \nu, T)$  is a distance along  $x'_1$  from a centre of the hollow to a point on a surface of the hollow.

If  $\beta_p < \beta_m$ , then we get  $R_{1p}(\varphi, \nu, T) > R_{1m}(\varphi, \nu, T)$ . Let the distance  $R_{1p}$  be changed to  $R_1$  for each value of the variables  $\varphi, \nu \in \langle 0, \pi/2 \rangle$ , where  $R_1 < R_{1p}$ . The change  $R_{1p}(\varphi, \nu, T) \rightarrow R_1$  is caused by the radial stress  $p_1 = p_1(\varphi, \nu, T)$  which acts, along the axis  $x'_1$ , on a surface of the separated particle. Due to  $\beta_p < \beta_m$ , the radial stress  $p_1$  is compressive regarding the surface of the separated particle. Additionally,  $[u'_{1p}(\varphi, \nu, T)]_{r=R_{1p}} = R_1 - R_{1p}$  represents a **thermal-stress induced radial displacement** on a surface of the separated particle (i.e. for  $r = R_{1p}$ ) at a point defined by the coordinates  $\varphi, \nu \in \langle 0, \pi/2 \rangle$ . The radial displacement  $(u'_{1p})_{r=R_{1p}}$  along the axis  $x'_1 = x_r$  (see Fig. 2) is induced by the radial stress  $p_1$ .

The separated particle can be put into the hollow provided that the distance  $R_{1m}$  is also changed to  $R_1$  for each value of the variables  $\varphi, \nu \in \langle 0, \pi/2 \rangle$ , where  $R_1 > R_{1m}$ . The change  $R_{1m}(\varphi, \nu, T) \rightarrow R_1(\varphi, \nu, T)$  is also caused by the radial stress  $p_1 = p_1(\varphi, \nu, T)$  which acts on a surface of the hollow in the matrix. Due to  $\beta_p < \beta_m$ , the radial stress  $p_1$  is also compressive regarding the surface of the hollow. Additionally,  $[u'_{1m}(\varphi, \nu, T)]_{r=R_{1m}} = R_1 - R_{1m}$  represents a **thermal-stress induced radial displacement** on a surface of the hollow (i.e. for  $r = R_{1m}$ ) at a point defined by the coordinates  $\varphi, \nu \in \langle 0, \pi/2 \rangle$ . The radial displacement  $(u'_{1m})_{r=R_{1m}}$  along the axis  $x'_1 = x_r$  (see Fig. 2) is also induced by the radial stress  $p_1$ .

After the embedding of the separated particle with the radius  $R_{1p}$  in the hollow with the radius  $R_{1m}$ , a surface of the particle with the radius  $R_1$  is pushed by a surface of the matrix, where  $R_{1p} > R_1 > R_{1m}$ . Similarly, a surface of the matrix is pushed by a surface of the particle. The same is also valid in case of the pulling for  $\beta_p > \beta_m$ . This analysis of the pushing or pulling which considers a concept of the imaginarily separated components is also valid for the multi-particle-envelope-matrix system.

### 2.3 Fundamental equations of solid continuum mechanics.

Cauchy's equations. The Cauchy's equations which represent geometric equations define relationships between displacements and strains of an infinitesimal part of a solid continuum. In case of the infinitesimal spherical cap at the arbitrary point  $P$  (see Fig. 2), the relationships between the radial displacement  $u'_1 = u_r$  along the axis  $x'_1 = x_r$  and the radial strain  $\varepsilon'_{11} = \varepsilon_r$  along  $x'_1 = x_r$ , the tangential strain  $\varepsilon'_{22} = \varepsilon_\varphi$  along  $x'_2 = x_\varphi$ , the tangential strain  $\varepsilon'_{33} = \varepsilon_\nu$  along  $x'_3 = x_\nu$ , the shear strains  $\varepsilon'_{12} = \sigma_{r\varphi}$ ,  $\varepsilon'_{13} = \sigma_{r\nu}$  are derived as

$$\varepsilon'_{11} = \frac{\partial u'_1}{\partial r}, \quad \varepsilon'_{22} = \varepsilon'_{33} = \frac{u'_1}{r}, \quad \varepsilon'_{12} = \frac{1}{r} \frac{\partial u'_1}{\partial \varphi}, \quad \varepsilon'_{13} = \frac{1}{r} \frac{\partial u'_1}{\partial \nu}. \quad (2)$$

With regard to the analysis in Sec. 2.2, we get the shear strain  $\varepsilon'_{23} = \varepsilon'_{\varphi\nu} \propto [(\partial u'_2/\partial \nu) + (\partial u'_3/\partial \varphi)] = 0$  due to  $u'_2 = u_\varphi = 0$ ,  $u'_3 = u_\nu = 0$ , where  $u'_2 = u_\varphi$  and  $u'_3 = u_\nu$  represent displacements of the infinitesimal spherical cap along  $x'_2$  and  $x'_3$ , respectively, i.e. along tangential directions.

Compatibility equations. Solid continuum mechanics considers such principle that a system which is continuous before deformation is required to exhibit this continuity after deformation as well, i.e. strains are required to be mutually compatible [52,53]. The compatibility equations for the infinitesimal spherical cap at the arbitrary point  $P$  (see Fig. 2) have the forms

$$\varepsilon'_{11} - \varepsilon'_{22} - r \frac{\partial \varepsilon'_{22}}{\partial r} = 0, \quad \frac{\partial \varepsilon'_{11}}{\partial \varphi} - \varepsilon'_{12} - r \frac{\partial \varepsilon'_{12}}{\partial r} = 0, \quad \frac{\partial \varepsilon'_{11}}{\partial \nu} - \varepsilon'_{13} - r \frac{\partial \varepsilon'_{13}}{\partial r} = 0, \quad \frac{\partial \varepsilon'_{22}}{\partial \varphi} - \varepsilon'_{12} = 0, \quad \frac{\partial \varepsilon'_{22}}{\partial \nu} - \varepsilon'_{13} = 0. \quad (3)$$

Equilibrium equations. Solid continuum mechanics also considers a principle of the equilibrium of forces which act within a solid continuum, strictly speaking, within on sides an infinitesimal part of the solid continuum. In case of the infinitesimal spherical cap, the equilibrium equations of the forces which act (along  $x'_1, x'_2, x'_3$ ) on sides of the infinitesimal spherical cap at the arbitrary point  $P$  (see Fig. 2) are derived as

$$2\sigma'_{11} - \sigma'_{22} - \sigma'_{33} + r \frac{\partial \sigma'_{11}}{\partial r} + \frac{\partial \sigma'_{12}}{\partial \varphi} + \frac{\partial \sigma'_{13}}{\partial \nu} = 0, \quad \frac{\partial \sigma'_{22}}{\partial \varphi} + 3\sigma'_{12} + r \frac{\partial \sigma'_{12}}{\partial r} = 0, \quad \frac{\partial \sigma'_{33}}{\partial \nu} + 3\sigma'_{13} + r \frac{\partial \sigma'_{13}}{\partial r} = 0. \quad (4)$$

As analysed in Sec. 2.2, the infinitesimal spherical cap exhibits the thermal-stress induced radial displacement  $u'_1$  along the axis  $x'_1$ . This radial displacement is caused by the radial stress  $p_1$  acting at the particle-matrix and particle-envelope boundary as well as by the radial stress  $p_2$  acting at the matrix-envelope boundary. Due to these radial stresses and radial displacement, we get  $\sigma'_{23} = \sigma_{\varphi\nu} = 0$ , where  $\sigma'_{23}$  is a shear stress which is determined in the Cartesian system  $(Px'_1x'_2x'_3)$  (see Fig. 2).

Hooke's law. With regard to  $\sigma'_{23} = 0$ , the Hooke's law for an **anisotropic** continuum is derived as [54]

$$\begin{aligned} \varepsilon'_{11} &= s'_{11}\sigma'_{11} + s'_{12}\sigma'_{22} + s'_{13}\sigma'_{33} + s'_{15}\sigma'_{13} + s'_{16}\sigma'_{12}, & \varepsilon'_{22} &= s'_{12}\sigma'_{11} + s'_{22}\sigma'_{22} + s'_{23}\sigma'_{33} + s'_{25}\sigma'_{13} + s'_{26}\sigma'_{12}, \\ \varepsilon'_{33} &= s'_{13}\sigma'_{11} + s'_{23}\sigma'_{22} + s'_{33}\sigma'_{33} + s'_{35}\sigma'_{13} + s'_{36}\sigma'_{12}, & \varepsilon'_{23} &= s'_{14}\sigma'_{11} + s'_{24}\sigma'_{22} + s'_{34}\sigma'_{33} + s'_{45}\sigma'_{13} + s'_{46}\sigma'_{12}, \\ \varepsilon'_{13} &= s'_{15}\sigma'_{11} + s'_{25}\sigma'_{22} + s'_{35}\sigma'_{33} + s'_{55}\sigma'_{13} + s'_{56}\sigma'_{12}, & \varepsilon'_{12} &= s'_{16}\sigma'_{11} + s'_{26}\sigma'_{22} + s'_{36}\sigma'_{33} + s'_{56}\sigma'_{13} + s'_{66}\sigma'_{12}. \end{aligned} \quad (5)$$

The elastic modulus  $s'_{ijkl}$  ( $\equiv s'_{11}, s'_{12}, \dots, s'_{56}, s'_{66}$ ) ( $i, j, k, l = 1, 2, 3$ ) in  $(Ox'_1x'_2x'_3)$  which is determined by  $s_{11}, s_{12}, \dots, s_{56}, s_{66}$  in  $(Ox_1x_2x_3)$  (see Fig. 2), the coefficient  $a_{vw} = \cos[\angle(x'_v, x_w)]$  ( $v, w = 1, 2, 3$ ), and transformations of subscripts are derived as [54]

$$\begin{aligned} s'_{ijkl} &= \sum_{r,s,t,u=1}^3 a_{ir} a_{js} a_{kt} a_{lu} s_{rstu} \quad i, j, k, l = 1, 2, 3; \\ a_{11} &= \cos \varphi \sin \nu, \quad a_{12} = \sin \varphi \sin \nu, \quad a_{13} = \cos \nu, \quad a_{21} = -\sin \varphi, \quad a_{22} = -\cos \varphi, \quad a_{23} = 0, \\ a_{31} &= -\cos \varphi \cos \nu, \quad a_{32} = -\sin \varphi \cos \nu, \quad a_{33} = -\sin \nu; \\ ij &\equiv ji; \quad i = j \rightarrow ij \equiv i; \quad i \neq j \rightarrow ij = 12 \equiv 6, \quad ij = 13 \equiv 5, \quad ij = 23 \equiv 4. \end{aligned} \quad (6)$$

In case of an **isotropic** continuum, we get [52,53,55]

$$\begin{aligned} \varepsilon'_{11} &= s_{11}\sigma'_{11} + s_{12}(\sigma'_{22} + \sigma'_{33}), \quad \varepsilon'_{22} = s_{12}(\sigma'_{11} + \sigma'_{33}) + s_{11}\sigma'_{22}, \quad \varepsilon'_{33} = s_{12}(\sigma'_{11} + \sigma'_{22}) + s_{11}\sigma'_{33}, \\ \varepsilon'_{13} &= s_{44}\sigma'_{13}, \quad \varepsilon'_{12} = s_{44}\sigma'_{12}; \quad s_{11} = \frac{1}{E}, \quad s_{12} = -\frac{\mu}{E}, \quad s_{44} = \frac{2(1+\mu)}{E}, \end{aligned} \quad (7)$$

where  $E$  and  $\mu$  are the Young's modulus and Poisson's ratio, respectively. As presented in [54], we get  $\mu = 0.25$ . In case of real materials, we get  $\mu < 0.5$  [56]. The elastic moduli  $s'_{11}, s'_{12}, \dots, s'_{56}, s'_{66}$ ;  $s_{11}, s_{12}, \dots, s_{56}, s_{66}$ ; the Young' modulus  $E$  and the Poisson's ratio  $\mu$  are related to the spherical particle ( $q = p$ ), spherical envelope ( $q = e$ ) and the cell matrix ( $q = m$ ). The transformations  $s'_{ij} \rightarrow s'_{ijq}$ ,  $s_{ij} \rightarrow s_{ijq}$ ,  $E \rightarrow E_q$ ,  $\mu \rightarrow \mu_q$  ( $i, j = 1, \dots, 6$ ;  $q = p, e, m$ ) are then required to be considered.

**2.4 Elastic energy.** The elastic energy density  $w_q$  accumulated at the arbitrary point in the spherical particle ( $q = p$ ), spherical envelope ( $q = e$ ) and cell matrix ( $q = m$ ), along with the elastic energy  $W_q$  accumulated in the volume  $V_q$  of these components have the forms [29,52]

$$w_q = \frac{1}{2} \left( \sum_{i=1}^3 \sigma'_{iiq} \varepsilon'_{iiq} + \sum_{i,j=1; i \neq j}^3 \sigma'_{ijq} \varepsilon'_{ijq} \right), \quad W_q = \int_{V_q} w_q dV_q = 8 \int_0^{\pi/2} \int_0^{\pi/2} \int_{r_1}^{r_2} w_q r^2 dr d\varphi d\nu, \quad q = p, e, m, \quad (8)$$

where  $dV_q = r^2 dr d\varphi d\nu$  is volume of the infinitesimal spherical cap for the angles  $\varphi, \nu \in \langle 0, \pi/2 \rangle$ . The integration boundaries  $r_1, r_2$  are as follows:  $r_1 = 0, r_2 = R_1$  for the spherical particle;  $r_1 = R_1, r_2 = R_2$  for the spherical envelope;  $r_1 = R_1, r_2 = r_c$  for the cell matrix of the multi-particle-matrix

system;  $r_1 = R_2$ ,  $r_2 = r_c$  for the cell matrix of the multi-particle-envelope-matrix system; where  $R_1$ ,  $R_2$  and  $r_c = r_c(R_1, v)$  are related to the temperature  $T \in \langle T_f, T_r \rangle$ .

Elastic energy of the multi-particle-matrix and multi-particle-envelope-matrix systems is represented by the elastic energy  $W_c = W_p + W_m$  and  $W_c = W_p + W_e + W_m$  of the cubic cell, respectively.

As analysed in Secs. 3.2, 4.2, a thermal stress-strain state in the model systems (see Fig. 1) is determined by mutually different solutions which result in mutually different values of  $W_c$ . Due to these different values, such solution is considered to exhibit minimal value of  $W_c$ . Strictly speaking, a principle of minimum total potential energy (i.e. the tendency of an elastic solid body to exhibit minimum total potential energy) [29] is required to be considered.

As presented in [29], the total potential energy  $W_t = W_d - (W_v + W_s)$  consists of the deformation energy  $W_d$ , and of the energy  $W_v$  and  $W_s$  which is induced by the volume and surface forces,  $\vec{F}_v$  and  $\vec{F}_s$ , respectively. In case of the model systems (see Fig. 1), we get  $\vec{F}_v = \vec{F}_s = 0$ , and then  $W_v = W_s = 0$ ,  $W_t = W_d$ . The deformation energy  $W_d$  of the model systems is then identical with  $W_c$ . Finally, in case of the model systems, the principle of minimum total potential energy is thus 'transformed' to a principle of minimum value of  $W_c$  due to  $W_t = W_d = W_c$ .

**2.5 Reason of thermal stresses.** In case of the multi-particle-matrix system, the thermal stresses are a consequence of the condition  $\alpha_p \neq \alpha_m$  as well as a consequence of a phase transformation which originates at the temperature  $T_{tq}$  ( $q = p, m$ ) at least in one component of this system. The thermal expansion coefficient  $\alpha_q$  ( $q = p, e, m$ ) along the axis  $x'_1 = x_r$  (see Fig. 2) is given by Eq. (12). The phase-transformation temperature  $T_{tq}$  is from the interval  $\langle T_f, T_r \rangle$ , where  $T_f$  is a final temperature of a cooling process, and  $T_r$  is a relaxation temperature of this model system. The phase transformation at  $T_{tq} \in \langle T_f, T_r \rangle$  induces the radial strain  $\varepsilon'_{11tq} = \varepsilon'_{11tq}(\varphi, \nu)$  along the axis  $x'_1$ . This phase-transformation radial strain is a consequence of a difference in dimensions of mutually transforming crystal lattices.

In case of the multi-particle-envelope-matrix system, the thermal stresses originate as a consequence of one of these conditions  $\alpha_p \neq \alpha_e = \alpha_m$ ,  $\alpha_p \neq \alpha_e \neq \alpha_m$   $\alpha_p = \alpha_e \neq \alpha_m$  as well as a consequence of  $\varepsilon'_{11tq} = \varepsilon'_{11tq}(\varphi, \nu)$  ( $q = p, e, m$ ) which is induced at  $T_{tq} \in \langle T_f, T_r \rangle$  ( $q = p, e, m$ ) at least in one component of this model system. The relaxation temperature  $T_r$  of the model systems is analysed below. The coefficient  $\beta_q$  which includes  $\alpha_q$  and  $\varepsilon'_{11tq}$  is determined below (see Eqs. (9)–(12)). The determination of  $\varepsilon'_{11tq} = \varepsilon'_{11tq}(\varphi, \nu)$  ( $q = p, e, m$ ) for anisotropic and isotropic crystal lattices is not presented due to a range of this brochure. This determination is presented in the doctoral dissertation.

Relaxation temperature. The thermal stresses originate during a cooling process. Additionally, the thermal stresses originate at the temperature  $T \in \langle T_f, T_r \rangle$ . As defined in [56], the relaxation temperature  $T_r$  is such temperature below that the stress relaxation as a consequence of thermal-activated processes does not occur in a material. The relaxation temperature is defined approximately by the relationship  $T_r = (0.35 - 0.4) \times T_m$  [56] and exactly by an experiment, where  $T_m$  is melting temperature of the model systems (see Sec. 1.2).

The analysis of  $T_m$  for the multi-particle-matrix system is as follows. If the particles precipitate from a liquid matrix, then  $T_m$  represents a minimum of the set  $\{T_{mp}, T_{mm}\}$ , where  $T_{mp}$  and  $T_{mm}$  are melting temperatures of the particles and the matrix, respectively. If the particles precipitate from a solid matrix, then  $T_m$  represents a melting temperature of the multi-particle-matrix system.

The analysis of  $T_m$  for the multi-particle-envelope-matrix system is as follows. If the particles and envelopes precipitate from a liquid matrix, then  $T_m$  represents a minimum of the set  $\{T_{mp}, T_{me}, T_{mm}\}$ , where  $T_{ep}$  is a melting temperature of the envelope. If the particles and envelopes precipitate from a solid matrix, then  $T_m$  represents a melting temperature of the multi-particle-envelope-matrix system.

Let the multi-particle-matrix system be considered. If  $\alpha_p = \alpha_m$ , then the thermal stresses originate at the temperature  $T_t$  which represents maximal temperature of the set  $\{T_{tp}, T_{tm}\}$ .  $T_{tp}$  and  $T_{tm}$  thus represent temperature of a phase transformation in the spherical particle and cell matrix, where  $T_{tq} \in \langle T_f, T_r \rangle$  ( $q = p, m$ ).

The same is also valid for multi-particle-envelope-matrix system. In this case (i.e. on the condition

$\alpha_p = \alpha_e = \alpha_m$ ),  $T_t$  represents maximal temperature of the set  $\{T_{tp}, T_{te}, T_{tm}\}$ , where  $T_{te} \in \langle T_f, T_r \rangle$  is temperature of a phase transformation in the spherical envelope.

Coefficients  $\beta_p, \beta_e, \beta_m$ . As mentioned in Sec. 2.2, a mutual interaction of components of the model systems is realized along the radial direction, i.e. along the axis  $x'_1 = x_r$  (see Fig. 2). Accordingly, the coefficient  $\beta_q$  ( $q = p, e, m$ ) is also related to  $x'_1$ .

Let the phase transformation originate at the temperature  $T_{tq} \in \langle T_f, T_r \rangle$  in the component which is related to the subscript  $q = p, e, m$ . Consequently, the coefficient  $\beta_q = \beta_q(T)$  at the temperature  $T \in \langle T_f, T_{tq} \rangle \subset \langle T_f, T_r \rangle$  has the form

$$\beta_q = \varepsilon'_{11tq} + \int_T^{T_{tq}} \alpha_{Iq} dT + \int_{T_{tq}}^{T_r} \alpha_{IIq} dT, \quad T_{tq} \in \langle T_f, T_r \rangle, \quad T \in \langle T_f, T_{tq} \rangle \subset \langle T_f, T_r \rangle, \quad (9)$$

where  $\alpha_{Iq} = \alpha_{Iq}(T)$  and  $\alpha_{IIq} = \alpha_{IIq}(T)$  (see Eq. (12)) represent a thermal expansion coefficient of the component at the temperature  $T \leq T_{tq}$  and  $T \geq T_{tq}$ , respectively. If  $T > T_{tq}$ , then the coefficient  $\beta_q = \beta_q(T)$  at the temperature  $T \in (T_{tq}, T_r) \subset \langle T_f, T_r \rangle$  has the form

$$\beta_q = \int_T^{T_r} \alpha_{IIq} dT, \quad T_{tq} \in \langle T_f, T_r \rangle, \quad T \in (T_{tq}, T_r) \subset \langle T_f, T_r \rangle. \quad (10)$$

Let the phase transformation do not originate at the temperature  $T_{tq} \in \langle T_f, T_r \rangle$ , i.e.  $T_{tq} \notin \langle T_f, T_r \rangle$ . The coefficient  $\beta_q = \beta_q(T)$  at the temperature  $T \in \langle T_f, T_r \rangle$  has the form

$$\beta_q = \int_T^{T_r} \alpha_q dT, \quad T_{tq} \notin \langle T_f, T_r \rangle, \quad T \in \langle T_f, T_r \rangle, \quad (11)$$

where  $\alpha_q = \alpha_q(T)$  (see Eq. (12)) is a thermal expansion coefficient on the condition  $T_{tq} \notin \langle T_f, T_r \rangle$ .

The thermal stresses are then a consequence of the condition  $\beta_{q1} \neq \beta_{q2}$ . In case of the multi-particle-matrix and multi-particle-envelope-matrix systems, we get  $q_1, q_2 = p, m$  and  $q_1, q_2 = p, e, m$ , respectively, where  $q_1 \neq q_2$ .

Let  $\alpha_{iq}$  represent a thermal expansion coefficient along the axis  $x_i$  ( $i = 1, 2, 3$ ) of the Cartesian system ( $Ox_1x_2x_3$ ) (see Fig. 2). The component for which one of these conditions  $\alpha_{1q} \neq \alpha_{2q} = \alpha_{3q}$  or  $\alpha_{1q} \neq \alpha_{2q} \neq \alpha_{3q}$  or  $\alpha_{1q} = \alpha_{2q} \neq \alpha_{3q}$  is valid is anisotropic. In case of an **anisotropic component** of the model systems (see Sec. 1.2), the thermal expansion coefficient  $\alpha_q$  along the axis  $x'_1$  is then derived as [57]

$$\alpha_q = a_{11}^2 \alpha_{1q} + a_{12}^2 \alpha_{2q} + a_{13}^2 \alpha_{3q}, \quad (12)$$

where the coefficient  $a_{ij} = \cos[\angle(x'_i, x_j)]$  ( $i = 1; i, j = 1, 2, 3$ ) is given by Eq. (6). In case of an **isotropic component**, we get  $\alpha_q = \alpha_{1q} = \alpha_{2q} = \alpha_{3q}$ . Due to the term  $\alpha_{Iq}$  in Eq. (9), the terms  $\alpha_{1q}, \alpha_{2q}, \alpha_{3q}$  in Eq. (12) are replaced by  $\alpha_{1Iq}, \alpha_{2Iq}, \alpha_{3Iq}$ , respectively. Consequently, in case of  $\alpha_{IIq}$ , the terms  $\alpha_{1q}, \alpha_{2q}, \alpha_{3q}$  in Eq. (12) are replaced by  $\alpha_{1IIq}, \alpha_{2IIq}, \alpha_{3IIq}$ , respectively.

**2.6 Formulae for determination of the radial stresses  $p_1, p_2$ .** In case of the multi-particle-matrix system (see Fig. 1a), the formula

$$(1 - \beta_m) (\varepsilon'_{22m})_{r=R_{1m}} - (1 - \beta_p) (\varepsilon'_{22p})_{r=R_{1p}} = \beta_m - \beta_p, \quad (13)$$

is considered for the determination of the radial stress  $p_1 = p_1(\varphi, \nu)$  acting at the particle-matrix boundary (i.e. for  $r = R_1$ ) along the axis  $x'_1$  (see Fig. 2). In case of multi-particle-envelope-matrix system (see Fig. 1b), and on the condition  $\beta_p \neq \beta_e$ , the formula

$$(1 - \beta_e) (\varepsilon'_{22e})_{r=R_{1e}} - (1 - \beta_p) (\varepsilon'_{22p})_{r=R_{1p}} = \beta_e - \beta_p \quad (14)$$

is considered for the determination of the radial stress  $p_1 = p_1(\varphi, \nu)$  which acts at the particle-envelope boundary. In case of  $\beta_m \neq \beta_e$ , the formula

$$(1 - \beta_m) (\varepsilon'_{22m})_{r=R_{2m}} - (1 - \beta_e) (\varepsilon'_{22e})_{r=R_{2e}} = \beta_m - \beta_e \quad (15)$$

is considered for the determination of the radial stress  $p_2 = p_2(\varphi, \nu)$  which acts at the matrix-envelope boundary.

### 3 Thermal stresses in the model systems with anisotropic components

**3.1 Radial, tangential and shear stresses.** Applying suitable mathematical procedures to the Cauchy's, compatibility and equilibrium equations as well as to the Hooke's law for an anisotropic continuum (see Sec. 2.3), we get

$$\begin{aligned} \sigma'_{11} &= \sum_{i=1}^n C_i r^{\lambda_i}, \quad \sigma'_{2+j2+j} = (\delta_{1j} - \delta_{0j}) \left( c_{135+j} \sigma'_{11} + c_{137+j} r \frac{\partial \sigma'_{11}}{\partial r} + c_{139+j} r^2 \frac{\partial^2 \sigma'_{11}}{\partial r^2} \right), \\ \sigma'_{12+j} &= c_{153+j} \sigma'_{11} + c_{155+j} r \frac{\partial \sigma'_{11}}{\partial r} + c_{157+j} r^2 \frac{\partial^2 \sigma'_{11}}{\partial r^2}, \quad j = 0, 1, \end{aligned} \quad (16)$$

where  $n$  is a number of boundary conditions,  $C_i$  is an integration constant which is determined by the boundary conditions, the exponent  $\lambda_i$  is required to represent a real number, and  $\delta_{0i}, \delta_{1i}$  ( $i = 0, 1$ ) are the Kronecker's symbols. The exponents  $\lambda_1, \dots, \lambda_n$  represent real roots of one of the following characteristics equations

$$c_{203+3i} \lambda^2 + (c_{202+3i} - c_{203+3i}) \lambda + c_{201+3i} = 0, \quad i = 0 - 5, \quad (17)$$

$$c_{540+4i} \lambda^3 + (c_{539+4i} - 3c_{540+4i}) \lambda^2 + (c_{538+4i} - c_{539+4i} + 2c_{540+4i}) \lambda + c_{537+4i} = 0, \quad i = 0 - 29, \quad (18)$$

The determination of Eqs. (16)–(18) is not presented due to a range of this thesis. This determination along with the coefficient  $c_i = c_i(\varphi, \nu)$  ( $i = 1, \dots, 656$ ) is presented in detail in the doctoral dissertation. Additionally, the doctoral dissertation also presents the determination of characteristics equations of an order of  $\lambda^4$  and  $\lambda^5$ . Similarly, due to a range of this brochure, the analyses in Secs. 3.1, 3.2 which are applied to these characteristics equations of an order of  $\lambda^4$  and  $\lambda^5$  are also presented in the doctoral dissertation.

Due to  $i = 0 - 5$ , the equation (17) represents six characteristic equations with the variable  $\lambda = \lambda(\varphi, \nu)$  and with the parameters  $\varphi, \nu$ . The parameters  $\varphi, \nu$  are included in  $s'_{11}, s'_{12}, \dots, s'_{56}, s'_{66}$  which are functions of  $a_{ij} = \cos[\angle(x'_i, x'_j)]$  ( $i, j = 1, 2, 3$ ) (see Eq. (6)). The elastic moduli  $s'_{11}, s'_{12}, \dots, s'_{56}, s'_{66}$  are included in the coefficients  $c_i, \dots, c_{15+i}$  which are then included in the coefficients  $c_{18+i}, \dots, c_{7766+6j}$  ( $i = 1 - 3; j = 0 - 63$ ).

The exponents  $\lambda_1^{(17)(i)} = \lambda_1^{(17)(i)}(\varphi, \nu)$ ,  $\lambda_2^{(17)(i)} = \lambda_2^{(17)(i)}(\varphi, \nu)$  which represent roots of the  $i$ -th characteristic equation ( $i = 0 - 5$ ) are derived as

$$\lambda_j^{(17)(i)} = \frac{1}{2c_{203+3i}} \left[ c_{203+3i} - c_{202+3i} + (\delta_{1j} - \delta_{2j}) \sqrt{(c_{203+3i} - c_{202+3i})^2 - 4c_{201+3i}c_{203+3i}} \right], \quad j = 1, 2. \quad (19)$$

Due to  $i = 0 - 5$ , the formula (19) represents six sets with the exponents  $\lambda_1^{(17)(i)}, \lambda_2^{(17)(i)}$  ( $i = 0 - 5$ ), i.e.  $\{\lambda_1^{(17)(0)}, \lambda_2^{(17)(0)}\}, \dots, \{\lambda_1^{(17)(5)}, \lambda_2^{(17)(5)}\}$ . If both exponents of each of the sets are imaginary, or none of these six sets consists of such real exponents which fulfil boundary conditions (see Sec. 3.3) for a component of the model systems (see Sec. 1.2), then the characteristic equation (18) is considered.

Due to  $i = 0 - 29$ , the equation (18) represents thirty characteristic equations with three roots in these thirty sets  $\{\lambda_1^{(18)(0)}, \lambda_2^{(18)(0)}, \lambda_3^{(18)(0)}\}, \dots, \{\lambda_1^{(18)(29)}, \lambda_2^{(18)(29)}, \lambda_3^{(18)(29)}\}$ . The exponents  $\lambda_1^{(18)(i)} = \lambda_1^{(18)(i)}(\varphi, \nu)$ ,  $\lambda_2^{(18)(i)} = \lambda_2^{(18)(i)}(\varphi, \nu)$ ,  $\lambda_3^{(18)(i)} = \lambda_3^{(18)(i)}(\varphi, \nu)$  represent roots of the  $i$ -th characteristic equation. The set  $\{\lambda_1^{(18)(i)}, \lambda_2^{(18)(i)}, \lambda_3^{(18)(i)}\}$  consists either of three real roots, or of one real and two imaginary roots. If none of these thirty sets consists of such real exponents which fulfil boundary conditions (see Sec. 3.3) for a component of the model systems (see Sec. 1.2), then a characteristic equation of an order of  $\lambda^4$  which is determined in the doctoral dissertation is considered.

Finally, these analyses concerning the characteristic equations (17), (18) are considered due to the determination of a sufficient number of the real exponent  $\lambda$  which is required to fulfill boundary conditions (see Sec. 3.3) for a component of the model systems (see Sec. 1.2).

Roots of the characteristic equation (18) are determined for a real component of the model systems (see Sec. 1.2) by a suitable numerical method. Strictly speaking, numerical values of the elastic moduli  $s_{11q}, s_{12q}, \dots, s_{56q}, s_{66q}$  (see Eq. (6)) are required to be substituted to the coefficients which are included in (18). Consequently, the suitable numerical method is required to be applied for the determination of these roots (the exponent  $\lambda \equiv \lambda_q$ ) of the characteristic equation (18). The subscripts  $q = p, q = p$  and  $q = p$  are related to the numerical values of  $s_{11q}, s_{12q}, \dots, s_{56q}, s_{66q}$  for the spherical particle, spherical envelope and cell matrix, respectively.

**3.2 Analysis of a number of solutions for the model systems.** Let  $n_q^{(17)(i)}$  represent a number of such real roots of the set  $\{\lambda_{1p}^{(17)(i)}, \lambda_{2p}^{(17)(i)}\}$  ( $i = 0, \dots, 5$ ) which fulfil the boundary conditions (see Sec. 3.3) for the spherical particle ( $q = p$ ), the spherical envelope ( $q = e$ ) and the cell matrix ( $q = m$ ). Let  $n_q$  be a number of the boundary conditions for the component of the model systems which is related to the subscript  $q = p, e, m$ , where  $n_q^{(17)(i)} \geq n_q$ . The set  $\{\lambda_{1q}^{(17)(i)}, \lambda_{2q}^{(17)(i)}\}$  ( $i = 0, \dots, 5$ ) (see Eq. (19)) represents the  $i$ -th set of these six sets  $\{\lambda_1^{(17)(0)}, \lambda_2^{(17)(0)}\}, \dots, \{\lambda_1^{(17)(5)}, \lambda_2^{(17)(5)}\}$  which are related to the characteristic equation (17). Let  $s_q^{(17)(i)}$  represent a number of solutions for the thermal stresses in the component of the model systems which is related to the subscript  $q = p, e, m$ . The number  $s_q^{(17)(i)}$  is related to the set  $\{\lambda_{1q}^{(17)(i)}, \lambda_{2q}^{(17)(i)}\}$ , and then we get

$$s_q^{(17)(i)} = \binom{n_q^{(17)(i)}}{n_q} = \frac{n_q^{(17)(i)}!}{n_q! (n_q^{(17)(i)} - n_q)!}. \quad (20)$$

The number  $s^{(17)}$  of solutions which determine a stress-strain state induced by the thermal stresses in the multi-particle-matrix system is derived as

$$s^{(17)} = \left( \sum_i s_p^{(17)(i)} \right) \times \left( \sum_i s_m^{(17)(i)} \right), \quad (21)$$

where  $s^{(17)}$  are related to the characteristic equation (17). In case of the multi-particle-envelope-matrix system, we get

$$s^{(17)} = \left( \sum_i s_p^{(17)(i)} \right) \times \left( \sum_i s_e^{(17)(i)} \right) \times \left( \sum_i s_m^{(17)(i)} \right). \quad (22)$$

The superscript  $i \in \{0, \dots, 5\}$  concerning the sum  $\sum_i$  in Eqs. (21), (22) is related to such  $n_q^{(17)(i)}$  for which the condition  $n_q^{(17)(i)} \geq n_q$  is valid ( $q = p, e, m$ ). The same analysis is valid for  $s^{(18)}$ , which includes  $s_q^{(18)(j)}$  for  $j = 0, \dots, 29$ . The parameter  $s_q^{(18)(j)}$  is related to  $\{\lambda_1^{(18)(j)}, \lambda_2^{(18)(j)}, \lambda_3^{(18)(j)}\}$  which represents the  $j$ -th set of these thirty sets  $\{\lambda_1^{(18)(0)}, \lambda_2^{(18)(0)}, \lambda_3^{(18)(0)}\}, \dots, \{\lambda_1^{(18)(29)}, \lambda_2^{(18)(29)}, \lambda_3^{(18)(29)}\}$ .

As an example, let the characteristic equations (17), (18) be considered for the determination of a stress-strain state in the model systems (see Sec. 1.2). In case of the multi-particle-matrix system, we get

$$s^{(17)(18)} = \left( \sum_j s_p^{(17)(i)} + \sum_l s_p^{(18)(i)} \right) \times \left( \sum_j s_m^{(17)(i)} + \sum_l s_m^{(18)(i)} \right). \quad (23)$$

In case of the multi-particle-envelope-matrix system, we get

$$s^{(17)(18)} = \left( \sum_j s_p^{(17)(i)} + \sum_l s_p^{(18)(i)} \right) \times \left( \sum_j s_e^{(17)(i)} + \sum_l s_e^{(18)(i)} \right) \times \left( \sum_j s_m^{(17)(i)} + \sum_l s_m^{(18)(i)} \right). \quad (24)$$

The superscripts  $j \in \{0, \dots, 5\}$  and  $l \in \{0, \dots, 29\}$  concerning the sums  $\sum_j, \sum_l$  in Eqs. (23), (24) are related to such  $n_q^{(17)(j)}$  and  $n_q^{(18)(l)}$  for which the conditions  $n_q^{(17)(j)} \geq n_q$  and  $n_q^{(18)(l)} \geq n_q$  are valid ( $q = p, e, m$ ), respectively.

### 3.3 Boundary conditions.

**Spherical particle.** The thermal stresses  $\sigma'_{iip}, \sigma'_{12+jp}$  ( $i = 1, 2, 3; j = 0, 1$ ) in the Cartesian system  $(Px'_1x'_2x'_3)$  (see Fig. 2), and the thermal-stress induced radial displacement  $u'_{1p}$  along the axis  $x'_1$  are required to fulfil these boundary conditions

$$(u'_{1p})_{r=0} = 0, \quad (25)$$

$$(\sigma'_{iip})_{r \rightarrow 0} \nrightarrow \pm\infty, \quad i = 1, 2, 3, \quad (26)$$

$$(\sigma'_{12+ip})_{r \rightarrow 0} \nrightarrow \pm\infty, \quad i = 0, 1, \quad (27)$$

$$(\sigma'_{11p})_{r=R_1} = -p_1. \quad (28)$$

Equations (25) and (26)–(28) represent geometric and stress boundary conditions, respectively. The boundary conditions (25)–(28) are considered for the multi-particle-matrix system on the condition  $\beta_p \neq \beta_m$ . The boundary conditions (25)–(28) are also considered for the multi-particle-envelope-matrix systems on the conditions  $\beta_p \neq \beta_e = \beta_m$ ,  $\beta_p \neq \beta_e \neq \beta_m$  (see Eqs. (9)–(12)). If  $\beta_p = \beta_e \neq \beta_m$ , then the boundary condition (28) is replaced by

$$(\varepsilon'_{22p})_{r=R_1} = (\varepsilon'_{22e})_{r=R_1} = \frac{(u'_{1e})_{r=R_1}}{R_1} = -p_2 \varrho_{1e}^{pe}, \quad (29)$$

In this case, i.e.  $\beta_p = \beta_e \neq \beta_m$ , the integration constant  $C_{1p}$  includes  $\varrho_{1e}^{pe}$ . The coefficient  $\varrho_{1e}^{pe}$  can be thus determined after the determination of the integration constant  $C_{1e}$ . As mentioned above, the integration constant  $C_{1e}$  for  $\beta_p = \beta_e \neq \beta_m$  is determined by the boundary condition (31). The determination of  $C_{1p}$  for  $\beta_p = \beta_e \neq \beta_m$  is then preceded by the determination of  $C_{1e}$  for  $\beta_p = \beta_e \neq \beta_m$ .

Equations (25)–(28) result in one integration constant only, and then we get  $n_p = 1$ , where  $n_p$  is a number of boundary conditions which are required for the spherical particle. The integration constant  $C_{1p} \neq 0$  is then determined by Eq. (28).

On each of these conditions,  $\beta_p \neq \beta_m$ ,  $\beta_p \neq \beta_e = \beta_m$ ,  $\beta_p \neq \beta_e \neq \beta_m$ ,  $\beta_p = \beta_e \neq \beta_m$ , the absolute value  $|u'_{1p}|$  is required to represent an increasing function of  $r \in \langle 0, R_1 \rangle$ . This increasing dependence  $|u'_{1p}| - r$  exhibits a maximal value at the particle-matrix or particle-envelope boundary, thus for  $r = R_1$ . Due to  $|u'_{1p}| \propto r^{\lambda_{1p}}$ , the condition  $\lambda_{1p} > 0$  is required to be fulfilled.

**Spherical envelope.** If  $\beta_p \neq \beta_e \neq \beta_m$  (see Eqs. (9)–(12)), then the following boundary conditions

$$(\sigma'_{11e})_{r=R_1} = -p_1, \quad (30)$$

$$(\sigma'_{11e})_{r=R_2} = -p_2, \quad (31)$$

are considered for the determination of the integration constants  $C_{1e} \neq 0$  and  $C_{2e} \neq 0$ , and then  $n_e = 2$ , where  $n_e$  is a number of boundary conditions for the spherical envelope. In case of  $\beta_p \neq \beta_e \neq \beta_m$ , the real exponents  $\lambda_{1e}$  and  $\lambda_{2e}$  are not required to be defined by additional conditions, in contrast to the condition  $\lambda_{1p} > 0$  for the spherical particle.

If  $\beta_p \neq \beta_e = \beta_m$ , then the boundary condition (30) is considered for the determination of the integration constant  $C_{1e} \neq 0$ , and then we get  $n_e = 1$ . In this case, i.e.  $\beta_p \neq \beta_e = \beta_m$ , the absolute value  $|u'_{1e}|$  is required to represent a decreasing function of the variable  $r \in \langle R_1, R_2 \rangle$  or, at the very most, a constant function of  $r \in \langle R_1, R_2 \rangle$ . This decreasing dependence  $|u'_{1e}| - r$  exhibits a maximal value at the particle-envelope boundary, thus for  $r = R_1$ . Due to  $|u'_{1e}| \propto r^{\lambda_{1e}+1}$ , the condition  $\lambda_{1e} \leq -1$  is required to be fulfilled.

If  $\beta_p = \beta_e \neq \beta_m$ , then the boundary condition (31) along with the condition  $n_e = 1$  are considered for the determination of the integration constant  $C_{1e} \neq 0$ . The absolute value  $|u'_{1e}|$  is required to represent an increasing function of  $r \in \langle R_1, R_2 \rangle$  or, at the very most, a constant function of

$r \in \langle R_1, R_2 \rangle$ . This increasing dependence  $|u'_{1e}| - r$  exhibits a maximal value at the matrix-envelope boundary, thus for  $r = R_2 = R_1 + t$ . Due to  $|u'_{1e}| \propto r^{\lambda_{1e}+1}$ , the condition  $\lambda_{1e} \geq -1$  is required to be fulfilled.

**Cell matrix.** The thermal stresses in the cell matrix are derived regarding the standard boundary conditions (32)–(34) which are mandatory. In addition to (32)–(34), the additional boundary conditions (36), (37) might be also considered. With regard to (36), the dependence  $u'_{1m} - r$  is required to be extremal on the cell surface, i.e. for  $r = r_c$ . With regard to (37), the dependence  $w_m - r$  is required to be extremal on the cell surface.

The mandatory boundary conditions for the multi-particle-matrix and multi-particle-envelope-matrix systems are as follows.

- In case of the multi-particle-matrix system, the conditions (32), (34) are considered.
- In case of the multi-particle-envelope-matrix system, the conditions (33), (34) are considered for  $\beta_p \neq \beta_e \neq \beta_m$  or  $\beta_p = \beta_e \neq \beta_m$  (see Eqs. (9)–(12)).
- In case of the multi-particle-envelope-matrix system, the conditions (34), (35) are considered for  $\beta_p \neq \beta_e = \beta_m$ .

Accordingly, the four following combinations of the mandatory and additional boundary conditions for the multi-particle-matrix and multi-particle-envelope-matrix systems are considered:

1. the mandatory boundary conditions (32), (34) or (33), (34).
2. the mandatory boundary conditions (32), (34) or (33), (34) along with the additional boundary condition (36).
3. the mandatory boundary conditions (32), (34) or (33), (34) along with the additional boundary condition (37).
4. the mandatory boundary conditions (32), (34) or (33), (34) along with the additional boundary conditions (36) and (37).

Mandatory boundary conditions. The thermal radial stress  $\sigma'_{11m}$  and the thermal-stress induced radial displacement  $u'_{1m}$  are required to fulfil these mandatory boundary conditions

$$(\sigma'_{11m})_{r=R_1} = -p_1, \quad (32)$$

$$(\sigma'_{11m})_{r=R_2} = -p_2, \quad (33)$$

$$(u'_{1m})_{r=r_c} = 0, \quad (34)$$

where the distance  $r_c$  is given by Eq. (1). Equations (32), (33) and (34), represent stress and geometric boundary conditions, respectively. The mandatory boundary conditions (32), (34) are considered for the multi-particle-matrix for  $\beta_p \neq \beta_m$ . The mandatory boundary conditions (33), (34) are also considered for the multi-particle-envelope-matrix system on the conditions  $\beta_p \neq \beta_e \neq \beta_m$  or  $\beta_p = \beta_e \neq \beta_m$ . If  $\beta_p \neq \beta_e = \beta_m$ , then the boundary condition (33) is replaced by

$$(\varepsilon'_{22m})_{r=R_2} = (\varepsilon'_{22e})_{r=R_2} = \frac{(u'_{1e})_{r=R_2}}{R_2} = -p_1 \varrho_{2e}^{me}, \quad (35)$$

In this case, i.e.  $\beta_p \neq \beta_e = \beta_m$ , the integration constants  $C_{1m}$ ,  $C_{2m}$  both include  $\varrho_{2e}^{me}$ . The coefficient  $\varrho_{2e}^{me}$  can be thus determined after the determination of the integration constant  $C_{1e}$ . As mentioned above, the integration constant  $C_{1e}$  for  $\beta_p \neq \beta_e = \beta_m$  is determined by the boundary condition (30). The determination of  $C_{1m}$ ,  $C_{2m}$  for  $\beta_p \neq \beta_e = \beta_m$  is then preceded by the determination of  $C_{1e}$  for  $\beta_p \neq \beta_e = \beta_m$ .

Equations (32)–(35) result in two integration constants, and then we get  $n_m = 2$  where  $n_m$  is a number of boundary conditions which are required for the cell matrix.

In case of the multi-particle-matrix system, the absolute value  $|u'_{1m}|$  is required to represent a decreasing function of  $r \in \langle R_1, r_c \rangle$  due to  $(u'_{1m})_{r=r_c} = 0$  (see Eq. (34)). This decreasing dependence  $|u'_{1m}| - r$  exhibits a maximal value at the particle-matrix boundary, thus for  $r = R_1$ . The same is also valid for the multi-particle-envelope-matrix system on each of the conditions  $\beta_p \neq \beta_e = \beta_m$ ,

$\beta_p \neq \beta_e \neq \beta_m$ ,  $\beta_p = \beta_e \neq \beta_m$ , The decreasing course of the dependence  $|u'_{1m}| - r$  in the cell matrix of the multi-particle-matrix and multi-particle-envelope-matrix systems is ensured by integration constants.

The determination of  $(u'_{1m})_{r=r_c} = 0$  is based on a concept of the imaginary separation of components of the model systems (see Fig. 1). This concept which is also considered for the determination of the Eshelby's model [51] is described in detail in Sec. 2.2.

Let the multi-particle-matrix system be considered. Let the components of this system be imaginarily separated at the relaxation temperature  $T_r$ . In this case, the spherical particles in the infinite matrix are replaced by spherical hollows. Let  $R_1 = R_1(T)$  be a temperature dependence of a radius of these separated particles. Let  $R_{1m} = R_{1m}(T)$  be a temperature dependence of a radius of the spherical hollows. Let these separated components be cooled down from the relaxation temperature  $T_r$  to the temperature  $T$ , where  $T < T_r$ .

A radius of the separated particle is thus changed from  $R_1(T_r)$  to  $R_1(T)$ , where  $R_1(T) < R_1(T_r)$ .

A radius of the hollow is thus changed from  $R_{1m}(T_r)$  to  $R_{1m}(T)$ , where  $R_{1m}(T) < R_{1m}(T_r)$ . Additionally, the condition  $R_1(T_r) = R_{1m}(T_r)$  is valid.

A dimension of the cubic cell is thus changed from  $d(T_r)$  to  $d(T)$ , where  $d(T) < d(T_r)$ .

Let the condition  $\beta_p \leq \beta_m$  be considered. If  $\beta_p \leq \beta_m$ , then  $R_1(T) \geq R_{1m}(T)$  for  $T < T_r$ .

As analysed in Sec. 2.2, the infinitesimal spherical cap exhibits a displacement along the axis  $x'_1$  (see Fig. 2). This displacement along  $x'_1$  results from the symmetry of the multi-particle-matrix system. The axis  $x'_1$  of the Cartesian system  $(Px'_1x'_2x'_3)$  defines a radial direction regarding the Cartesian system  $(Ox_1x_2x_3)$  (see Fig. 2).

Let the separated particle with the radius  $R_1(T)$  be put into the spherical hollow with the radius  $R_{1m}(T)$  of the cubic cell with with the dimension  $d(T)$ . After the embedding of the separated particle in the hollow at the temperature  $T < T_r$ , a surface of the particle is pushed or pulled by a surface of the matrix due to  $R_1(T) > R_{1m}(T)$  or  $R_1(T) < R_{1m}(T)$ , respectively. Similarly, a surface of the matrix is pushed or pulled by a surface of the particle due to  $R_1(T) > R_{1m}(T)$  or  $R_1(T) < R_{1m}(T)$ , respectively. The pushing or pulling at  $T < T_r$  within the spherical particle and cell matrix is expressed by the thermal-stress induced radial displacements  $u'_{1p}$  and  $u'_{1m}$  along the axis  $x'_1$ , i.e. along a radial direction.

The same is also valid for the multi-particle-envelope-matrix system as well as for the thermal-stress induced radial displacement  $u'_{1e}$  in the spherical envelope.

The pushing or pulling, which is induced in the cubic cell *after* the embedding at  $T < T_r$ , is related to the cell dimension  $d(T)$  at the temperature  $T < T_r$ . This fact is required to be considered within the following analysis which concerns the determination of the mandatory boundary condition  $(u'_{1m})_{r=r_c} = 0$ .

An analysis of the mandatory boundary condition  $(u'_{1m})_{r=r_c} = 0$  is as follows.

Let  $C$  be an arbitrary point on the surface  $1234$  (see Fig. 3). The surface  $1234$  with the normal  $x_2$  represents a common surface of two neighbouring cubic cells  $A$  and  $B$  with the centres  $O_A$  and  $O_B$ , respectively. These neighbouring cubic cells with the dimension  $d(T)$  at the temperature  $T < T_r$  are cells of the multi-particle-matrix system or the multi-particle-envelope-matrix system.

A position of the arbitrary point  $C$  on the surface  $1234$  of the cell  $A$  is determined by the spherical coordinates  $(r_{cA}, \varphi_A, \nu_A)$  regarding the Cartesian system  $(O_Ax_{1A}x_{2A}x_{3A})$ , where  $r_{cA} = |\overline{O_A C}|$ . Let the axis  $x'_{1A}$  (see Figs. 2, 3) define a radial displacement in the cubic cell  $A$ . Let  $u'_{1mA} = u'_{1mA}(r, \varphi_A, \nu_A)$  represent the thermal-stress induced radial displacement along the axis  $x'_{1A}$  in the cell matrix of the cell  $A$ .

A position of the arbitrary point  $C$  on the surface  $1234$  of the cell  $B$  is determined by the spherical coordinates  $(r_{cB}, \varphi_B, \nu_B)$  regarding the Cartesian system  $(O_Bx_{1B}x_{2B}x_{3B})$ , where  $r_{cB} = |\overline{O_B C}|$ . Let the axis  $x'_{1B}$  (see Figs. 2, 3) define a radial displacement in the cubic cell  $B$ . Let  $u'_{1mB} = u'_{1mB}(r, \varphi_B, \nu_B)$  represent the thermal-stress induced radial displacement along the axis  $x'_{1B}$  in the cell matrix of the cell  $B$ .

The distances  $r_{cA} = r_{cA}(d, \varphi_A, \nu_A)$ ,  $r_{cB} = r_{cB}(d, \varphi_B, \nu_B)$  are given by Eq. (1).



this extreme for  $r = r_c$  represents the minimum, where the dependences  $|u'_{1m}| - r$  and  $w_m - r$  are decreasing. If  $u'_{1m} < 0$ , then this extreme for  $r = r_c$  represents the maximum.

With regard to Eq. (2), the additional boundary conditions for the cell matrix of the model systems (see Fig. 1) are derived as

$$(\varepsilon'_{11m})_{r=r_c} = \left( \frac{\partial u'_{1m}}{\partial r} \right)_{r=r_c} = 0, \quad (36)$$

$$\left( \frac{\partial w_m}{\partial r} \right)_{r=r_c} = 0. \quad (37)$$

## 4 Thermal stresses in the model systems with isotropic components

**4.1 Radial, tangential and shear stresses.** Applying suitable mathematical procedures to the Cauchy's, compatibility and equilibrium equations as well as to the Hooke's law for an isotropic continuum (see Sec. 2.3), we get

$$\begin{aligned} \sigma'_{11} &= (c_1 + c_2) \frac{\partial u'_1}{\partial r} - 2c_2 \frac{u'_1}{r}, & \sigma'_{22} &= \sigma'_{33} = -c_2 \frac{\partial u'_1}{\partial r} + c_1 \frac{u'_1}{r}, & \sigma'_{12} &= \frac{1}{s_{44}r} \frac{\partial u'_1}{\partial \varphi}, & \sigma'_{13} &= \frac{1}{s_{44}r} \frac{\partial u'_1}{\partial \nu}, \\ c_1 &= \frac{E}{(1 + \mu)(1 - 2\mu)}, & c_2 &= -\mu c_1, & c_3 &= -4(1 - \mu). \end{aligned} \quad (38)$$

The radial displacement  $u'_{1q} = u'_{1q}(r, \varphi, \nu)$  along the axis  $x'_1$  (see Fig. 2) in the spherical particle ( $q = p$ ), the spherical envelope ( $q = e$ ) and the cell matrix ( $q = m$ ) which is determined by four different mathematical procedures has the form

$$\begin{aligned} u'_{1q} &= \sum_{i=1}^2 C_{iq}^{(1)} \xi_{iq}^{(1)} u_{irq}^{(1)}, & u_{irq}^{(1)} &= r^{\lambda_{iq}}, & \xi_{iq}^{(1)} &= \frac{1}{3s_{44}(c_1 + c_2)} \left( \frac{1}{\lambda_{iq} + 2} - \frac{1}{\lambda_{iq} - 1} \right), \\ \lambda_{iq} &= \frac{1}{2} \left[ 1 + (\delta_{1i} - \delta_{2i}) \sqrt{D_q} \right], & D_q &= 1 + 16(1 - \mu_q)[1 + 4(1 - \mu_q)], & i &= 1, 2, \end{aligned} \quad (39)$$

$$\begin{aligned} u'_{1q} &= \sum_{i=1}^3 C_{iq}^{(2)} \xi_{iq}^{(2)} u_{irq}^{(2)}, & u_{1rq}^{(2)} &= r \left( \frac{1}{3} - \ln r \right), & u_{2rq}^{(2)} &= r^{c_{3q}}, & u_{3rq}^{(2)} &= 1, \\ \xi_{1q}^{(2)} &= \frac{1}{3s_{44q}(c_{1q} + c_{2q})}, & \xi_{2q}^{(2)} &= \xi_{1q}^{(2)} \left( \frac{1}{c_{3q} + 2} - \frac{1}{c_{3q} - 1} \right), & \xi_{3q}^{(2)} &= \frac{3\xi_{1q}^{(2)}}{2}, \end{aligned} \quad (40)$$

$$\begin{aligned} u'_{1q} &= \sum_{i=1}^3 C_{iq}^{(3)} \xi_{iq}^{(3)} u_{irq}^{(3)}, & u_{1rq}^{(3)} &= r \left( \frac{4}{3} - \ln r \right), & u_{2rq}^{(3)} &= r^{c_{3q}}, & u_{3rq}^{(3)} &= \frac{1}{2} + \ln r, \\ \xi_{1q}^{(3)} &= c_{3q} \xi_{1q}^{(2)}, & \xi_{2q}^{(3)} &= 3\xi_{1q}^{(3)} \left[ \frac{1}{2c_{3q}} - \frac{1}{3(c_{3q} - 1)} - \frac{1}{6(c_{3q} + 2)} \right], & \xi_{3q}^{(3)} &= \frac{3\xi_{1q}^{(3)}}{2}, \end{aligned} \quad (41)$$

$$u'_{1q} = \sum_{i=1}^3 C_{iq}^{(4)} u_{irq}^{(4)}, \quad u_{1rq}^{(4)} = r, \quad u_{2rq}^{(4)} = r^{c_{3q}}, \quad u_{3rq}^{(4)} = \frac{1}{r^2}, \quad (42)$$

where detailed analyses of the four mathematical procedures are presented in the doctoral dissertation. In case of an elastic solid continuum, we get  $\mu = 0.25$  [54]. In case of a real isotropic material, we get  $\mu < 0.5$  [56], and then  $c_{3q} < 0$ , we get  $D_q > 0$ , and the real exponents  $\lambda_{1q} > 3$ ,  $\lambda_{2q} < -2$ . Accordingly,  $u_{1rq}^{(1)} = u_{1rq}^{(1)}(r)$ ,  $u_{3rq}^{(3)} = u_{3rq}^{(3)}(r)$ ,  $u_{1rq}^{(4)} = u_{1rq}^{(4)}(r)$  and  $u_{2rq}^{(1)} = u_{2rq}^{(1)}(r)$ ,  $u_{2rq}^{(2)} = u_{2rq}^{(2)}(r)$ ,  $u_{2rq}^{(3)} = u_{2rq}^{(3)}(r)$ ,  $u_{2rq}^{(4)} = u_{2rq}^{(4)}(r)$ ,  $u_{3rq}^{(4)} = u_{3rq}^{(4)}(r)$  are increasing and decreasing functions of the variable  $r$ , respectively, and  $u_{3rq}^{(2)} \neq f(r)$  is a constant function.

The function  $u_{1rq}^{(2)} = u_{1rq}^{(2)}(r)$  increases or decreases on the condition  $\partial u_{1rq}^{(2)}/\partial r > 0$  or  $\partial u_{1rq}^{(2)}/\partial r < 0$ , respectively. The conditions  $\partial u_{1rq}^{(2)}/\partial r > 0$  and  $\partial u_{1rq}^{(2)}/\partial r < 0$  result in  $r < e^{-2/3} \approx 0.51342$  m and

$r > e^{-2/3} \approx 0.51342$  m, respectively, where  $e \approx 2.71828$  is the Euler's number [58]. In case of real two- and three-component materials, we get  $R_1 < 0.51342$  m,  $R_2 < 0.51342$  m,  $d < 0.51342$  m, and then  $r < 0.51342$  m. Finally, due to  $r < 0.51342$  m for real two- and three-component materials, the function  $u_{1rq}^{(2)} = u_{1rq}^{(2)}(r)$  represents an increasing function of the variable  $r$ . Similarly, the condition  $\partial u_{1rq}^{(3)}/\partial r \geq 0$  results in  $r \leq e^{1/3} \approx 1.39561$  m, and then  $u_{1rq}^{(3)} = u_{1rq}^{(3)}(r)$  represents an increasing function of the variable  $r$ .

**4.2 Analysis of a number of solutions for the model systems.** The analysis in Sec. 3.3 which concern a course of the dependence  $|u'_{1q}| - r$  is also valid for an isotropic component. The course of  $|u'_{1q}| - r$  results from courses of the functions  $u_{irq}^{(1)} = u_{irq}^{(1)}(r)$ ,  $u_{jrq}^{(2)} = u_{jrq}^{(2)}(r)$ ,  $u_{jrq}^{(3)} = u_{jrq}^{(3)}(r)$ ,  $u_{jrq}^{(4)} = u_{jrq}^{(4)}(r)$  ( $i=1,2$ ;  $j=1,2,3$ ;  $q=p,e,m$ ) (see Eqs. (39)–(42)). The analysis of courses of these functions regarding the boundary conditions which is presented in detail in the doctoral dissertation is as follows.

Let  $s_q^{iso}$  represent a number of solutions which are determined by the four mathematical procedures for the thermal stresses in the isotropic spherical particle ( $q=p$ ), the isotropic spherical envelope ( $q=e$ ) and the isotropic cell matrix ( $q=m$ ).

Spherical particle. If  $\beta_p \neq \beta_m$ ;  $\beta_p \neq \beta_e = \beta_m$  and  $\varepsilon'_{11te} \neq \varepsilon'_{11tp}$ ;  $\beta_p \neq \beta_e \neq \beta_m$ ;  $\beta_p = \beta_e \neq \beta_m$ ; then  $s_p^{iso} = 4$ . If  $\beta_p \neq \beta_e = \beta_m$  and  $\varepsilon'_{11te} = \varepsilon'_{11tp}$ , then  $s_p^{iso} = 1$ .

Spherical envelope. If  $\beta_p \neq \beta_e = \beta_m$  and  $\varepsilon'_{11te} \neq \varepsilon'_{11tp}$ , then  $s_e^{iso} = 4$ . If  $\beta_p \neq \beta_e = \beta_m$  and  $\varepsilon'_{11te} = \varepsilon'_{11tp}$ , then  $s_e^{iso} = 1$ . If  $\beta_p = \beta_e \neq \beta_m$ , then  $s_e^{iso} = 6$ . If  $\beta_p \neq \beta_e \neq \beta_m$ , then  $s_e^{iso} = 10$ .

Cell matrix. In case of the cell matrix, we get  $s_m^{iso} = 13$ , where the mandatory boundary conditions without or with the additional boundary condition (36) are considered. The additional boundary condition (37) is not considered due to the following analysis.

With regard to Eq. (8), the thermal-stress induced elastic energy density  $w_m = w_m(r, \varphi, \nu) > 0$  in the cell matrix includes the shear stresses  $\sigma'_{12m}$  and  $\sigma'_{13m}$  as well as the shear strains  $\varepsilon'_{12m}$  and  $\varepsilon'_{13m}$  which are functions of  $\partial u'_{1m}/\partial \varphi$  and  $\partial u'_{1m}/\partial \nu$  (see Eq. (2)), respectively. The terms  $\partial u'_{1m}/\partial \varphi$  and  $\partial u'_{1m}/\partial \nu$  are functions of the terms  $\partial C_{im}/\partial \varphi$  and  $\partial C_{im}/\partial \nu$  ( $i=1, \dots, n$ ), respectively.

On the one hand, the additional boundary condition (37) concerning a course of the dependence  $w_m - r$  on a surface of the cubic cell might be considered to be a reasonable assumption. Equation (37) thus includes the terms  $\partial C_{im}/\partial \varphi$ ,  $\partial C_{im}/\partial \nu$ , where  $C_{im} \equiv C_{im}^{(j)}$  ( $i=1, \dots, 3$ ;  $j=2,3,4$ ) (see Eqs. (40)–(42)). On the other hand, no conditions exist for the determination of  $\partial C_{im}/\partial \varphi$ ,  $\partial C_{im}/\partial \nu$ . Accordingly, if the model systems (see Fig. 1) consist of isotropic components, then the additional boundary condition (37) can not be considered in case of the cell matrix.

**4.3 Number of solutions for the model systems.** The stress-strain state which is induced by the thermal stresses in the multi-particle-matrix system with isotropic components (see Fig. 1a) is described by  $s = s_p^{iso} \times s_m^{iso} = 4 \times 13 = 52$  mathematical solutions which fulfil the boundary conditions (see Sec. 3.3). In case of the multi-particle-envelope-matrix system with isotropic components (see Fig. 1b) for  $\beta_p \neq \beta_e = \beta_m$ , we get  $s = 208$  and  $s = 13$  for  $\varepsilon'_{11e} \neq \varepsilon'_{11p}$  and  $\varepsilon'_{11e} = \varepsilon'_{11p}$ , respectively. If  $\beta_p \neq \beta_e \neq \beta_m$ , then we get  $s = 520$ . If  $\beta_p = \beta_e \neq \beta_m$ , then we get  $s = 312$ .

**4.4 Thermal stresses in the model systems with isotropic and anisotropic components.** The determination of an analytical model of the thermal stresses in such model system (see Fig. 1) which consists of anisotropic and isotropic components is as follows.

In case of an anisotropic component, formulae for the thermal stresses and strains as well as formulae for thermal-stress induced radial displacement, thermal-stress induced elastic energy density and elastic energy (see Sec. 2.4) are taken from Chap. 3. In case of an isotropic component, these formulae are taken from Chap. 4. These formulae for anisotropic and isotropic components includes the radial stresses  $p_1$ ,  $p_2$  which are determined by the formulae (13)–(15).

The formulae (13)–(15) include tangential strains in components of the model systems (see Fig. 1). In case of an anisotropic component, a formula for the tangential strain which is included in Eqs. (13)–

(15) is taken from Chap. 4. Similarly, in case of an isotropic component, a formula for the tangential strain which is included in Eqs. (13)–(15) is taken from Chap. 3.

Let  $s$  represent a number of solutions of the model system which consists of anisotropic and isotropic components. As an example, in case of the multi-particle-matrix system with anisotropic spherical particles and an isotropic matrix, we get  $s = s_p^{aniso} + s_m^{iso}$ . The numbers  $s_p^{aniso}$  and  $s_m^{iso}$  of solutions for the isotropic particle and cell matrix are taken from Chaps. 3 and 4, respectively. In case of the multi-particle-envelope-matrix system, a formula for  $s$  can be analogically determined.

Finally, if  $s > 1$ , then a principle of minimum total potential energy of an elastic solid body [29] is required to be considered (see Sec. 2.4).

## 5 Related phenomena

**5.1 Analytical model of crack formation.** The analytical modelling of crack formation<sup>2</sup> is based on the comparison of thermal-stress induced elastic energy in the cubic cell with energy for the creation of the surface of a crack. This comparison results from the analysis which is applied to a solid continuum of a general shape (see Fig. 4a)<sup>3</sup>.

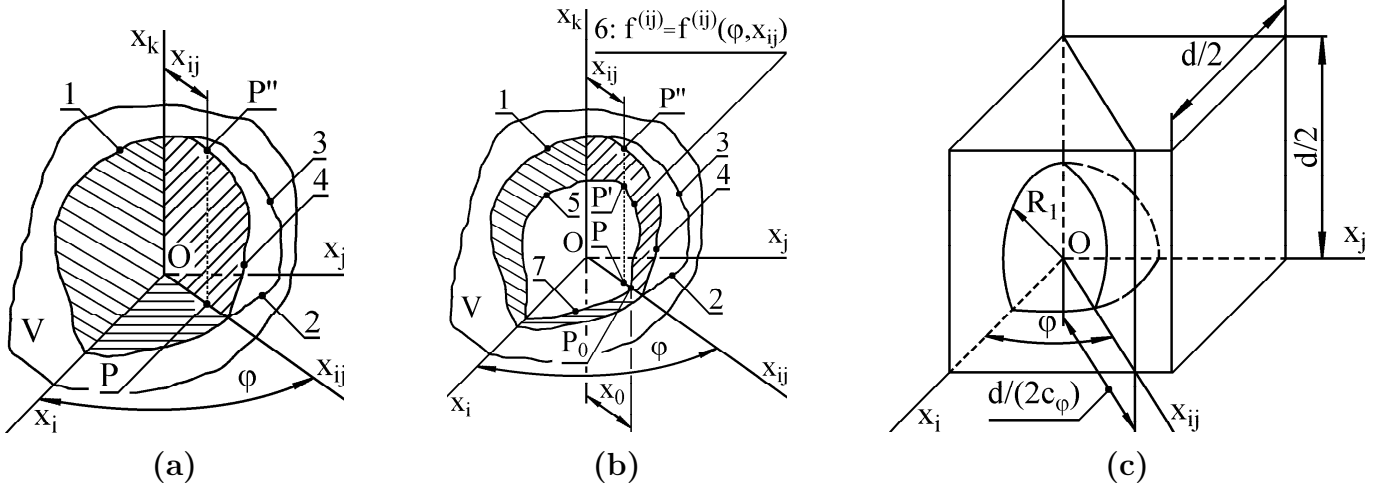


Figure 4: The solid continuum with a general shape with the volume  $V$  in the Cartesian system  $(Ox_i x_j x_k)$  ( $i, j, k = 1, 2, 3; i \neq j \neq k$ ); (a) without and (b) with a crack. The crack is formed in the plane  $x_i x_j$ . The shaded area represents cuts of the solid continuum in the planes  $x_i x_j$ ,  $x_i x_k$ ,  $x_j x_k$ , where  $x_{ij} \subset x_i x_j$ ,  $\varphi = \angle(x_i, x_{ij}) \in \langle 0, 2\pi \rangle$ . The curves 1, 2, 3, 4 on a surface of the solid continuum are outlines of the cuts in the planes  $x_i x_k$ ,  $x_i x_j$ ,  $x_j x_k$ ,  $x_{ij} x_k$ , respectively.  $P$  and  $P''$  are points on the axis  $x_{ij}$  and the curve 4, respectively, where  $|OP| = x_{ij}$ ,  $\overline{PP''} \parallel x_k$ . The curves 5 and 6 represent the crack shape in the planes  $x_i x_k$  and  $x_{ij} x_k$ , respectively. The planes  $x_i x_k$ ,  $x_{ij} x_k$  are perpendicular to the crack formation plane  $x_i x_j$ . The curve 7 determines a position of the crack tip in the crack formation plane  $x_i x_j$ . The function  $f^{(ij)} = f^{(ij)}(x_{ij}, \varphi, x_k)$  related to the curve 6 describes the crack shape in the plane  $x_{ij} x_k$ . The point  $P_0 \in x_i x_j$  with the coordinate  $x_{ij} = x_0(\varphi)$  represents the crack tip related to the plane  $x_{ij} x_k$ . In case of the multi-particle-matrix system (see Fig. 1a), one eighth of the cubic cell with the central spherical particle with the radius  $R_1$  is considered, where  $d$  is the cubic cell dimension. The coefficient  $c_\varphi = c_\varphi(\varphi)$  is given by Eq. (1).

<sup>2</sup>The term 'crack formation' which is used in the doctoral dissertation includes the crack initiation (in the plane  $x_i x_j$  for  $R_1 = R_{1cq}^{(ij)}$  ( $q = p, m$ ) and the crack propagation (in the plane  $x_i x_j$  for  $R_1 > R_{1cq}^{(ij)}$ ). The crack initiation is followed by the crack propagation.

<sup>3</sup>Due to a range of the doctoral dissertation, this analytical model of the crack formation induced by the thermal stresses is determined for the multi-particle-matrix system with anisotropic and/or isotropic components (see Fig 1a). Results for the multi-particle-envelope-matrix system (see Fig 1b) which are presented in [D18] can be determined analogically.

This comparison results in the formula

$$\frac{\partial f^{(ij)}}{\partial x_{ij}} = \pm \frac{1}{s_{kk} [K_{IC}^{(ij)}]^2} \sqrt{[W_c^{(ij)}]^2 - \left\{ s_{kk} [K_{IC}^{(ij)}]^2 \right\}^2}, \quad (43)$$

for the function  $f^{(ij)} = f^{(ij)}(x_{ij}, \varphi, x_k)$  (see the curve 6, Fig. 1b) which describes the crack shape in the plane  $x_{ij}x_k$  ( $i, j, k = 1, 2, 3; i \neq j \neq k$ ), where  $x_{ij} \subset x_i x_j$ ,  $\varphi = \angle(x_i, x_{ij}) \in \langle 0, 2\pi \rangle$ . The plane  $x_{ij}x_k$  is perpendicular to the crack formation plane  $x_i x_j$ .  $K_{IC}^{(ij)}$  is fracture toughness in the crack formation plane  $x_i x_j$ . Additionally, the formula (43) is considered for  $W_c^{(ij)} - s_{kk} [K_{IC}^{(ij)}]^2 \geq 0$ . Finally,  $W_c^{(ij)} = W_c^{(ij)}(x_{ij}, \varphi) = \int_{PP''} w^{(ij)} dx_k$  represent a curve integral of the thermal-stress induced elastic energy density  $w = w^{(ij)} = w^{(ij)}(x_{ij}, \varphi, x_k)$  along the curve  $PP''$ , where  $w = w^{(ij)} = w^{(ij)}(x_{ij}, \varphi, x_k)$  is determined by the cylindrical coordinates  $(x_{ij}, \varphi, x_k)$ .

Let the multi-particle-matrix system be considered. In case of thermal stresses,  $W_c^{(ij)} = W_{cp}^{(ij)} = W_{cp}^{(ij)}(x_{ij}, \varphi, R_1, v)$  and  $W_c^{(ij)} = W_{cm}^{(ij)} = W_{cm}^{(ij)}(x_{ij}, R_1, v, \varphi)$  represent increasing and decreasing functions of the variable  $x_{ij} \in \langle 0, R_1 \rangle$  and  $x_{ij} \in \langle R_1, d/(2c_\varphi) \rangle$ , respectively, where the interval  $\varphi \in \langle 0, \pi/2 \rangle$  is sufficient to be considered due to the symmetry of the multi-particle-matrix system (see Sec. 2.1). Accordingly,  $f_p^{(ij)} = f_p^{(ij)}(x_{ij}, \varphi, R_1, v)$  and  $f_m^{(ij)} = f_m^{(ij)}(x_{ij}, \varphi, R_1, v)$  are assumed to be also increasing and decreasing functions of  $x_{ij}$ , where the sign "+" and "-" in Eq. (43) is considered, respectively. Additionally, formula (43) is considered for  $W_{cq}^{(ij)} - s_{kkq} [K_{ICq}^{(ij)}]^2 \geq 0$ .

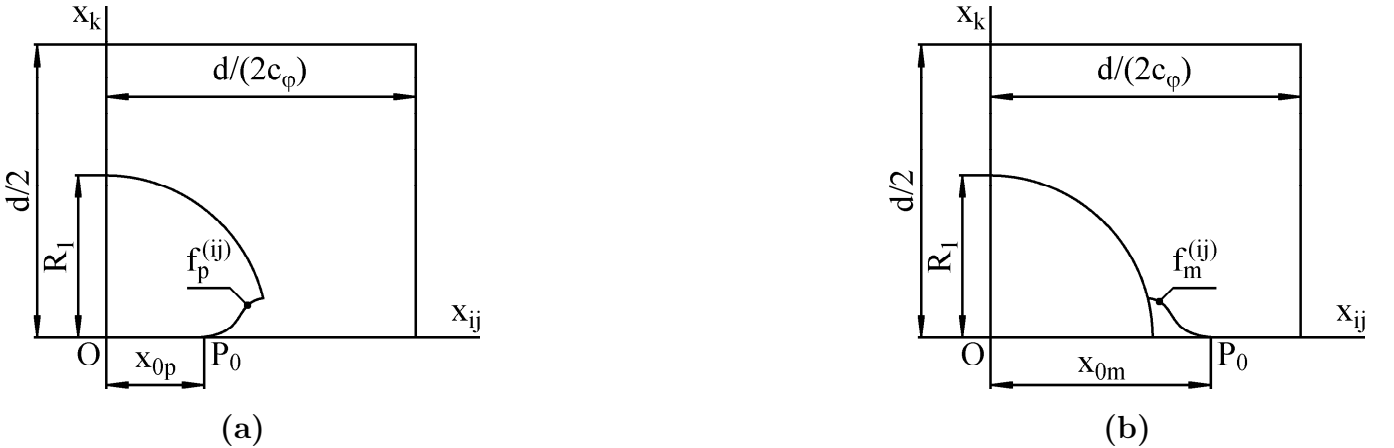


Figure 5: A schematic illustration of a shape of cracks in the plane  $x_{ij}x_k$  (see Fig. 4c). The crack with a tip in the point  $P_0$  is formed in the plane  $x_i x_j$  in (a) the spherical particle and (b) the cell matrix. The crack shape in the plane  $x_{ij}x_k$  is described by the increasing and decreasing functions  $f_p^{(ij)} = f_p^{(ij)}(x_{ij}, \varphi, R_1, v)$  and  $f_m^{(ij)} = f_m^{(ij)}(x_{ij}, \varphi, R_1, v)$  of the variable  $x_{ij} \in \langle x_{0p}, R_1 \rangle$  and  $x_{ij} \in \langle R_1, x_{0m} \rangle$  for  $R_1 > R_{1cp}^{(ij)}$  and  $R_1 > R_{1cm}^{(ij)}$  (see Eqs. (44)–(46)), respectively. The coefficient  $c_\varphi = c_\varphi(\varphi)$  is given by Eq. (1).

Consequently, the increasing and decreasing functions  $f_p^{(ij)} = f_p^{(ij)}(x_{ij}, \varphi, R_1, v)$  and  $f_m^{(ij)} = f_m^{(ij)}(x_{ij}, \varphi, R_1, v)$  of the variable  $x_{ij} \in \langle x_{0p}, R_1 \rangle$  and  $x_{ij} \in \langle R_1, x_{0m} \rangle$  which describe the crack shape in the plane  $x_{ij}x_k$  in the spherical particle and the cell matrix, respectively, are derived as (see Fig. 5)

$$f_p^{(ij)} = \frac{1}{s_{kkp} [K_{ICp}^{(ij)}]^2} \left[ \int \sqrt{[W_{cp}^{(ij)}]^2 - \left\{ s_{kkp} [K_{ICp}^{(ij)}]^2 \right\}^2} dx_{ij} - C_p^{(ij)} \right], \quad x_{ij} \in \langle x_{0p}, R_1 \rangle, \quad R_1 > R_{1cp}^{(ij)}, \quad (44)$$

$$f_m^{(ij)} = \frac{1}{s_{kkm} [K_{ICm}^{(ij)}]^2} \left[ C_m^{(ij)} - \int \sqrt{[W_{cm}^{(ij)}]^2 - \left\{ s_{kkm} [K_{ICm}^{(ij)}]^2 \right\}^2} dx_{ij} \right], \quad x_{ij} \in \langle R_1, x_{0m} \rangle, \quad R_1 > R_{1cm}^{(ij)}, \quad (45)$$

where  $\varphi \in \langle 0, \pi/2 \rangle$ ,  $R_1$  and  $v \in (0, \pi/6)$  (see Sec. 1.3) represent parameters of these functions. The integration constant  $C_q^{(ij)}$  ( $q = p, m$ ) which is determined by the boundary condition  $\left[ f_q^{(ij)} \right]_{x_{ij}=x_{0q}} = 0$  has the form

$$C_q^{(ij)} = \left[ \int \sqrt{[W_{cq}^{(ij)}]^2 - \left\{ s_{kkq} [K_{ICq}^{(ij)}]^2 \right\}^2} dx_{ij} \right]_{x_{ij}=x_{0q}}, \quad q = p, m. \quad (46)$$

The condition

$$[W_{cq}^{(ij)}(x_{ij}, \varphi, R_1, v)]_{x_{ij}=R_1} - s_{kkq} [K_{ICq}^{(ij)}]^2 = 0, \quad q = p, m, \quad (47)$$

represents an equation with the variable  $R_1$  and the parameters  $\varphi, v$ . The root  $R_{1cq}^{(ij)} = R_{1cq}^{(ij)}(\varphi, v)$  of Eq. (47) represents a critical particle radius which is a reason of the crack initiation in the plane  $x_i x_j$  in the spherical particle ( $q = p$ ) or cell matrix ( $q = m$ ) of the multi-particle-matrix system. The determination of  $R_{1cp}^{(ij)}$  or  $R_{1cm}^{(ij)}$  is related to such position  $x_{ij} \in \langle 0, R_1 \rangle$  or  $x_{ij} \in \langle R_1, d/(2c_\varphi) \rangle$  at which the dependence  $W_{cp}^{(ij)} - x_{ij}$  or  $W_{cm}^{(ij)} - x_{ij}$  is maximal, respectively. In case of the thermal stresses, we get  $x_{ij} = R_1$  for  $W_{cp}^{(ij)} - x_{ij}$  and  $W_{cm}^{(ij)} - x_{ij}$ .

The critical particle radius  $R_{1cq}^{(ij)}$  thus defines a *limit state* with respect to the crack initiation in the plane  $x_i x_j$  in the spherical particle ( $q = p$ ) and cell matrix ( $q = m$ ). The crack initiation in the plane  $x_i x_j x_k$  is then followed by the crack propagation for  $R_1 > R_{1cq}^{(ij)}$ .

Let the condition  $R_1 > R_{1cq}^{(ij)}(\varphi, v)$  be valid. The condition

$$W_{cq}^{(ij)}(x_{ij}, \varphi, R_1, v) - s_{kkq} [K_{ICq}^{(ij)}]^2 = 0, \quad R_1 > R_{1cq}^{(ij)}, \quad q = p, m, \quad (48)$$

represents an equation with the variable  $x_{ij}$  and the parameters  $\varphi, R_1, v$ . The root  $x_{0q} = x_{0q}(\varphi, R_1, v)$  which is a function of the variable  $\varphi$  defines a position of the crack tip point  $P_0$  on the axis  $x_{ij}$  (see Fig. 4b), where  $R_1, v$  represent parameters of this function. The point  $P_0 \in x_i x_j$  with the coordinate  $x_{ij} = x_{0q}(\varphi, R_1, v)$  represents the crack tip related to the plane  $x_i x_j x_k$ . The dependence  $x_{0q} - \varphi$  thus defines the crack shape in the plane  $x_i x_j$  in the spherical particle ( $q = p$ ) or cell matrix ( $q = m$ ). With regard to Fig. 4b, the dependence  $x_{0q} - \varphi$  thus defines the curve  $\gamma$ .

As mentioned above, the critical particle radius  $R_{1cq}^{(ij)} = R_{1cq}^{(ij)}(\varphi, v)$  defines such limit state which is related to one value of the variable  $\varphi \in \langle 0, \pi/2 \rangle$ . Consequently, the minimal value  $R_{1cq\min}^{(ij)}$  of the dependence  $R_{1cq}^{(ij)} - \varphi$  defines a limit state related to such plane  $x_i x_j x_k$  which corresponds to maximal value of the dependence  $W_{cq}^{(ij)}$ . The maximal value  $R_{1cq\max}^{(ij)}$  of the dependence  $R_{1cq}^{(ij)} - \varphi$  then defines a 'total' limit state of the crack initiation in the plane  $x_i x_j$  in the spherical particle ( $q = p$ ) or cell matrix ( $q = m$ ).

The analysis which results in Eqs. (43)–(48) is valid disregarding the determination of the curve integral  $W_{cq}^{(ij)}$  ( $q = p, m$ ). On the one hand, the thermal stresses are modified (changed) during the crack propagation for  $R_1 > R_{1cq}^{(ij)}$ . Accordingly,  $W_{cq}^{(ij)}$  is also modified (changed) during the crack propagation. Such modification might be analytically and/or computationally determined, and then this modification can be applied to Eqs. (43)–(48). On the other hand, formulae for  $W_{cq}^{(ij)}$  (see Eqs. (50), (51)) do not consider the modification of  $W_{cq}^{(ij)}$  during the crack propagation. These formulae for  $W_{cq}^{(ij)}$  are thus determined for a stress-strain state which is induced by the thermal stresses before the crack initiation. Consequently, these formulae are then required to be considered only in case of a two-component material with ceramic components. In general, a ceramic component

exhibits a high-speed crack propagation [39]–[41] during which the modification (change) of  $W_{cq}^{(ij)}$  can be assumed to be neglected.

Finally, the determination of  $R_{1cq}^{(ij)}$  which considers the thermal stresses *before* the crack initiation is valid for any two-component material.

Due to a range of this brochure, the curve integral  $W_{cq}^{(ij)} = W_{cq}^{(ij)}(x_{ij}, \varphi, R_1, \nu)$  ( $q = p, m$ ) is determined for the multi-particle-matrix system (see Fig. 1a) on the condition  $\beta_p(\varphi, \nu) = \beta_m(\varphi, \nu)$  for  $\nu = \nu_{pm}(\varphi)$ . If the multi-particle-matrix system does not exhibit a phase transformation at the temperature  $T \in \langle T_f, T_r \rangle$ , then the condition  $\beta_p = \beta_m$  is transformed to  $\alpha_p(\varphi, \nu) = \alpha_m(\varphi, \nu)$ . Consequently, an analysis of the condition  $\alpha_p(\varphi, \nu) - \alpha_m(\varphi, \nu) = 0$  is as follows.

1. If the differences  $\alpha_{1p} - \alpha_{1m}$ ,  $\alpha_{2p} - \alpha_{2m}$ ,  $\alpha_{3p} - \alpha_{3m}$  exhibits identical signs, i.e.  $\alpha_{1p} \geq \alpha_{1m}$ ,  $\alpha_{2p} \geq \alpha_{2m}$ ,  $\alpha_{3p} \geq \alpha_{3m}$ , then the condition  $\alpha_p(\varphi, \nu) \neq \alpha_m(\varphi, \nu)$  is valid for  $\varphi, \nu \in \langle 0, \pi/2 \rangle$ . Otherwise, the following analysis is considered.
2. If  $\alpha_{1p} \geq \alpha_{1m}$ ,  $\alpha_{2p} \geq \alpha_{2m}$ ,  $\alpha_{3p} \leq \alpha_{3m}$ , then the condition  $\alpha_p(\varphi, \nu) = \alpha_m(\varphi, \nu)$  is valid for  $\varphi \in \langle 0, \pi/2 \rangle$  and for  $\nu = \nu_{pm}$ , where the function  $\nu_{pm} = \nu_{pm}(\varphi)$ , along with the angle  $\varphi_{pm}$ , mentioned below, which is determined by the condition  $\alpha_p(\varphi, \nu) - \alpha_m(\varphi, \nu) = 0$  for  $\alpha_{3p} = \alpha_{3m}$ , have the forms

$$\begin{aligned} \nu_{pm} &= \arcsin \left( \sqrt{\frac{\alpha_{3m} - \alpha_{3p}}{(\alpha_{1p} - \alpha_{1m}) \cos^2 \varphi + (\alpha_{2p} - \alpha_{2m}) \sin^2 \varphi + \alpha_{3m} - \alpha_{3p}}} \right), \\ \varphi_{pm} &= \arcsin \left( \sqrt{\frac{\alpha_{1m} - \alpha_{1p}}{\alpha_{2p} - \alpha_{2m}}} \right). \end{aligned} \quad (49)$$

3. If  $\alpha_{1p} \geq \alpha_{1m}$ ,  $\alpha_{2p} \leq \alpha_{2m}$ ,  $\alpha_{3p} \leq \alpha_{3m}$ , then the condition  $\alpha_p(\varphi, \nu) = \alpha_m(\varphi, \nu)$  is valid for  $\varphi \in \langle 0, \varphi_{pm} \rangle$  and for  $\nu = \nu_{pm}$ .
4. If  $\alpha_{1p} \geq \alpha_{1m}$ ,  $\alpha_{2p} \leq \alpha_{2m}$ ,  $\alpha_{3p} \geq \alpha_{3m}$ , then the condition  $\alpha_p(\varphi, \nu) = \alpha_m(\varphi, \nu)$  is valid for  $\varphi \in \langle \varphi_{pm}, \pi/2 \rangle$  and for  $\nu = \nu_{pm}$ .
5. If  $\alpha_{3p} = \alpha_{3m}$ , then the following analysis is considered.
  - (a) If  $\alpha_{1p} \geq \alpha_{1m}$ ,  $\alpha_{2p} \geq \alpha_{2m}$ , then the condition  $\alpha_p(\varphi, \nu) = \alpha_m(\varphi, \nu)$  is valid for  $\nu = 0$ .
  - (b) If  $\alpha_{1p} \geq \alpha_{1m}$ ,  $\alpha_{2p} \leq \alpha_{2m}$ , then the condition  $\alpha_p(\varphi, \nu) = \alpha_m(\varphi, \nu)$  is valid for  $\varphi = \varphi_{pm}$  and for  $\nu \in \langle 0, \pi/2 \rangle$ .

Let the plane  $x_1x_2$  (see Fig. 2) in the component which is related to the subscript  $q_1$  be isotropic. In case of this uni-axial anisotropy, we get  $\alpha_{1q_1} = \alpha_{2q_1}$ .

If  $\varepsilon'_{11tp}(\varphi, \nu) \neq \varepsilon'_{11tm}(\varphi, \nu)$  at  $T \in \langle T_f, T_r \rangle$ , then the function  $\nu_{pm} = \nu_{pm}(\varphi)$  and the angle  $\varphi_{pm} \in \langle 0, \pi/2 \rangle$  which both result from the condition  $\beta_p(\varphi, \nu) - \beta_m(\varphi, \nu) = 0$  are determined by numerical methods for a real two-component material (see Sec. 1.1). In case of  $\varepsilon'_{11tp}(\varphi, \nu) \neq \varepsilon'_{11tm}(\varphi, \nu)$  at  $T \in \langle T_f, T_r \rangle$ , the condition  $\beta_p(\varphi, \nu) - \beta_m(\varphi, \nu) = 0$  thus represents a transcendental equation regarding the variables  $\varphi, \nu \in \langle 0, \pi/2 \rangle$ .

If the spherical particles and matrix are isotropic and anisotropic, respectively, then we get  $\alpha_{1p} = \alpha_{2p} = \alpha_{3p} = \alpha_p$ . Similarly, if the spherical particles and matrix are anisotropic and isotropic, respectively, then we get  $\alpha_{1m} = \alpha_{2m} = \alpha_{3m} = \alpha_m$ .

The angle  $\nu_{pm}$  thus defines the intervals  $\nu \in \langle 0, \nu_{pm} \rangle$  and  $\nu \in \langle \nu_{pm}, \pi/2 \rangle$  for which the conditions  $\alpha_p \leq \alpha_m$  and  $\alpha_p \geq \alpha_m$  are valid, respectively. The determination of  $W_{cp}^{(ij)}$  and  $W_{cm}^{(ij)}$  then considers the intervals  $\nu_{pm} \in \langle 0, \nu_R \rangle$ ,  $\nu_{pm} \in \langle \nu_R, \nu^* \rangle$ ,  $\nu_{pm} \in \langle \nu^*, \pi/2 \rangle$ . The angle  $\nu^* = \nu^*(\varphi)$  which is given by Eq. (1), and the angle  $\nu_R = \arctan(2R_1/d)$  are shown in Fig. 6, where this figure also shows the angle  $\nu_{pm}$  for the interval  $\nu_{pm} \in \langle \nu^*, \pi/2 \rangle$ .

On the conditions  $\nu_{pm} \in \langle 0, \nu_R \rangle$  and  $\nu_{pm} \in \langle \nu_R, \nu^* \rangle$ , the determination of  $W_{cp}^{(ij)} = W_{cp}^{(ij)}(x_{ij}, \varphi, R_1, \nu)$  for  $x_{ij} \in \langle 0, R_1 \rangle$  and  $W_{cm}^{(ij)} = W_{cm}^{(ij)}(x_{ij}, \varphi, R_1, \nu)$  for  $x_{ij} \in \langle R_1, d/(2c_\varphi) \rangle$  is not presented due to a range of this brochure. This determination is presented in the doctoral dissertation.

The curve integral  $W_{cq}^{(ij)} = W_{cq}^{(ij)}(x_{ij}, \varphi, R_1, v)$  ( $q = p, m$ ) is then determined for the interval  $\nu_{pm} \in \langle \nu^*, \pi/2 \rangle$  by the two following methods.

**Method 1.** This method of determination of  $W_{cp}^{(ij)}$  and  $W_{cm}^{(ij)}$  is based on an assumption that the thermal-stress induced elastic energy accumulated in the cubic cell volume which is related to  $\nu_{pm} \in \langle \nu^*, \pi/2 \rangle$  is released by the crack formation in the plane  $x_i x_j$  in the spherical particle for  $\alpha_p > \alpha_m$  or in the cell matrix for  $\alpha_p < \alpha_m$ .

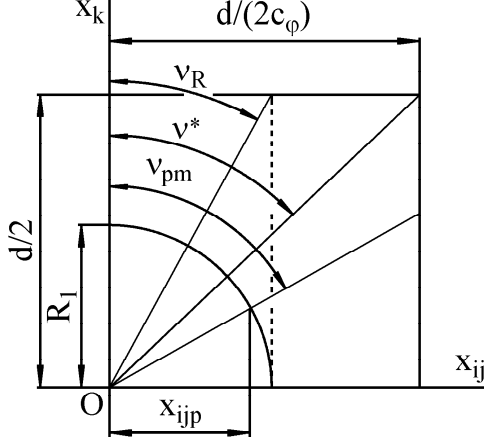


Figure 6: The angles  $\nu^* = \nu^*(\varphi)$  (see Eq. (1)),  $\nu_R = \arctan(2R_1/d)$  along with the angle  $\nu_{pm}$  which is shown for the interval  $\nu_{pm} \in \langle \nu^*, \pi/2 \rangle$ , where  $x_{ijp} = R_1 \sin \nu_{pm}$ . The coefficient  $c_\varphi = c_\varphi(\varphi)$  is given by Eq. (1).

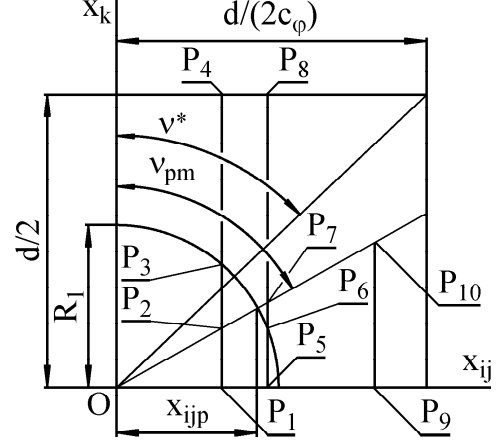


Figure 7: The abscissae  $\overline{P_1P_2}$ ,  $\overline{P_2P_3}$ ,  $\overline{P_3P_4}$ ,  $\overline{P_5P_6}$ ,  $\overline{P_6P_7}$ ,  $\overline{P_7P_8}$ ,  $\overline{P_9P_{10}}$  along which the curve integrals  $W_{cp}^{(ij),1}$ ,  $W_{cp}^{(ij),2}$ ,  $W_{cm}^{(ij),1}$  are determined for  $\nu_{pm} \in \langle \nu^*, \pi/2 \rangle$  (see Eqs. (50), (51)). The abscissae  $\overline{P_1P_2P_3P_4}$ ,  $\overline{P_5P_6P_7P_8}$  and  $\overline{P_9P_{10}}$  are related to the plane  $x_{ij}x_k$  (see Fig. 4c). The coefficient  $c_\varphi = c_\varphi(\varphi)$  is given by Eq. (1).

With regard to Fig. 7, the curve integral  $W_{cp}^{(ij),1} = W_{cp}^{(ij),1}(x_{ij}, \varphi, R_1, v)$  for  $x_{ij} \in \langle 0, x_{ijp} \rangle$  and  $x_{ij} \in \langle x_{ijp}, R_1 \rangle$ , and the curve integral  $W_{cm}^{(ij),1} = W_{cm}^{(ij),1}(x_{ij}, \varphi, R_1, v)$  for  $x_{ij} \in \langle R_1, d/(2c_\varphi) \rangle$  are derived as <sup>4</sup>

$$\begin{aligned}
 W_{cp}^{(ij),1} &= \int_{\overline{P_1P_2}} w_p^{(ij)} dx_k = \int_0^{x_{k0}} w_p^{(ij)} dx_k, \quad x_{ij} \in \langle 0, x_{ijp} \rangle, \quad x_{ijp} = R_1 \sin \nu_{pm}, \quad x_{k0} = x_{ij} \cot \nu_{pm}, \\
 W_{cp}^{(ij),1} &= \int_{\overline{P_5P_6}} w_p^{(ij)} dx_k + \int_{\overline{P_6P_7}} w_m^{(ij)} dx_k = \int_0^{\sqrt{R_1^2 - x_{ij}^2}} w_p^{(ij)} dx_k + \int_{\sqrt{R_1^2 - x_{ij}^2}}^{x_{k0}} w_m^{(ij)} dx_k, \quad x_{ij} \in \langle x_{ijp}, R_1 \rangle, \\
 W_{cm}^{(ij),1} &= \int_{\overline{P_9P_{10}}} w_m^{(ij)} dx_k = \int_0^{x_{k0}} w_m^{(ij)} dx_k, \quad x_{ij} \in \left\langle R_1, \frac{d}{2c_\varphi} \right\rangle. \tag{50}
 \end{aligned}$$

**Method 2.** This method is based on an assumption that the crack can be formed in the spherical particle or cell matrix in the plane  $x_i x_j$  in spite of the condition  $\beta_p < \beta_m$  or  $\beta_p > \beta_m$ , respectively. The following analysis can then explain such paradoxical behaviour of the cracking which is observed in a real two-component material [39]–[41]. This analysis results from an assumption that the release of energy of a system considers 'minimal resistance' of the system, i.e. the energy of a system is released through 'minimal resistance' of the system. Due to a range of this brochure, this analysis

<sup>4</sup>The superscripts 1 and 2 in  $W_{cp}^{(ij),1}$ ,  $W_{cm}^{(ij),1}$  and  $W_{cp}^{(ij),2}$  are related to the method 1 and method 2, respectively.

is determined for the spherical particle only. The analysis for the cell matrix is presented in the doctoral dissertation.

Let the condition  $\alpha_p < \alpha_m$  be valid for  $\nu \in (\nu_{pm}, \pi/2)$ . Let  $R_{1cp}^{(jk),1} = R_{1cp}^{(jk),1}(\varphi, \nu)$  represent a critical particle radius for the crack initiation in the spherical particle in the plane  $x_j x_k$ . Let  $R_{1cp}^{(jk),1} = R_{1cp}^{(jk),1}(\varphi, \nu)$  be determined by the curve integral  $W_{cp}^{(jk),1} = W_{cp}^{(jk),1}(x_{jk}, \varphi, R_1, \nu)$  for  $\varphi = \angle(x_j, x_{jk})$ ,  $x_{jk} \subset x_j x_k$  (see Eq. (47)). Let  $W_{cp}^{(jk),1}$  be determined by the *method 1*.

Let  $R_{1cp}^{(ki),1} = R_{1cp}^{(ki),1}(\varphi, \nu)$  represent a critical particle radius for the crack initiation in the spherical particle in the plane  $x_k x_i$ . Let  $R_{1cp}^{(ki),1} = R_{1cp}^{(ki),1}(\varphi, \nu)$  be determined by the curve integral  $W_{cp}^{(ki),1} = W_{cp}^{(ki),1}(x_{ki}, \varphi, R_1, \nu)$  for  $\varphi = \angle(x_k, x_{ki})$ ,  $x_{ki} \subset x_k x_i$  (see Eq. (47)). Let  $W_{cp}^{(ki),1}$  be also determined by the *method 1*.

Let  $R_{1cm}^{(ij),1} = R_{1cm}^{(ij),1}(\varphi, \nu)$  represent a critical particle radius for the crack initiation in the cell matrix in the plane  $x_k x_i$ . Let  $R_{1cm}^{(ij),1} = R_{1cm}^{(ij),1}(\varphi, \nu)$  be determined by the curve integral  $W_{cm}^{(ij),1} = W_{cm}^{(ij),1}(x_{ij}, \varphi, R_1, \nu)$  for  $\varphi = \angle(x_i, x_{ij})$ ,  $x_{ij} \subset x_i x_j$  (see Eq. (47)). Let  $W_{cm}^{(ij),1}$  be also determined by the *method 1*.

Finally, let  $R_{1cp}^{(ij),2} = R_{1cp}^{(ij),2}(\varphi, \nu)$  represent a critical particle radius for the crack initiation in the spherical particle in the plane  $x_k x_i$ . Let  $R_{1cp}^{(ij),2} = R_{1cp}^{(ij),2}(\varphi, \nu)$  be determined by the curve integral  $W_{cp}^{(ij),2} = W_{cp}^{(ij),2}(x_{ij}, \varphi, R_1, \nu)$  for  $\varphi = \angle(x_i, x_{ij})$ ,  $x_{ij} \subset x_i x_j$  (see Eq. (47)). With regard to Fig. 7, the curve integral  $W_{cp}^{(ij),2}$  which is determined by the *method 2* for  $x_{ij} \in \langle 0, x_{ijp} \rangle$  and  $x_{ij} \in \langle x_{ijp}, R_1 \rangle$  have the form

$$\begin{aligned}
W_{cp}^{(ij),2} &= \int_{\frac{P_2 P_3}{P_2 P_3}} w_p^{(ij)} dx_k + \int_{\frac{P_3 P_4}{P_3 P_4}} w_m^{(ij)} dx_k - \int_{\frac{P_1 P_2}{P_1 P_2}} w_p^{(ij)} dx_k \\
&= \int_{x_{k0}}^{\sqrt{R_1^2 - x_{ij}^2}} w_p^{(ij)} dx_k + \int_{\sqrt{R_1^2 - x_{ij}^2}}^{d/2} w_m^{(ij)} dx_k - \int_0^{x_{k0}} w_p^{(ij)} dx_k \geq 0, \quad x_{ij} \in \langle 0, x_{ijp} \rangle, \quad x_{k0} = x_{ij} \cot \nu_{pm} \\
W_{cp}^{(ij),2} &= \int_{\frac{P_7 P_8}{P_7 P_8}} w_m^{(ij)} dx_k - \left[ \int_{\frac{P_5 P_6}{P_5 P_6}} w_p^{(ij)} dx_k + \int_{\frac{P_6 P_7}{P_6 P_7}} w_m^{(ij)} dx_k \right] \\
&= \int_{x_{k0}}^{d/2} w_m^{(ij)} dx_k - \left[ \int_0^{\sqrt{R_1^2 - x_{ij}^2}} w_p^{(ij)} dx_k + \int_{\sqrt{R_1^2 - x_{ij}^2}}^{x_{k0}} w_m^{(ij)} dx_k \right] \geq 0, \quad x_{ij} \in \langle x_{ijp}, R_1 \rangle. \tag{51}
\end{aligned}$$

Additionally,  $W_{cp}^{(ij),2} = W_{cp}^{(ij),2}(x_{ij}, \varphi, R_1, \nu)$  is defined for such interval  $x_{ij} \in \langle x_{ijp0}, R_1 \rangle \subset \langle 0, R_1 \rangle$  for which the condition  $W_{cp}^{(ij),2} \geq 0$  is valid, where  $x_{ijp0}$  is determined by the condition  $W_{cp}^{(ij),2} = 0$ . In case of the thermal stresses,  $W_{cp}^{(ij),2}$  represents an increasing function of  $x_{ij} \in \langle x_{ijp0}, R_1 \rangle$ .

If the conditions

$$R_{1cp}^{(ij),2} < R_{1cp}^{(jk),1}, \quad R_{1cp}^{(ij),2} < R_{1cp}^{(ki),1}, \quad R_{1cp}^{(ij),2} < R_{1cm}^{(ij),1} \tag{52}$$

are simultaneously valid, then the crack is formed in the plane  $x_i x_j$  in the spherical particle

- in spite of the fact that the condition  $\alpha_p < \alpha_m$  for  $\nu \in (\nu_{pm}, \pi/2)$  is valid,
- and in spite of the fact that the crack would be expected to be formed in the cell matrix regarding  $\alpha_p < \alpha_m$  for  $\nu \in (\nu_{pm}, \pi/2)$ .

The critical particle radius  $R_{1cp}^{(ij),2}$  which is a minimal value of the set  $\{R_{1cp}^{(ij),2}, R_{1cp}^{(jk),1}, R_{1cp}^{(ki),1}, R_{1cm}^{(ij),1}\}$  thus represents the 'minimal resistance' through which energy of the cubic cell is released.

**5.2 Analytical model of energy barrier.** The definition of the energy barriers  $W_{bi} = W_{bi}(x_i)$ ,  $W_{bj} = W_{bj}(x_j)$ ,  $W_{bk} = W_{bk}(x_k)$  which represent energy gradients along the axes  $x_i$ ,  $x_j$ ,  $x_k$ , respectively, is as follows. Let a solid continuum with a general shape shown in Fig. 8 be considered. Let  $W = \int_V w dV$  be energy accumulated in the volume  $V$  of this solid continuum, and then we get

$$\begin{aligned} W &= \int_{x_{i1}}^{x_{i2}} \int_{x_{j1}}^{x_{j2}} \int_{x_{k1}}^{x_{k2}} w dx_i dx_j dx_k \\ &= \int_{x_{i1}}^{x_{i2}} \int_{S_i} w dx_i dS_i = \int_{x_{j1}}^{x_{j2}} \int_{S_j} w dx_j dS_j = \int_{x_{k1}}^{x_{k2}} \int_{S_k} w dx_k dS_k, \end{aligned} \quad (53)$$

where the energy density  $w = w(x_i, x_j, x_k)$  is represented e.g. by thermal-stress induced elastic energy density.  $x_{i1}, x_{i2}$ ;  $x_{j1}, x_{j2}$ ;  $x_{k1}, x_{k2}$  are integration boundaries related to the variables  $x_i$ ;  $x_j$ ;  $x_k$ , respectively. The surfaces  $S_i, S_j, S_k$  in positions given by  $x_i \in \langle x_{i1}, x_{i2} \rangle$ ,  $x_j \in \langle x_{j1}, x_{j2} \rangle$ ,  $x_k \in \langle x_{k1}, x_{k2} \rangle$  represent cross-sections of the solid continuum, where these surfaces are perpendicular to the axes  $x_i, x_j, x_k$ , respectively. As an example (see Fig. 8), the surface  $S_i$  with the normal  $x_i$  is related to the plane  $x_j''x_k''$  which is parallel to  $x_jx_k$ .

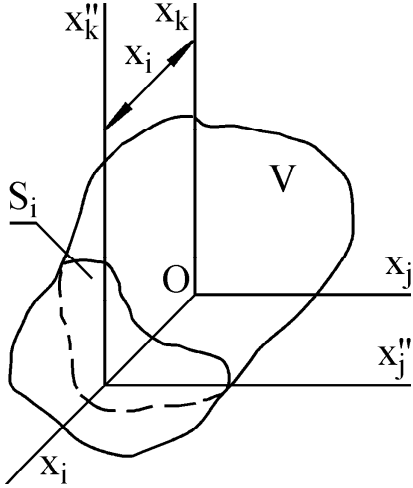


Figure 8: The solid continuum with a general shape with the volume  $V$ , and with the surface  $S_i$  in a position given by  $x_i \in \langle x_{i1}, x_{i2} \rangle$ , where the difference  $x_{i2} - x_{i1}$  represents length of the solid continuum along the axis  $x_i$ . The surface  $S_i$  with the normal  $x_i$  is a cross-section of the solid continuum. The cross-section is given by the plane  $x_j''x_k''$  which is parallel to the plane  $x_jx_k$ .

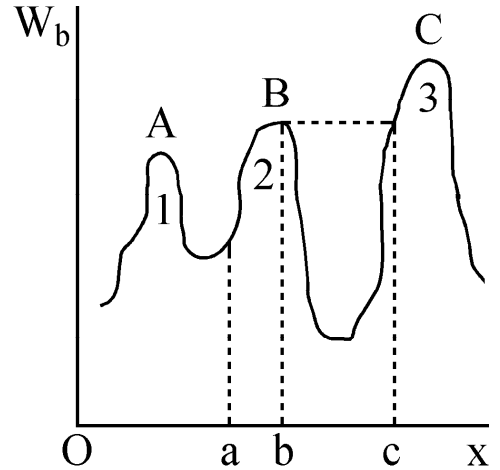


Figure 9: The energy barriers 1, 2, 3 with maximal values in the points A, B, C, respectively. The energy barrier 2 exhibits the maximum in the position  $x = b$ .

Consequently,  $W_{bi} = W_{bi}(x_i) = \partial W / \partial x_i$ ,  $W_{bj} = W_{bj}(x_j) = \partial W / \partial x_j$ ,  $W_{bk} = W_{bk}(x_k) = \partial W / \partial x_k$  which represent surface integrals related to  $S_i, S_j, S_k$ , respectively, have the forms

$$W_{bi} = \int_{x_{j1}}^{x_{j2}} \int_{x_{k1}}^{x_{k2}} w dx_j dx_k, \quad W_{bj} = \int_{x_{i1}}^{x_{i2}} \int_{x_{k1}}^{x_{k2}} w dx_i dx_k, \quad W_{bk} = \int_{x_{i1}}^{x_{i2}} \int_{x_{j1}}^{x_{j2}} w dx_i dx_j. \quad (54)$$

This definition of an energy barrier, i.e.  $W_{bi} = \partial W / \partial x_i$ ,  $W_{bj} = \partial W / \partial x_j$ ,  $W_{bk} = \partial W / \partial x_k$ , is also presented in [59].

In general, energy barriers influence motion of dislocations, magnetic domain walls, etc., where a magnetic domain wall represents a front between magnetic domains with and without ordered

magnetic moments [59]. As an example, a planar magnetic domain wall in a magnetic material is shifted along the axis  $x$  from the position  $x = a$  to the position  $x = b$  due to the change  $\Delta H_{ba} = H_b - H_a$  of the magnetic field intensity  $H$  (see Fig 9). As presented in Fig 9, the point  $B$  with the position  $x = b$  represents a maximum of the energy barrier  $\mathcal{2}$ . Consequently, this magnetic domain wall moves along the axis  $x$  to the position  $x = c$  at the constant intensity  $H_b = H_c$ . The wall is then stopped by the energy barrier  $\mathcal{3}$  which is higher than the energy barrier  $\mathcal{2}$ . The position change  $\Delta x_{cb} = c - b$  of the wall results in the change  $\Delta M_{cb}$  of the magnetic moment  $M$  of the magnetic material. Accordingly,  $\Delta M_{ba}$  related to  $\Delta x_{cb} = c - b$  results in a discrete change of the magnetization hysteresis loop at zero change of  $H$ , i.e. for  $\Delta H_{cb} = H_c - H_b = 0$ . This discrete change at the constant intensity  $H_b = H_c$  induces a voltage impulse in a pickup coil. The voltage impulse is known as the Barkhausen jump. Additionally, maximal values of the energy barriers  $\mathcal{1}$ ,  $\mathcal{2}$ ,  $\mathcal{3}$  are reasons of the coercivity of magnetic materials including magnetic multi-component materials [59].

Due to a range of this brochure, formulae for the energy barrier in the model systems (see Fig. 1) are determined in the doctoral dissertation.

**5.3 Analytical model of strengthening.** The analytical model of the micro-strengthening  $\sigma_{si} = \sigma_{si}(x_i)$ ,  $\sigma_{sj} = \sigma_{si}(x_j)$ ,  $\sigma_{sk} = \sigma_{si}(x_k)$  and the macro-strengthening  $\bar{\sigma}_{si}$ ,  $\bar{\sigma}_{sj}$ ,  $\bar{\sigma}_{sk}$  along the axes  $x_i$ ,  $x_j$ ,  $x_k$  ( $i, j, k = 1, 2, 3; i \neq j \neq k$ ) (see Fig. 8) is based on the following energy analysis.

Let a solid continuum with a general shape and with the volume  $V$  shown in Fig. 8 be considered. Let the surface  $S_i$  in a position given by  $x_i \in \langle x_{i1}, x_{i2} \rangle$  be a cross-section of this solid continuum, where  $S_i(x_i)$  is an area of  $S_i$ . The cross-section  $S_i$  with the normal  $x_i$  is related to the plane  $x_j''x_k''$  (see Fig. 8), where  $x_j''x_k'' \parallel x_jx_k$ . The surface  $S_i$  is described by the coordinates  $x_j \in \langle x_{j1}, x_{j2} \rangle$  and  $x_k \in \langle x_{k1}, x_{k2} \rangle$ .

Let the micro-strengthening  $\sigma_{si} = \sigma_{si}(x_i)$  along the axis  $x_i$  which is required to be determined within this analysis represent a normal stress acting on the surface  $S_i$ . Additionally, let  $\sigma_{si} = \sigma_{si}(x_i)$  be constant regarding each point of the surface  $S_i$ , i.e.  $\sigma_{si} = \sigma_{si}(x_i) \neq f(x_j, x_k)$  is not a function of  $x_j \in \langle x_{j1}, x_{j2} \rangle$  and  $x_k \in \langle x_{k1}, x_{k2} \rangle$ .

Consequently, let the stress  $\sigma_{si} = \sigma_{si}(x_i)$  induce the elastic strain  $\varepsilon_{sii} = \varepsilon_{sii}(x_i) = s_{ii}\sigma_{si}(x_i)$  along the axis  $x_i$ . Accordingly, the elastic energy density  $W_{\sigma_{si}} = W_{\sigma_{si}}(x_i)$  accumulated on the surface area  $S_i = S_i(x_i)$  has the form

$$W_{\sigma_{si}} = W_{\sigma_{si}}(x_i) = \frac{\sigma_{si} \varepsilon_{sii} S_i}{2} = \frac{s_{ii} S_i \sigma_{si}^2}{2}, \quad s_{ii} = \frac{1}{E_i}, \quad (55)$$

where  $E_i$  is the Young's modulus along the axis  $x_i$ .

Let  $\sigma_i = \sigma_i(x_i, x_j, x_k) = \sum_{n_1=1}^3 a_{n_1 i} \sigma'_{n_1 n_1} + \sum_{n_1, n_2=1; n_1 \neq n_2}^3 a_{n_1 i} \sigma'_{n_1 n_2}$  be a thermal stress which acts along the axis  $x_i$  in the solid continuum, where the term  $a_{n_1 i} \sigma'_{n_1 n_2}$  represents a projection ('coordinate') of the stress  $\sigma'_{n_1 n_2}$  to a direction represented by the axis  $x_i$ , and the coefficient  $a_{n_1 i}$  ( $i, j, k, n_1, n_2 = 1, 2, 3$ ) is given by Eq. (6). Let  $w_i = w_i(x_i, x_j, x_k) = \varepsilon_{ii} \sigma_i / 2 = s_{ii} \sigma_i^2 / 2$  be elastic energy density which is induced by  $\sigma_i = \sigma_i(x_i, x_j, x_k)$ .

Accordingly, the thermal-stress induced elastic energy density  $W_i = W_i(x_i)$  accumulated on the surface area  $S_i = S_i(x_i)$  is derived as

$$W_i = W_i(x_i) = \int_{S_i} w_i dS_i. \quad (56)$$

With regard to a sign of the stress  $\sigma_{si} = \sigma_{si}(x_i)$ , the determination of the integral in Eq. (56) is required to consider the following conditions:

1. If  $\sigma_i(x_i, x_j, x_k) < 0$  at a point with the coordinates  $(x_i, x_j, x_k)$  on the surface  $S_i$ , then  $w_i = w_i(x_i, x_j, x_k)$  at this point is considered to be  $-w_i$ .
2. If  $\sigma_i(x_i, x_j, x_k) > 0$  at a point with the coordinates  $(x_i, x_j, x_k)$  on the surface  $S_i$ , then  $w_i = w_i(x_i, x_j, x_k)$  at this point is considered to be  $+w_i$ .

The micro-strengthening  $\sigma_{si} = \sigma_{si}(x_i)$  along the axis  $x_i$  which is determined by the condition

$$W_{\sigma_{si}} = W_i. \quad (57)$$

The macro-strengthening  $\bar{\sigma}_{si}$  along the axis  $x_i$  which represents a mean value of  $\sigma_{si} = \sigma_{si}(x_i)$  regarding the interval  $x_i \in \langle x_{1i}, x_{2i} \rangle$ , are then derived as

$$\begin{aligned} \sigma_{si} = \sigma_{si}(x_i) &= \pm \sqrt{\frac{2|W_i|}{s_{ii} S_i}}, \\ \bar{\sigma}_{si} &= \frac{1}{x_{2i} - x_{1i}} \int_{x_{1i}}^{x_{2i}} \sigma_{si} dx_i = \frac{1}{x_{2i} - x_{1i}} \sqrt{\frac{2}{s_{ii}}} \int_{x_{1i}}^{x_{2i}} \pm \sqrt{\frac{|W_i|}{S_i}} dx_i, \quad s_{ii} = \frac{1}{E_i}, \end{aligned} \quad (58)$$

where the signs '+' and '-' in Eq. (57) are considered for  $W_i > 0$  and  $W_i < 0$ , respectively. Additionally, the following conditions are considered:

3. If  $W_i(x_i) > 0$  in a position given by the coordinate  $x_i$ , then the sign '+' in Eq. (58) is considered.
4. If  $W_i(x_i) < 0$  in a position given by the coordinate  $x_i$ , then the sign '-' in Eq. (58) is considered.

Finally, the following analysis concerning a sign of  $\bar{\sigma}_{si}$  is considered:

5. If  $\bar{\sigma}_{si} < 0$ , then the macro-strengthening  $\bar{\sigma}_{si}$  represents a 'resistance' against compressive mechanical loading.
6. If  $\bar{\sigma}_{si} > 0$ , then the macro-strengthening  $\bar{\sigma}_{si}$  represents a 'resistance' against tensile mechanical loading.

With regard to the micro-/macro-strengthening along the axes  $x_j$  and  $x_k$ , the transformations  $i \rightarrow j, j \rightarrow i, k \rightarrow k$  and  $i \rightarrow k, j \rightarrow j, i \rightarrow k$  of the subscripts  $i, j, k$  are considered in Eqs. (55)–(57), respectively.

Due to a range of this brochure, formulae for the micro-/macro-strengthening in the model systems (see Fig. 1) are determined in the doctoral dissertation.

**5.4 Methods of lifetime prediction.** The analytical-computational and analytical-experimental-computational methods of the lifetime prediction are applicable to the three-component material defined in Item 4, Sec. 1.1. This three-component material consists of grains with and without a continuous component (envelope) on a grain surface. The grains with the continuous component and the grains without the continuous component are identical or different regarding their crystal lattices, and thus exhibit identical or different thermal expansion coefficients, respectively.

With regard to analytical modelling of the thermal stresses, this three-component material is replaced by the multi-particle-envelope-matrix system (see Fig. 1b). The grains (with the radius  $R_1$  and with the volume fraction  $v$ ) with the envelope with the thickness  $t$  correspond to the spherical particles with the radius  $R_1$  of this model system. The grains without the envelope correspond to the matrix of this model system. The parameters  $R_1, t, v$  of the multi-particle-envelope-matrix system represent microstructural parameters of the three-component material.

Each of the lifetime prediction methods considers a dependence of  $\bar{p}_i = \bar{p}_i(R_1, t, v)$  ( $i = 1, 2$ ) on these microstructural parameters, where  $\bar{p}_i = \bar{p}_i(R_1, t, v) = (2/\pi)^2 \times \int_0^{\pi/2} \int_0^{\pi/2} p_i d\varphi d\nu$  represents a mean value [58] of the function  $p_i = p_i(\varphi, \nu, R_1, t, v)$  of the variables  $\varphi \in \langle 0, \pi/2 \rangle, \nu \in \langle 0, \pi/2 \rangle$ . The radial stresses  $p_1 = p_1(\varphi, \nu, R_1, t, v)$  and  $p_2 = p_2(\varphi, \nu, R_1, t, v)$  act at the particle-envelope and matrix-envelope boundaries, respectively. The integration is sufficient to be determined within one eighth of the cubic cell, i.e. for  $\varphi \in \langle 0, \pi/2 \rangle$  and  $\nu \in \langle 0, \pi/2 \rangle$ . As analysed in Sec. 2.1, this is a

consequence of symmetry of the multi-particle-envelope-matrix system due to the matrix infinity and the periodical distribution of the spherical particles and the spherical envelopes (see Fig. 1b).

On the one hand, the following analyses concern a stress-strain state which is induced by the thermal stresses. On the other hand, these analyses are also applicable to a stress-strain state with the radial stress  $\sigma'_{11q}$ , tangential stresses  $\sigma'_{22q}$ ,  $\sigma'_{33q}$  and shear stresses  $\sigma'_{12q}$ ,  $\sigma'_{13q}$  in the spherical particle ( $q=p$ ) and cell matrix ( $q=m$ ) which are required to fulfilled the following conditions, i.e. which have the forms  $\sigma'_{11p} = -p_1 f_{11p}$ ,  $\sigma'_{11m} = -p_2 f_{11m}$ ;  $\sigma'_{22p} = -p_1 f_{22p}$ ,  $\sigma'_{33p} = -p_1 f_{33p}$ ,  $\sigma'_{22m} = -p_2 f_{22m}$ ,  $\sigma'_{33m} = -p_2 f_{33m}$ ;  $\sigma'_{12p} = -p_1 f_{12p}$ ,  $\sigma'_{13p} = -p_1 f_{13p}$ ,  $\sigma'_{12m} = -p_2 f_{12m}$ ,  $\sigma'_{13m} = -p_2 f_{13m}$ , where  $f_{ijp}$  and  $f_{ijm}$  ( $i, j = 1, 2, 3$ ) are functions of a position in the spherical particle and cell matrix, respectively.

Resistive and contributory effects of thermal stresses. In case of the multi-particle-matrix system, the compressive or tensile radial stress  $\bar{p}_1(R_1, v) > 0$  or  $\bar{p}_1(R_1, v) < 0$  which acts at the particle-matrix boundary corresponds to the condition  $\beta_p < \beta_m$  or  $\beta_p > \beta_m$  (see Eqs. (9)–(12)), respectively.

In case of the multi-particle-envelope-matrix system, the radial stresses  $\bar{p}_1(R_1, t, v) \geq 0$  and  $\bar{p}_2(R_1, t, v) \geq 0$  can or need not correspond to the conditions  $\beta_e \geq \beta_p$  and  $\beta_m \geq \beta_e$  (see Eqs. (9)–(12)), respectively. This fact results from a dependence of  $\bar{p}_i$  ( $i = 1, 2$ ) on  $R_1, t, v$ .

Consequently, the radial stress  $\bar{p}_i = \bar{p}_i(R_1, t, v)$  ( $i = 1, 2$ ) can exhibit zero values at  $R_{1ci}, t_{ci}$ . Accordingly,  $R_{1ci}, t_{ci}$  represent such critical values of the microstructural parameters  $R_1, t$  at which  $\bar{p}_i$  is transformed from compressive to tensile or vice versa.

If  $\bar{p}_1$  is compressive (i.e.  $\bar{p}_1(R_1, t, v) > 0$ ), then radial and tangential thermal stresses in the spherical particle (i.e. in the grain with the envelope on the grain surface) are also compressive. The compressive radial and tangential thermal stresses in the spherical particle thus represent 'resistance' against the compressive radial stress  $\sigma_{r1} < 0$ . The radial stress  $\sigma_{r1}$  acting at the particle-envelope boundary is explained below.

Similarly, if  $\bar{p}_1$  is tensile (i.e.  $\bar{p}_1(R_1, t, v) < 0$ ), then radial and tangential thermal stresses in the spherical particle (i.e. in the grain with the envelope on the grain surface) are also tensile. The tensile radial and tangential thermal stresses in the spherical particle thus represent 'resistance' against the tensile radial stress  $\sigma_{r1} > 0$ .

If  $\bar{p}_2$  is compressive (i.e.  $\bar{p}_2(R_1, t, v) > 0$ ), then radial and tangential thermal stresses in the cell matrix (i.e. in the grain without the envelope on the grain surface) are compressive and tensile, respectively. The compressive radial and tensile tangential thermal stresses in the cell matrix thus represent 'resistance' against the compressive radial stress  $\sigma_{r2} < 0$ . The radial stress  $\sigma_{r2}$  acting at the matrix-envelope boundary is explained below.

Similarly, if  $\bar{p}_2$  is tensile (i.e.  $\bar{p}_2(R_1, t, v) < 0$ ), then radial and tangential thermal stresses in the cell matrix (i.e. in the grain without the envelope on the grain surface) are tensile and compressive, respectively. The tensile radial and compressive tangential thermal stresses in the cell matrix thus represent 'resistance' against the tensile radial stress  $\sigma_{r2} > 0$ .

The critical microstructural parameters  $R_{1c1}, t_{c1}$  for  $v \in (0, v_{max})$  (see Sec. 1.3) thus represent such critical values at which the radial and tangential thermal stresses in the spherical particle change from positive (or negative) to negative (or positive). Accordingly, this resistive effect of the thermal stresses in the spherical particle is transformed to a contributory effect or vice versa.

Similarly,  $R_{1c2}, t_{c2}$  for  $v \in (0, v_{max})$  (see Sec. 1.3) thus represent such critical values at which the radial/tangential thermal stresses in the cell matrix change from positive/negative (or negative/positive) to negative/positive (or positive/negative). Accordingly, this resistive effect of the thermal stresses in the cell matrix is transformed to a contributory effect or vice versa.

Due to mechanical loading mentioned below, the following analysis, which is based on the analysis presented above, also considers an quasi-resistive effect.

Let the three-component material be loaded by mechanical loading. Let the mechanical loading be represented by the stresses  $\sigma_{1mech}, \sigma_{2mech}, \sigma_{3mech}$  which act along the axes  $x_1, x_2, x_3$  (see Fig. 2). Let  $\sigma_{1mech}, \sigma_{2mech}, \sigma_{3mech}$  induce the radial stresses  $\sigma_{r1} = \sigma_{r1}(\varphi, \nu, R_1, t, v)$  and  $\sigma_{r2} = \sigma_{r2}(\varphi, \nu, R_1, t, v)$

which act at the particle-envelope and matrix-envelope boundaries, respectively <sup>5</sup>. Let the term  $\overline{\sigma_{ri}} = \overline{\sigma_{ri}}(R_1, t, v)$  ( $i=1,2$ ) represent a mean value of the function  $\overline{\sigma_{ri}} = \overline{\sigma_{ri}}(R_1, t, v)$  of the variables  $\varphi \in \langle 0, 2\pi \rangle$ ,  $\nu \in \langle 0, \pi \rangle$ .

Consequently, the condition  $|\overline{p_i}(R_1, t, v)| = |\overline{\sigma_{ri}}(R_1, t, v)|$  results in the dependence  $R_{1Ac} = f_i(t_{Ac}, v, \overline{\sigma_{ri}})$  between the variables  $R_1, t$  of the function  $\overline{\sigma_{ri}} = \overline{\sigma_{ri}}(R_1, t, v)$  with the parameter  $v \in (0, v_{max})$  (see Sec. 1.3).

Similarly, the condition  $\overline{p_i}(R_1, t, v) = 0$  results in the dependence  $R_{1Bc} = f_i(t_{Bc}, v)$  between the variables  $R_1, t$  of the function  $\overline{p_i} = \overline{p_i}(R_1, t, v)$  with the parameter  $v \in (0, v_{max})$ .

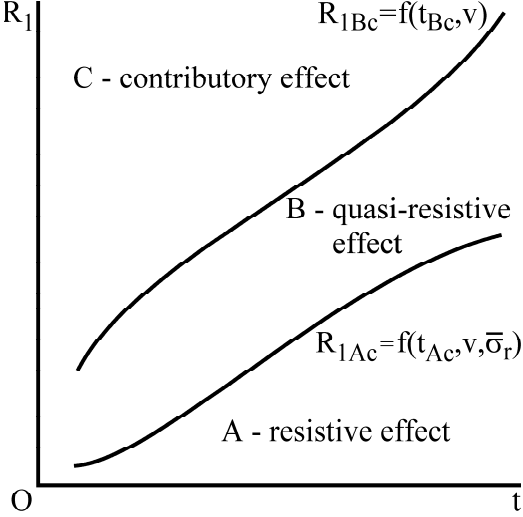


Figure 10: A schematic illustration of the dependences  $R_{1Ac} = f(t_{Ac}, v, \overline{\sigma_r})$  and  $R_{1Bc} = f(t_{Bc}, v)$  which result from the conditions  $|\overline{p_i}(R_1, t, v)| = |\overline{\sigma_{ri}}(R_1, t, v)|$  and  $\overline{p_i}(R_1, t, v) = 0$ , respectively, where  $f(t_{Ac}, v, \overline{\sigma_r}) \equiv f_i(t_{Ac}, v, \overline{\sigma_{ri}})$ ,  $f(t_{Bc}, v) \equiv f_i(t_{Bc}, v)$  for  $v \in (0, v_{max})$  (see Sec. 1.3).

Fig. 10 shows a schematic illustration of the dependences  $R_{1Ac} = f(t_{Ac}, v, \overline{\sigma_r})$  and  $R_{1Bc} = f(t_{Bc}, v)$  for  $v \in (0, v_{max})$  (see Sec. 1.3) which define the areas  $A, B, C$ , where  $f(t_{Ac}, v, \overline{\sigma_r}) = f_i(t_{Ac}, v, \overline{\sigma_{ri}})$ ,  $f(t_{Bc}, v) = f_i(t_{Bc}, v)$  ( $i=1,2$ ).

The area  $A$  is characterized by such coordinates  $(R_1, t)$  of the microstructural parameters  $R_1, t$  for which the thermal stresses exhibit the resistive effect against the mechanical loading, and additionally  $|\overline{p_i}(R_1, t, v)| \geq |\overline{\sigma_{ri}}(R_1, t, v)|$ , and  $\overline{p_i}(R_1, t, v) \times \overline{\sigma_{ri}}(R_1, t, v) < 0$ .

The area  $B$  is characterized by such coordinates  $(R_1, t)$  of the microstructural parameters  $R_1, t$  for which the thermal stresses exhibit the quasi-resistive effect against the mechanical loading, i.e.  $|\overline{p_i}(R_1, t, v)| \in \langle 0, |\overline{\sigma_{ri}}(R_1, t, v)| \rangle$ , and  $\overline{p_i}(R_1, t, v) \times \overline{\sigma_{ri}}(R_1, t, v) \leq 0$ .

The area  $C$  is characterized by such coordinates  $(R_1, t)$  of the microstructural parameters  $R_1, t$  for which the thermal stresses exhibit the contributory effect regarding the mechanical loading, and  $\overline{p_i}(R_1, t, v) \times \overline{\sigma_{ri}}(R_1, t, v) > 0$ .

With regard to Fig. 10, material scientists are able to design and develop microstructure of the three-component material with such microstructural parameters  $R_1, t, v$  which result in this thermal-stress induced resistance against required mechanical loading. The microstructure can be thus tailored regarding the required mechanical loading.

Additionally, let the microstructure be time-dependent. If a time development of the microstructure is determined analytically or experimentally, then the time  $\tau_c$  when the three-component material exhibits the critical microstructural parameters  $R_{1c}, t_c$  for  $v \in (0, v_{max})$  (see Sec. 1.3) can be determined.

The determination of  $\tau_{c1}$  and  $\tau_{c2}$  which are related to  $\overline{p_1} = \overline{p_1}(R_1, t, v)$  and  $\overline{p_2} = \overline{p_2}(R_1, t, v)$ , respectively, is as follows.

Analytical-computational method. The transformation of the resistive effect of the thermal stresses to contributory effect with respect to mechanical loading is considered for the determination of a

<sup>5</sup>Such radial stresses (i.e.  $\sigma_{r1}, \sigma_{r2}$ ) can be determined by e.g. the Eshelby's model. The Eshelby's model and its development [20,21,28,51] which are based on the Green's function, ordinary Newtonian potential and biharmonic potential define the disturbance of an applied stress-field in a solid continuum, where the applied stress-field is disturbed due to the presence of inclusions in a solid continuum.

method of the lifetime prediction. The lifetime prediction method is applicable to e.g. structural steels which are used within high-temperature applications, e.g. superheater and reheater tubing and piping in power plants. With regard to the high-temperature applications, these structural steels are creep-resistant [60]–[64]. Creep-resistant steels represent multi-component materials which exhibit changes of microstructure during years of an application at high temperature. In general, these microstructural changes are a reason of a degradation of strength of creep-resistant steels. The components of a power plant are usually designed with respect to a service life of 20 years (184 080 hours) [63,64].

The analytical-computational method represents a connection of analytical and computational techniques. The analytical technique is based on the 'resistance-contribution' transformation. The computational technique is represented by a computational simulation of the time development of microstructure at the temperature  $T$ . The temperature  $T$  is a parameter of this analytical-computational method.

Microstructure of a creep-resistant steel thus exhibits changes during the time-temperature exploitation. An initial state of the microstructure at the beginning of the time-temperature exploitation is characterized by the presence of grains with aperiodically distributed precipitates of more or less defined shape. The grain matrix is ferritic ( $\text{Fe}_\alpha\text{-C}$ ) or austenitic ( $\text{Fe}_\gamma\text{-C}$ ), with the substitutive atoms Mn, Cr, Mo, W. The precipitates are represented by the carbonitride MX ( $M = \text{Nb, V, Ti}$ ;  $X = \text{C, N}$ ), various carbide types of Cr, Mo, V, W, and inter-metallic phases (Laves and sigma phases) [60]–[64]. As presented in [64], the ability of steels to resist creep deformation depends on the presence of such precipitates in a matrix of grains.

Consequently, a final state of the microstructure of the structural steel at the end (regarding the lifetime) of the time-temperature exploitation is characterized by the presence of grains with an envelope on the grain surface as well as by the presence of grains without an envelope on the grain surface.

The matrix of grains without the envelope and the matrix of grains with the envelope are ferritic ( $\text{Fe}_\alpha\text{-C}$ ) or austenitic ( $\text{Fe}_\gamma\text{-C}$ ). The envelope is represented by the carbides  $\text{M}_{23}\text{C}_6$ ,  $\text{M}_6\text{C}$ , and/or inter-metallic phases (Laves and sigma phases) [60]–[64].

Microstructure of this final state of a creep-resistant steel thus corresponds to the microstructure which is defined in Item 4, Sec. 1.1.

The lifetime prediction method determines the critical time  $\tau_{Ac}$  and  $\tau_{Bc}$  when the microstructure exhibits the critical parameters  $R_{1Ac}$ ,  $t_{1Ac}$  and  $R_{1Bc}$ ,  $t_{1Bc}$ , respectively, where  $\tau_{Ac} < \tau_{Bc}$ . The determination of  $\tau_{Ac}$ ,  $\tau_{Bc}$  is as follows.

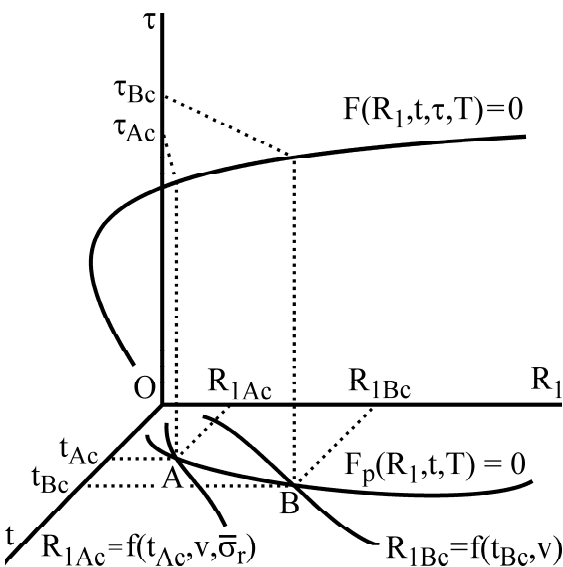


Figure 11: The function  $F(R_1, t, \tau, T) = 0$  which is determined by a computational simulation represents the time development of microstructure of the three-component material defined in Item 4, Sec. 1.1. The radius  $R_1$  of the grains which are covered by the envelope on their surfaces, the thickness  $t$  of the component (envelope) on the grain surface, and the time  $\tau$  represent variables of the function  $F(R_1, t, \tau, T) = 0$ . The exploitation temperature  $T$  ( $\equiv T_e$ ) is a parameter of  $F(R_1, t, \tau, T) = 0$ , where  $T < T_r$  and  $T_r$  is relaxation temperature (see Sec. 2.5). The function  $F_p(R_1, t, T) = 0$  represents a projection of  $F(R_1, t, \tau, T) = 0$  into the plane  $R_1 - t$ . The functions  $R_{1Ac} = f(t_{Ac}, v, \overline{\sigma}_r)$ ,  $R_{1Bc} = f(t_{Bc}, v)$  for  $v \in (0, v_{max})$  (see Sec. 1.3) are shown in Fig. 10, where  $f(t_{Ac}, v, \overline{\sigma}_r) \equiv f_i(t_{Ac}, v, \overline{\sigma}_{ri})$ ,  $f(t_{Bc}, v) \equiv f_i(t_{Bc}, v)$  ( $i = 1, 2$ ).

As shown in Fig. 11, let the Cartesian system  $(ORt\tau)$  with the functions  $R_{1Ac} = f(t_{Ac}, v, \overline{\sigma}_r)$  and

$R_{1Bc} = f(t_{Bc}, v)$  in the plane  $R - t$  for  $v \in (0, v_{max})$  (see Sec. 1.3) which are shown in Fig. 10 be considered, and then we get  $f(t_{Ac}, v, \overline{\sigma_r}) \equiv f_i(t_{Ac}, v, \overline{\sigma_{ri}})$ ,  $f(t_{Bc}, v) \equiv f_i(t_{Bc}, v)$  ( $i = 1, 2$ ).

Let  $F(R_1, t, \tau, T) = 0$  in Fig. 11 represent a function which is determined by a computational simulation of the time development of microstructure of the three-component material defined in Item 4, Sec. 1.1. The grain radius  $R_1$ , the thickness  $t$  of the component (envelope) on the grain surface, and the time  $\tau$  represent variables of the function  $F(R_1, t, \tau, T) = 0$ . The exploitation temperature  $T$  ( $\equiv T_e$ ) is a parameter of the function  $F(R_1, t, \tau, T) = 0$ , where  $T < T_r$  and  $T_r$  is relaxation temperature (see Sec. 2.5). The  $F(R_1, t, \tau, T) = 0$  thus defines a time dependence of both  $R_1$  and  $t$  at the exploitation temperature  $T$ .

Consequently, let the function  $F_p(R_1, t, T) = 0$  represent a projection of  $F(R_1, t, \tau, T) = 0$  into the plane  $R_1 - t$  as shown in Fig. 11.

The points  $A$  and  $B$  with the coordinates  $(R_{1Ac}, t_{Ac})$  and  $(R_{1Bc}, t_{Bc})$  represent intersections of  $F_p(R_1, t, T) = 0$  with  $R_{1Ac} = f(t_{Ac}, v, \overline{\sigma_r})$  and  $R_{1Bc} = f(t_{Bc}, v)$ , respectively, where  $f(t_{Ac}, v, \overline{\sigma_r}) \equiv f_i(t_{Ac}, v, \overline{\sigma_{ri}})$ ,  $f(t_{Bc}, v) \equiv f_i(t_{Bc}, v)$  ( $i = 1, 2$ ).

The substitution of  $R_1 = f(t_{Ac}, v, \overline{\sigma_r})$  and  $R_1 = f(t_{Bc}, v)$  to the function  $F_p(R_1, t, T) = 0$  results in the conditions  $F_p(f(t_{Ac}, v, \overline{\sigma_r}), t_{Ac}, T) = 0$  and  $F_p(f(t_{Bc}, v), t_{Bc}, T) = 0$ , respectively. The conditions  $F_p(f(t_{Ac}, \overline{\sigma_r}), t_{Ac}, T) = 0$  and  $F_p(f(t_{Bc}), t_{Bc}, T) = 0$  with the variables  $t_{Ac}$  and  $t_{Bc}$  are considered for the determination of the  $t$ -coordinates,  $t_{Ac}$  and  $t_{Bc}$ , of the point  $A$  and  $B$  in the plane  $R_1 - t$ , respectively.

Consequently, the substitution of the coordinates  $t_{Ac}$  and  $t_{Bc}$  to  $R_{1Ac} = f(t_{Ac}, v, \overline{\sigma_r})$  and  $R_{1Bc} = f(t_{Bc}, v)$  results in the determination of the coordinates  $R_{1Ac}$  and  $R_{1Bc}$  of the points  $A$  and  $B$ , respectively.

The substitution of the coordinates  $(R_{1Ac}, t_{Ac})$  and  $(R_{1Bc}, t_{Bc})$  to  $F(R_1, t, \tau, T) = 0$  results in the condition  $F(R_{1Ac}, t_{Ac}, \tau_{Ac}, T) = 0$  and  $F(R_{1Bc}, t_{Bc}, \tau, T) = 0$ , respectively. The conditions  $F(R_{1Ac}, t_{Ac}, \tau, T) = 0$  and  $F(R_{1Bc}, t_{Bc}, \tau_{Bc}, T) = 0$  with the variables  $\tau_{Ac}$  and  $\tau_{Bc}$  are considered for the determination of the time  $\tau_{Ac}$  and  $\tau_{Bc}$ , respectively, where  $\tau_{Ac} = \tau_{Ac}(v, \overline{\sigma_r})$ ,  $\tau_{Bc} = \tau_{Bc}(v)$ .

Consequently, the intervals  $\tau < \tau_{Ac}(v, \overline{\sigma_r})$ ,  $\tau \in \langle \tau_{Ac}, \tau_{Bc} \rangle$ ,  $\tau > \tau_{Bc}$  defines the time  $\tau$  which is related to the resistive, quasi-resistive, contributory effects of the thermal stresses against the mechanical loading, respectively. The intervals  $\tau < \tau_{Ac}$ ,  $\tau \in \langle \tau_{Ac}, \tau_{Bc} \rangle$ ,  $\tau > \tau_{Bc}$  determine non-critical, quasi-critical, critical time periods of the exploitation, respectively.

The critical time  $\tau_{Ac}$  and  $\tau_{Bc}$  is assumed to represent contribution to the total lifetime related to the thermal-stress induced resistive effects of a three-component material. As analysed above,  $\tau_{Ac}$  is determined for  $|\overline{p_1}(R_1, t, v)| = |\overline{\sigma_{r1}}(R_1, t, v)|$  or  $|\overline{p_2}(R_1, t, v)| = |\overline{\sigma_{r2}}(R_1, t, v)|$ , and then  $\tau_{Ac} \rightarrow \tau_{Ac1}(v, \overline{\sigma_{r1}})$  or  $\tau_{Ac} \rightarrow \tau_{Ac2}(v, \overline{\sigma_{r2}})$ , respectively, where  $\tau_{Aci} = \tau_{Aci}(v, \overline{\sigma_{ri}})$  ( $i = 1, 2$ ). Similarly,  $\tau_{Bc}$  is determined for  $|\overline{p_1}(R_1, t, v)| = 0$  or  $|\overline{p_2}(R_1, t, v)| = 0$ , and then  $\tau_{Bc} \rightarrow \tau_{Bc1}(v)$  or  $\tau_{Bc} \rightarrow \tau_{Bc2}(v)$ , respectively, where  $\tau_{Bci} = \tau_{Bci}(v)$  ( $i = 1, 2$ ).

Finally,  $\tau_{Acmin}$  and  $\tau_{Bcmin}$  which represent minimal values of the sets  $\{\tau_{Ac1}, \tau_{Ac2}\}$  and  $\{\tau_{Bc1}, \tau_{Bc2}\}$  are considered to represent the lifetime regarding the 'resistance-(quasi-resistance)' and '(quasi-resistance)-contribution' transformations (see Fig. 10), respectively.

Analytical-computational-experimental method. The analytical-computational-experimental method represents a connection of an analytical model of the thermal stresses with computational simulation of the time development of microstructure as well as with experimental results. The temperature  $T$  is a parameter of this analytical-computational-experimental method. The determination of the analytical-computational-experimental method is as follows.

Let the computational simulation be represented by a time development of the thickness  $t$  of the component (envelope) on grain surfaces. Let this time development be represented by the function  $t = g(\tau)$ , where  $\tau = f(t)$  is an inverse function of  $t = g(\tau)$ . Let  $\log \tau = f(\log t)$  be derived by the Taylor series in terms of  $\log t$  regarding the time interval  $\tau \in \langle 0, 200000 \rangle$  [hour]. Consequently, the function  $\log \tau = f(\log t)$  has the form

$$\log \tau = \sum_{i=0}^n c_i^{(\tau)} (\log t)^i. \quad (59)$$

The experimental results are represented by a time development of the radius  $R_1$  of the grains which are covered by the component (envelope) on their surfaces. Let the dependence  $R_1 - \tau$  for  $\tau \in \langle 0, 200000 \rangle$  [hour] be derived as

$$\log R_1 = \sum_{j=0}^m c_j^{(R_1)} (\log \tau)^j. \quad (60)$$

With regard to Eqs. (59), (60), we get

$$\log R_1 = \sum_{j=0}^m c_j^{(R_1)} \left( \sum_{i=0}^n c_i^{(\tau)} (\log t)^i \right)^j. \quad (61)$$

An analytical model of the thermal stresses is represented by the functions  $R_{1Ac} = f(t_{Ac}, v, \overline{\sigma_r})$  and  $R_{1Bc} = f(t_{Bc}, v)$  (see Fig. 10), strictly speaking by the functions  $\log R_{1Ac} = \log [f(t_{Ac}, v, \overline{\sigma_r})]$  and  $\log R_{1Bc} = \log [f(t_{Bc}, v)]$ , where  $f(t_{Ac}, v, \overline{\sigma_r}) \equiv f_i(t_{Ac}, v, \overline{\sigma_{ri}})$ ,  $f(t_{Bc}, v) \equiv f_i(t_{Bc}, v)$  ( $i=1,2$ ). With regard to Eq. (61), and considering  $t \rightarrow t_{Ac}$ , we get

$$\log [f(t_{Ac}, v, \overline{\sigma_r})] - \sum_{j=0}^m c_j^{(R_1)} \left( \sum_{i=0}^n c_i^{(\tau)} (\log t_{Ac})^i \right)^j = 0. \quad (62)$$

Similarly, considering  $t \rightarrow t_{Bc}$ , we get

$$\log [f(t_{Bc}, v)] - \sum_{j=0}^m c_j^{(R_1)} \left( \sum_{i=0}^n c_i^{(\tau)} (\log t_{Bc})^i \right)^j = 0. \quad (63)$$

Consequently, the roots  $t_{Ac} = t_{Ac}(v, \overline{\sigma_r})$  and  $t_{Bc} = t_{Bc}(v)$  of Eqs. (62) and (63) are determined by a numerical method. Substituting  $t_{Ac} = t_{Ac}(v, \overline{\sigma_r})$  and  $t_{Bc} = t_{Bc}(v)$  to Eq. (59), the critical time  $\tau_{Ac}$  and  $\tau_{Bc}$  has the form

$$\tau_{Qc} = \exp \left[ (\ln 10) \sum_{i=0}^n c_i^{(\tau)} (\log t_{Qc})^i \right], \quad Q = A, B. \quad (64)$$

Finally, Equations (59) and (60) can be also determined from experimental results and a computational simulation, respectively. The analysis concerning  $\tau_{Acmin}$ ,  $\tau_{Bcmin}$  and the sets  $\{\tau_{Ac1}, \tau_{Ac2}\}$  and  $\{\tau_{Bc1}, \tau_{Bc2}\}$  is also considered for this analytical-computational-experimental method.

## 6 Conclusions and applications

This doctoral dissertation presents analytical models of thermal stresses and of thermal-stress induced phenomena in components of two- and three-component materials (see Sec. 1.1). With regard to the analytical modelling, these real multi-component materials with finite dimensions are replaced by two- and three-component model systems with infinite dimensions (see Secs. 1.2–1.4), i.e. multi-particle-matrix and multi-particle-envelope-matrix systems, respectively (see Figure 1). The analytical determination of a thermal stress-strain state is based on a cell model which considers a cubic cell (see Figure 1). The cell model is usually used in case of the analytical and computational modelling of phenomena in periodic model systems [19]–[28]. Additionally, as presented in [28], the case when an infinite matrix is considered within analytical modelling of phenomena in real multi-component materials with finite dimensions is of particular interest for the mathematical simplicity of analytical solutions. As presented in [28], such analytical solutions are assumed to exhibit sufficient accuracy due to the size of material components (e.g. precipitates, envelopes) which is relatively small in comparison with the size of macroscopic material samples, macroscopic structural elements, etc.

The thermal stresses which originate below relaxation temperature (see Sec. 2.5) during a cooling process are a consequence of the difference in dimensions of the components. This difference is a consequence of different thermal expansion coefficients and/or a consequence of the phase-transformation

induced strain which is determined in Sec. 2.5 for anisotropic and isotropic crystal lattices. This coefficient and strain are included in the coefficient  $\beta_q$  for the spherical particle ( $q = p$ ), the spherical envelope ( $q = e$ ) and the cell matrix ( $q = m$ ) (see Eqs. (9)–(12)).

This cooling process is characterized by a homogeneous temperature change. The homogeneous temperature change which is considered in this doctoral dissertation is then characterized by the condition  $\partial T/\partial r = \partial T/\partial \varphi = \partial T/\partial \nu = 0$ , where  $T$  is temperature and  $(r, \varphi, \nu)$  are spherical coordinates (see Fig. 2).

The analytical modelling of the thermal stresses results from fundamental equations of solid continuum mechanics which are represented by the Hooke's law for an anisotropic and isotropic continuum (see Eqs. (5)–(7)), and by the Cauchy's, compatibility and equilibrium equations (see Eqs. (2)–(4)) which are determined by the spherical coordinates  $(r, \varphi, \nu)$  (see Figure 2). The analytical models of the thermal stresses are determined for the model systems which consists of either anisotropic, or isotropic, or anisotropic and isotropic components (see Secs. 3.1, 3.2, 4.1–4.4). The thermal stress-strain state in each component of the model systems is determined by several mutually different solutions which fulfil the boundary conditions which are determined in Sec. 3.3. In case of the cell matrix, mandatory and additional boundary conditions are determined (see Eqs. (32)–(37)). Due to these different solutions, a principle of minimum total potential energy of an elastic solid body [29] is then required to be considered (see Sec. 2.4).

Strictly speaking, such solutions or a combination of solutions are considered to exhibit minimum total potential energy of the model systems (see Figure 1). As analysed in Sec. 2.4, the total potential energy  $W_t$  of the model systems is represented by the deformation energy  $W_d$ . The deformation energy of the model systems is represented by the thermal-stress induced elastic energy  $W_c$  which is accumulated in the cubic cell, and then  $W_t = W_d = W_c$ .

The analytical results of thermal-stress induced phenomena in this doctoral dissertation includes analytical models of crack formation (see Sec. 5.1), of the energy barrier (see Sec. 5.2), of the micro- and macro-strengthening (see Sec. 5.3) along with the analytical-computational and analytical-computational-experimental methods of the lifetime prediction (see Sec. 5.4).

As presented in Sec. 5.2, the crack formation in the multi-particle-matrix system includes crack initiation which is followed by crack propagation. With regard to the crack initiation, *no* mathematically defined crack is present in this model system *before* the thermal-stress loading. This is in contrast to the analytical and/or computational investigation in [33]–[38]. This investigation is applied to a model system with a crack which is mathematically defined, e.g. a penny-shaped crack. Strictly speaking, this mathematically defined crack exists in a model system before the loading of the model system.

The crack formation analysis in Sec. 5.1 is based on the comparison of energy which is accumulated in the cubic cell with energy for the creation of a new surface (i.e. a surface of a crack). This comparison is used e.g. in [39]–[41]. The crack formation analysis then considers a curve integral of the thermal-stress induced elastic energy density  $w$  (see Eqs. (50), (51)) along a curve in the cubic cell. The condition (see Eq. (47)) which defines a limit state with respect to the crack initiation in the cracking plane  $x_i x_j$  ( $i, j = 1, 2, 3; i \neq j$ ) in the spherical particle ( $q = p$ ) or cell matrix ( $q = m$ ) is determined, where the limit state is thus defined by the critical particle radius  $R_{1cq}^{(ij)}$ . With regard to the crack propagation at  $R_1 > R_{1cq}^{(ij)}$ , the condition (see Eq. (48)) for the determination of a position of the crack tip in  $x_i x_j$  (see Fig. 4c) in components of the multi-particle-matrix system is determined. Formulae (see Eqs. (44)–(46)) which define the crack shape in the plane  $x_{ij} x_k$  (see Fig. 4c) which is perpendicular to the cracking plane  $x_i x_j$  in components of the multi-particle-matrix system are also determined. These results concerning the crack propagation are valid for ceramic components which are characterized by a high-speed crack propagation. Additionally, the crack formation analysis concerning the Method 2 (see p. 24) explains paradoxical behaviour of the cracking which is experimentally observed in a real two-component material [39]–[41].

In contrast to the crack propagation results, the determination of the limit state is applicable

disregarding a 'character' of components of the multi-particle-matrix system (ceramic=brittle, elastic, elastoplastic components).

The energy barrier represents a surface integral of thermal-stress induced elastic energy density over a surface in the cubic cell (see Eq. (54)). Due to a range of this brochure, formulae for the energy barrier in the model systems (see Fig. 1) are determined in the doctoral dissertation.

In addition to experimental methods [42]–[44], strengthening of multi-component materials is also investigated analytically and/or computationally. Such analytical and/or computational determination is based on e.g. the finite element methods, Orowan and modified Oldroyd models, a simulation of dislocation dynamics [45]–[50].

As presented in Sec. 5.3, the micro- and macro-strengthening,  $\sigma_{si}$  and  $\bar{\sigma}_{si}$  (see Eq. (58)), respectively, along the axis  $x_i$  ( $i = 1,2,3$ ) (see Fig. 1) is also based on a surface integral of the thermal-stress induced elastic energy density  $w_i$  over a surface in the cubic cell (see Sec. 5.3). Additionally, within this doctoral dissertation, the micro- and macro-strengthening is defined as thermal-stress resistance against mechanical loading. In this case,  $w_i = w_i(x_i)$  represents such elastic energy density which is induced by the thermal stress  $\sigma_i = \sigma_i(x_i)$  which act along the axis  $x_i$  (see Sec. 5.3), where  $\bar{\sigma}_{si}$  represents a mean value of  $\sigma_{si} = \sigma_{si}(x_i)$  for  $x_i \in \langle 0, d/2 \rangle$  in the cubic cell. Due to a range of this brochure, formulae for the micro-/macro-strengthening in the model systems (see Fig. 1) are determined in the doctoral dissertation.

With regard to the analytical modelling, the lifetime prediction methods (see Sec. 5.4) are based on a transformation of the 'resistive' effect of the thermal stresses to the 'contributory' effect with respect to mechanical loading. This transformation results in the analytical determination of critical microstructural parameters (a radius of grains and thickness of an envelope which is segregated on a surface of the grains). The lifetime prediction methods also consider results which are obtained by a computational simulation of the microstructural parameters during a time-temperature-dependent development of microstructure (the analytical-computational method) as well as experimental results concerning this microstructural development (the analytical-computational-experimental method).

Additionally, the analytical models of the crack formation, of the energy barrier and of the micro- and macro-strengthening along with the methods of lifetime prediction exhibit a general validity. These analytical models and these lifetime prediction methods are then valid for the thermal-stress induced elastic energy density as well as for energy density which is induced by any stresses acting in the multi-particle-matrix and multi-particle-envelope-matrix systems. In case of the lifetime prediction methods, conditions which are required with respect to this general validity are presented (see p. 29). Due to a range of this brochure, illustrative examples of applications of the analytical models of these phenomena to real engineering materials (superconductive and structural ceramics, a creep-resistant steel) are presented in the doctoral dissertation.

Results of this doctoral dissertation are applicable within *basic research* (solid continuum mechanics, theoretical physics, materials science) as well as *engineering practice*.

With regard to the basic research, the analytical models of the thermal stresses in the model systems with either anisotropic components, or isotropic components, or anisotropic and isotropic components can be incorporated to the Eshelby's model [51]. The Eshelby's model and its development [20,21,28,51] which are based on the Green's function, ordinary Newtonian potential and biharmonic potential define the disturbance of an applied stress-field in a solid continuum. The applied stress-field (e.g. mechanical loading) is disturbed due to the presence of inclusions in a solid continuum. This incorporation thus defines a stress-strain state in a multi-component material which is loaded by thermal and mechanical stresses [28].

The analytical models of the thermal stresses can be incorporated into experimental and computational methods for the determination of residual stresses [65]–[67].

The analytical model of the thermal-stress induced energy barrier can be also incorporated into analytical and/or computational models which are created by e.g. theoretical physicists, and which describe an interaction of an energy barrier with dislocations or magnetic domain walls [68,69].

Similarly, the analytical model of the thermal-stress induced micro- and macro-strengthening can

be also incorporated into analytical, computational or experimental models of strengthening.

The thermal stresses can be incorporated into these models in a form of the thermal-stress induced field of stresses and/or strains, or in a form of the thermal-stress induced elastic energy density.

The same (i.e. this incorporation) is also valid for the analytical-computational-experimental lifetime prediction methods which can be considered within other analytical, computational and experimental techniques for the determination of the lifetime.

As presented in [39]–[41,52,70], material scientists often numerically determine a thermal stress-strain state in a real two-component material by an analytical model which is determined for a one-particle-matrix system. As presented in [52,70], this one-particle-matrix system with the particle volume fraction  $v = 0$  consists of an isotropic spherical particle and an isotropic infinite matrix. However, real two- and three components materials are characterized by  $v > 0$ . The analytical models in Chaps. 3,4 for the multi-particle model systems in Fig. 1, both with  $v > 0$ , thus enable to numerically determine the thermal stress-strain state with respect to different values of the particle volume fraction. Additionally, such numerical determination for the multi-particle model systems with anisotropic and/or isotropic components is assumed to be more considerable in comparison with numerical results for the one-particle-matrix system with isotropic components.

Concerning engineering practice, materials scientists and engineers are able to numerically determine the limit state (the critical particle radius) with respect to the crack initiation. Consequently, this numerical determination can be helpful for the determination of 'suitable' heat treatment parameters. These 'suitable' heat treatment parameters are expected to lead to non-critical radii of precipitates (particles) in microstructure of real two-component material of the precipitate-matrix type (see Sec. 1.1).

Materials scientists and engineers are also able to numerically determine the lifetime of creep-resistant steels by the analytical-computational and analytical-computational-experimental prediction methods. This lifetime is related to the transformation of the resistance effect to the contributory effect of the thermal stresses with respect to mechanical loading. This numerical determination requires experimental and/or computational determination of all material components and/or phases which create the envelope on a surface of grains. Additionally, the volume fraction of each of these material components and/or phases are also required to be experimentally and/or computationally determined. These volume fractions are then considered within a numerical determination of elastic moduli and a thermal expansion coefficient of this multi-component envelope. Finally, this 'thermal-stress induced' lifetime represents a part of total lifetime.

## Bibliography

- D1. L.Ceniga. Thermal stresses in triaxial anisotropic particle-matrix system. *Journal of Thermal Stresses* 27 (2004) 471–489 (IF: 0.951).
- D2. L.Ceniga. Thermal stresses and related phenomena in composite ceramics. *Journal of Materials Science* 42 (2007) 1202–1227 (IF: 1.855).
- D3. L.Ceniga. Analytical models of thermal-stress induced phenomena in isotropic multi-particle-matrix system. *Journal of Thermal Stresses* 31 (2008) 862–891 (IF: 0.951).
- D4. L.Ceniga. Thermal stresses in model materials. *Journal of Thermal Stresses* 31 (2008) 728–758 (IF: 0.951).
- D5. L.Ceniga. A new analytical model for thermal stresses in multi-phase materials and lifetime prediction methods. *Acta Mechanica Sinica* 24 (2008) 189–206 (IF: 0.749).
- D6. L.Ceniga. Thermal-stress induced phenomena in two-component material. Part I. *Acta Mechanica Sinica* 25 (2009) 811–820 (IF: 0.749).
- D7. L.Ceniga. Thermal-stress induced phenomena in two-component material. Part II. *Acta Mechanica Sinica* 26 (2010) 101–106 (IF: 0.749).

- D8. L.Ceniga. Thermal stresses in two- and three-component anisotropic materials. *Acta Mechanica Sinica* 26 (2010) 695–709 (IF: 0.749).
- D9. L.Ceniga. Analytical model of thermal stresses in two- and three-component materials. *International Journal of Engineering Science* 48 (2010) 290–311 (IF: 1.656).
- D10. L.Ceniga. Analytical model of thermal stresses in two- and three-component materials II. *International Journal of Engineering Science* 48 (2010) 1824–1841 (IF: 1.656).
- D11. L.Ceniga. Analytical model of thermal-stress induced cracking in two-component material with anisotropic component. *International Journal of Engineering Science* 49 (2011) 354–368 (IF: 1.656).
- D12. L.Ceniga. A novel analytical model and energy analysis of thermal stresses in two-phase composites. *Meccanica* 47 (2012) 845–855 (IF: 1.558).
- D13. L.Ceniga. Thermal stresses in particle-matrix system and related phenomena. Application to SiC-Si<sub>3</sub>N<sub>4</sub> Ceramics. In *Ceramics and Composite Materials: New Research*. Ed. B.M.Caruta. Nova Science Publishers, New York, 2005, ISBN: 1-59454-370-4, pp. 147-195.
- D14. L.Ceniga. Thermal stresses in isotropic multi-particle-envelope-matrix system. Application to SiC-YbN<sub>20</sub>-Si<sub>3</sub>N<sub>4</sub> ceramics. In *New Developments in Material Science Research*. Ed. B.M.Caruta. Nova Science Publishers, New York, 2007, ISBN: 1-59454-854-4, pp. 139-180.
- D15. L.Ceniga. New analytical model of thermal stresses and analytical fracture mechanics in two-component materials. Application to two-component ceramics. In *Ceramic Matrix Composites*. Eds. E.Dimitriou, M.Petralia. Nova Science Publishers, New York, 2010, ISBN: 978-1-60741-896-2, pp. 247–296.
- D16. L.Ceniga. Analytical Models of Thermal Stresses in Composite Materials I. Nova Science Publishers, New York, 2008, ISBN: 978-1-60456-085-5 (319 pages).
- D17. L.Ceniga. Analytical Models of Thermal Stresses in Composite Materials II. Nova Science Publishers, New York, 2007, ISBN: 1-60021-809-1 (200 pages).
- D18. L.Ceniga. Analytical Models of Thermal Stresses in Composite Materials III. Nova Science Publishers, New York, 2011, ISBN: 978-1-61324-710-5 (214 pages).
19. T.Mizutani. Residual strain energy in composites containing particles. *Journal of Materials Science* 11 (1996) 483–494.
20. S.Li, R.A.Sauer, G.Wang. The Eshelby tensors in a finite spherical domain - part I: Theoretical formulations. *Journal of Applied Mechanics* 74 (2007) 770–783.
21. S.Li, R.A.Sauer, G.Wang. The Eshelby tensors in a finite spherical domain - part II: Applications to homogenization. *Journal of Applied Mechanics* 74 (2007) 784–797.
22. V.I.Kushch. Effective elastic moduli of an isotropic medium weakened by identically oriented disk-shaped cracks. *International Applied Mechanics* 36 (2000) 225-233.
23. V.I.Kushch. The stress intensity factors in an isotropic elastic body weakened by equioriented disk cracks. *International Applied Mechanics* 36 (2000) 623-630.
24. M.Guagliano. A numerical model to investigate the role of residual stresses on the mechanical behavior of Al/Al<sub>2</sub>O<sub>3</sub> particulate composites. *Journal of Materials Engineering and Performance* 7 (1998) 183–189.
25. K.B.Broberg. The cell model of materials. *Computational Mechanics* 19 (1997) 447–452.
26. M.Šejnoha, J.Zeman. Micromechanical modeling of imperfect textile composites. *International Journal of Engineering Science* 46 (2008) 513-526.
27. M.Šejnoha, J.Zeman. Overall viscoelastic response of random fibrous composites with statistically quasi uniform distribution of reinforcements. *Computer Methods in Applied Mechanics and Engineering* 191 (2002) 5027-5044.

28. T.Mura. *Micromechanics of Defects in Solids*. Martinus Nijhoff Publishers, Dordrecht, 1987.
29. M.Brdička, L.Samek, B.Sopko. *Mechanics of Continuum*. Academia, Prague, 2000 (in Czech).
30. L.Hegedúsová, M.Kašiarová, J.Dusza, M.Hnatko, Šajgalík. Mechanical properties of carbon-derived  $\text{Si}_3\text{N}_4+\text{SiC}$  micro/nano-composite. *International Journal of Refractory Metals and Hard Materials* 27 (2009) 438–442.
31. F.Trebuňa, M.Buršák. *Limit States and Fractures (Medzné stavy a lomy)*. Edition of technical and scientific literature, Mechanical Engineering Faculty, Technical University in Košice, ManaCon Prešov, 2002 (in Slovak).
32. F.Trebuňa, F.Šimčák, J.Bocko, P.Trebuňa, M.Pátor, P.Šarga. Analysis of crack initiation in the press frame and innovation of the frame to ensure its further operation. *Engineering Failure Analysis* 18 (2011) 244–255.
33. Z.W.Gao, Y.H.Zhou. Fracture behaviors induced by thermal stress in an anisotropic half plane superconductor. *Physics Letters A* 372 (2008) 5261–5264.
34. P.Gudmundson. Anisotropic microcrack nucleation in brittle materials. *Journal of Mechanics and Physics of Solids* 38 (1990) 531–551.
35. S.G.Lekhnitskii. *Theory of Elasticity of an Anisotropic Elastic Body*. MIR Publishers, Moscow, 1981.
36. L.Ma, Y.Chen. Weight functions for interface cracks in dissimilar anisotropic materials. *Acta Mechanica Sinica* 20 (2004) 82–88.
37. F.Desrumaux, F.Meraghni, M.L.Benzeggagh. Generalised Mori-Tanaka scheme to model anisotropic damage using numerical Eshelby tensor. *Journal of Composite Materials* 35 (2001) 603–624.
38. T.Mori, K.Tanaka. Average stress in matrix and average elastic energy of materials with misfitting inclusions. *Acta Metallurgica* 21 (1973) 571–574.
39. P.Diko. Cracking in melt-processed REBaCuO superconductors. *Supercond. Sci. Technol.* 11 (1998) 68–72.
40. P.Diko. Cracking in melt-grown REBaCuO single-grain bulk superconductors. *Supercond. Sci. Technol.* 17 (2004) R45–R58.
41. P.Diko, Thermal stresses and microcracking caused by 211-particles in Y-Ba-Cu-O melt-processed bulks. *Mater. Sci. Eng.* B83 (1998) 149–153.
42. U.Lagerpusch, V.Mohles, D.Baither, B.Anczykowski, E.Nembach. Double strengthening of copper by dissolved gold-atoms and by incoherent  $\text{SiO}_2$ -particles: How do the two strengthening contributions superimpose? *Acta Materialia* 48 (2000) 3647–3656.
43. G.Liu, G.J.Zhang, X.D.Ding, J.Sun, K.H.Chen. Modeling the strengthening response to aging process of heat-treatable aluminum alloys containing plate/disc- or rod/needle-shaped precipitates. *Materials Science and Engineering A* 344 (2003) 113–124.
44. Z.Trojanová, Z.Drozd, S. Kúdela, Z.Száráz, P.Lukáč. Strengthening in MgLi matrix composites. *Composites Science and Technology* 67 (2007) 1965–1973.
45. L.Farrissey, S.Schmauder, M.Dong, E.Soppa, M.H.Poeh, P.McHugh. Investigation of the strengthening of particulate reinforced composites using different analytical and finite element models. *Computational Materials Science* 15 (1999) 1–10.
46. Z.Zhang, D.L.Chen. Consideration of Orowan strengthening effect in particulate-reinforced metal matrix nanocomposites: A model for predicting their yield strength.
47. N.Ramakrishnan. An analytical study on strengthening of particulate reinforced metal matrix composites. *Acta Materialia* 44 (1996) 69–77.

48. D.A.Terentyev, G.Bonny, L.Malerba. Strengthening due to coherent Cr precipitates in FeCr alloys: Atomistic simulations and theoretical models. *Acta Materialia* 56 (2008) 3229-3235.
49. S.Lefebvre, B.Devincre, T.Hoca. Yield stress strengthening in ultrafine-grained metals: A two-dimensional simulation of dislocation dynamics. *Journal of the Mechanics and Physics of Solids* 55 (2007) 788-802.
50. S.Queyreau, G.Monnet, B.Devincre. Orowan strengthening and forest hardening superposition examined by dislocation dynamics simulations. *Acta Materialia* 58 (2010) 5586-5595.
51. J.D.Eshelby. The determination of the elastic field of an ellipsoidal inclusion, and related problems. *Proc. Royal Soc. London A* 241 (1957) 376-396.
52. S.P.Timoshenko, J.N.Goodier. *Theory of Elasticity*. McGraw-Hill International Edition, 1970.
53. F.Kuba. *Theory of Elasticity and Selected Applications*. SNTL/Alfa, Prague, 1982 (in Czech).
54. R.F.S.Hearmon. *Introduction to Applied Anisotropic Elasticity*. SNTL, Prague, 1965 (in Czech); translation from English: The Clarendon Press, Oxford, 1961.
55. F.Trebuňa, F.Šimčák, V.Jurica. *Elasticity and Strength I (Pružnosť a pevnosť I)*. Edition of technical and scientific literature, Mechanical Engineering Faculty, Technical University in Košice, 2005 (in Slovak).
56. P.Skočovský, O.Bokúvka, P.Palček. *Materials Science*. EDIS, Žilina, 1996 (in Slovak).
57. S.I.Novikova. Anisotropy of thermal expansion of solids. *Measurement Techniques* 27 (1984) 933-938.
58. K.Rektorys. *Review of Applied Mathematics*. SNTL, Prague, 1973 (in Czech).
59. V.Hajko, L.Potocký, A.Zentko. *Magnetization Processes*. Alfa, Bratislava, 1982.
60. J.Hald. Microstructure and long-term creep properties of 9-12% Cr steels. *International Journal of Pressure Vessels and Piping* 85 (2008) 30-37.
61. A.Výrostková, V.Homolová, J.Pecha, M.Svoboda. Phase evolution in P92 and E911 weld metals during ageing. *Materials Science and Engineering A* 480 (2008) 289-298.
62. G.Dimmler, P.Weinert, E.Kozeschnik, H.Cerjak. Quantification of the Laves phase in advanced 9-12% Cr steels using a standard SEM. *Materials Characterization* 51 (2003) 341-352.
63. F.Abe, T.-U.Kern, R.Viswanathan. *Creep-Resistant Steels*. Woodhead Publishing Limited, Cambridge, 2008.
64. J.D.Robson, H.K.D.H.Bhadeshia. Kinetics of precipitation in power plant steels. *Calphad* 20 (1996) 447-460.
65. F.Trebuňa, P.Bigoš. *Intensification of Technical Capability of Heavy Supporting Structures (Intenzifikácia technickej spôsobilosti ťažkých nosných konštrukcií)*. Edition of technical and scientific literature, Mechanical Engineering Faculty, Technical University in Košice, Vienaľa, Košice, 1998 (in Slovak).
66. F.Trebuňa, F.Šimčák, J.Bocko, P.Šarga, P.Trebuňa, M.Pátor, J.Mihok. Quantification of residual stresses in the weld by the hole-drilling method. *Metalurgija* 47 (2008) 133-137.
67. F.Trebuňa, F.Šimčák, M.Buršák, J.Bocko, P.Šarga, M.Pátor, P.Trebuňa. Quantification of residual stresses in hot rolled steel sheets by the hole drilling method. *Metalurgija* 46 (2007) 41-46.
68. H.Shin, Y.Y.Earmme. Interaction of screw dislocation and anisotropic (or isotropic) circular inclusion in isotropic (or anisotropic) matrix. *International Journal of Fracture* 126 (2004) L35-L40.
69. J.Y.Li, M.L.Dunn. Anisotropic coupled-field inclusion and inhomogeneity problems. *Philosophical Magazine A* 77 (1998) 1341-1350.
70. R.W.Davidge, T.J.Green. The strength of two-phase ceramic/glass materials. *Journal of Materials Science* 3 (1968) 629-634.

## List of the author's publications

### Papers in international journals with an impact factor

- A1. A.Zentková, S.Uličiansky, A.Zentko, L.Ceniga. On the shape of individual Barkhausen pulse. *Materials Science Forum* 235-238 (Part 2) (1997) 795-800 (IF: 0.399).
- A2. L.Ceniga, A.Zentko, M.Zentková. Dynamics of the remagnetization process in the rapidly quenched FeCuNbSiB alloys *Materials Science Forum* 235-238 (Part 2) (1997) 755-758 (IF: 0.399).
- A3. L.Ceniga, L.Novák. The magnetic properties and the Barkhausen noise of the hydrogenated Fe-V-B amorphous alloy. *Acta Physica Polonica A* 97 (2000) 611-614 (IF: 0.467).
- A4. L.Ceniga, L.Novák, E.Kisdi-Koszó. The influence of heat treatment on the Barkhausen effect in the Fe-Cr-B amorphous alloy. *Journal of Magnetism and Magnetic Materials* 197 (1999) 154-155 (IF: 1.689).
- A5. L.Ceniga, L.Novák, A.Zentko. The magnetic properties and the Barkhausen noise of the annealed Fe-V-B amorphous alloy. *Acta Physica Polonica A* 97 (2000) 575-578 (IF: 0.467).
- A6. L.Ceniga. Internal stresses and Barkhausen noise of Fe<sub>80</sub>B<sub>20</sub> amorphous alloy treated by annealing and hydrogenation-dehydrogenation processes. *Materials Science and Engineering B* 79 (2001) 154-158 (IF: 2.614).
- A7. L.Ceniga, F.Kováč. Influence of annealing and hydrogenation-dehydrogenation processes on internal stresses and Barkhausen noise of Fe<sub>83</sub>B<sub>17</sub> amorphous alloy. *Journal of Materials Science* 36 (2001) 4125-4129 (IF: 1.855).
- A8. L.Ceniga, F.Kováč. Cracking of isotropic particle-matrix system: globular shape particle. *Materials Science and Engineering B* 86 (2001) 178-181 (IF: 2.614).
- A9. L.Ceniga, P.Diko. Matrix crack formation in Y-Ba-Cu-O superconductor. *Physica C* 385 (2003) 329-336 (IF: 1.407).
- A10. L.Ceniga. Thermal stresses in surface-coated Fe-3%Si sheet. *Journal of Materials Science* 38 (2003) 3709-3712 (IF: 1.855).
- A11. L.Ceniga. Thermal stresses in triaxial anisotropic particle-matrix system. *Journal of Thermal Stresses* 27 (2004) 471-489 (IF: 0.951).
- A12. L.Ceniga. Thermal stresses in isotropic cell-divided particle-matrix system: spherical and cubic cells. *Journal of Thermal Stresses* 27 (2004) 425-432 (IF: 0.951).
- A13. L.Ceniga. Thermal stresses in SiC-Si<sub>3</sub>N<sub>4</sub> cubic-cell-divided multi-particle-matrix system. *Key Engineering Materials* 290 (2005) 320-323 (IF: 0.224).
- A14. P.Diko, S.Kračunovská, L.Ceniga, J.Bierlich, M.Zeisberger, W.Gawalek. Microstructure of top seeded melt-grown YBCO bulks with holes. *Superconductor Science and Technology* 18 (2005) 1400-1404 (IF: 2.402).
- A15. L.Ceniga. Thermal stresses and related phenomena in composite ceramics. *Journal of Materials Science* 42 (2007) 1202-1227 (IF: 1.855).
- A16. L.Ceniga. Stresses in superconductor during oxygenation. *Journal of Materials Science* 42 (2007) 6895-6900 (IF: 1.855).
- A17. L.Ceniga, P.Diko. Analytical model of oxygenation-induced stresses in YBCO superconductor. *Physica C* 467 (2007) 179-185 (IF: 1.407).
- A18. L.Ceniga. Analytical models of thermal-stress induced phenomena in isotropic multi-particle-matrix system. *Journal of Thermal Stresses* 31 (2008) 862-891 (IF: 0.951).
- A19. L.Ceniga. Thermal stresses in model materials. *Journal of Thermal Stresses* 31 (2008) 728-758 (IF: 0.951).

- A20. L.Ceniga. A new analytical model for thermal stresses in multi-phase materials and lifetime prediction methods. *Acta Mechanica Sinica* 24 (2008) 189–206 (IF: 0.749).
- A21. L.Ceniga. Thermal-stress induced phenomena in two-component material. Part I. *Acta Mechanica Sinica* 25 (2009) 811–820 (IF: 0.749).
- A22. J.Král, M.Ferdinandy, D.Kottfer, I.Maňková, L.Ceniga. Tribological and refractory properties of TiAl3 inter-metallic alloy. *Surface Review and Letters* 16 (2009) 623–629 (IF: 0.372).
- A23. L.Ceniga. Thermal-stress induced phenomena in two-component material. Part II. *Acta Mechanica Sinica* 26 (2010) 101–106 (IF: 0.749).
- A24. L.Ceniga. Thermal stresses in two- and three-component anisotropic materials. *Acta Mechanica Sinica* 26 (2010) 695–709 (IF: 0.749).
- A25. L.Ceniga. Analytical model of thermal stresses in two- and three-component materials. *International Journal of Engineering Science* 48 (2010) 290–311 (IF: 1.656).
- A26. L.Ceniga. Analytical model of thermal stresses in two- and three-component materials II. *International Journal of Engineering Science* 48 (2010) 1824–1841 (IF: 1.656).
- A27. L.Ceniga. Thermal stresses in isotropic-triaxial-anisotropic particle-matrix system. *Meccanica* 45 (2010) 73–77 (IF: 1.558).
- A28. L.Hegedúsová, A.Kovalčková, L.Ceniga, J.Dusza. Contact strength and crack formation in monolithic ceramic materials. *Materials Science Engineering A* 527 (2010) 1179–1184 (IF: 2.319).
- A29. L.Ceniga. Analytical model of thermal-stress induced cracking in two-component material with anisotropic component. *International Journal of Engineering Science* 49 (2011) 354–368 (IF: 1.656).
- A30. L.Ceniga. A novel analytical model and energy analysis of thermal stresses in two-phase composites. *Meccanica* 47 (2012) 845–855 (IF: 1.558).
- A31. L.Hegedúsová, L.Ceniga, J.Dusza. Bending and contact strength of monolithic ceramic materials. *International Journal of Damage Mechanics* 21 (2012) 293–305 (IF: 1.958).
- A32. L.Hegedúsová, L.Ceniga. Contact strength and cracking of laminar ceramics. *High Temperature Materials and Processes* 31 (2012) 173–179 (IF: 0.355).

### Chapters in multi-authored international monographs

- A33. L.Ceniga. Thermal stresses in particle-matrix system and related phenomena. Application to SiC-Si<sub>3</sub>N<sub>4</sub> Ceramics. In *Ceramics and Composite Materials: New Research*. Ed. B.M.Caruta. Nova Science Publishers, New York, 2005, ISBN: 1-59454-370-4, pp. 147-195.
- A34. L.Ceniga. Thermal stresses in isotropic multi-particle-envelope-matrix system. Application to SiC-YbN<sub>20</sub>-Si<sub>3</sub>N<sub>4</sub> ceramics. In *New Developments in Material Science Research*. Ed. B.M.Caruta. Nova Science Publishers, New York, 2007, ISBN: 1-59454-854-4, pp. 139-180.
- A35. L.Ceniga. New analytical model of thermal stresses and analytical fracture mechanics in two-component materials. Application to two-component ceramics. In *Ceramic Matrix Composites*. Eds. E.Dimitriou, M.Petralia. Nova Science Publishers, New York, 2010, ISBN: 978-1-60741-896-2, pp. 247–296.
- A36. L.Hegedúsová, L.Ceniga, J.Dusza. Contact strength of ceramic materials. In *Ceramic Matrix Composites*. Eds. E.Dimitriou, M.Petralia. Nova Science Publishers, New York, 2010, ISBN: 978-1-60741-896-2, pp. 195–246.

### Sole-authored international monographs

- A37. L.Ceniga. Analytical Models of Thermal Stresses in Composite Materials I. Nova Science Publishers, New York, 2008, ISBN: 978-1-60456-085-5 (319 pages).

- A38. L.Ceniga. Analytical Models of Thermal Stresses in Composite Materials II. Nova Science Publishers, New York, 2007, ISBN: 1-60021-809-1 (200 pages).
- A39. L.Ceniga. Analytical Models of Thermal Stresses in Composite Materials III. Nova Science Publishers, New York, 2011, ISBN: 978-1-61324-710-5 (214 pages).

#### **Papers in Czech and Slovak journals with an impact factor**

- A40. A.Zentková, K.Šterbáková, L.Ceniga. The power spectrum of the correlated Barkhausen impulses. *Acta Physica Slovaca* 48 (1998) 631–634 (IF: 3.25).
- A41. L.Ceniga, L.Novák, M.Zentková. The effect of hydrogenation on the magnetization reversal process in amorphous ferromagnets. *Czechoslovak Journal of Physics* 49 (1999) 549–554 (IF: 0.42).
- A42. L.Novák, L.Ceniga, F.Kováč. Influence of hydrogenation-dehydrogenation process on magnetic properties and Barkhausen noise of the Fe-W-B amorphous alloy *Czechoslovak Journal of Physics* 52 (Suppl. A) (2002) A77–A80 (IF: 0.42).
- A43. L.Ceniga, F.Kováč. Influence of annealing process on magnetic properties and Barkhausen noise of the Fe-W-B amorphous alloy. *Czechoslovak Journal of Physics* 52 (Suppl. A) (2002) A73–A76 (IF: 0.42).
- A44. L.Ceniga, P.Diko. Internal stresses in superconductors. *Czechoslovak Journal of Physics* 52 (Suppl. A) (2002) A229–A232 (IF: 0.42).
- A45. A.Bidulská, R.Bidulský, L.Ceniga, T.Kvačkaj, M.Cabibbo, E.Evangelista. Hot Workability Evaluation of Zr-stabilized Aluminium alloy 2014 by Means of Torsion Test. *Metallic Materials* 46 (2008) 151–155 (IF: 0.81).
- A46. L.Hegedúsová, L.Ceniga, J.Dusza, M.Hnatko, P.ajgalík. Contact strength of monolithic and composite ceramic materials. *Metallic Materials* 47 (2009) 389–399 (IF: 0.81).
- A47. L.Hegedúsová, L.Ceniga, J.Dusza. Contact strength and crack formation in laminar ceramics. *Chemické listy* 105 (2011) 520–522 (IF: 0.62).